5-2002

A Study of the Photodegredation of Carbaryl: The Influence of Natural Organic Matter and the Use of Silver Zeolite Y As a Catalyst

Marsha Kanan

A STUDY OF THE PHOTODEGRADATION OF CARBARYL: THE INFLUENCE OF NATURAL ORGANIC MATTER AND THE USE OF SILVER ZEOLITE Y AS A CATALYST

By

Marsha Kanan

B.S. The University of Maine, 2001

A THESIS

Submitted in Partial Fulfillment of the

Requirements for the Degree of

Master of Science

(in Chemistry)

The Graduate School

The University of Maine

May, 2002

Advisory Committee:

Howard H. Patterson, Professor of Chemistry, Advisor

Alice E. Bruce, Associate Professor of Chemistry

Carl P. Tripp, Associate Professor of Chemistry

Rachel N. Austin, Assistant Professor of Chemistry, Bates College

A STUDY OF THE PHOTODEGRADATION OF CARBARYL: THE INFLUENCE OF NATURAL ORGANIC MATTER AND THE USE OF SILVER ZEOLITE Y AS A CATALYST

By Marsha Kanan

Thesis Advisor: Dr. Howard H. Patterson

An Abstract of the Thesis Presented
in Partial Fulfillment of the Requirements for the
Degree of Master of Science
(in Chemistry)
May, 2002

The photodegradation of carbaryl in the presence of Suwannee River natural organic matter (NOM) as well as the presence of AgY zeolites was studied. Two NOM samples were purchased in 2000 and 2001 and labeled as NOM-2000 and NOM-2001, respectively. The synchronous-scan luminescence spectra (SSLS) indicate the presence of different luminophores in the two samples. This suggests that although the compositions of the two NOM samples are similar, isomers composing the NOM mixtures are different. This difference was observed in the effect the two Suwannee River NOM samples had on the photodegradation of carbaryl. In particular, the photodecomposition of carbaryl in the presence of NOM-2001 follows first-order kinetics; whereas, in the presence of NOM-2000 the photodecomposition of carbaryl did not follow first-order kinetics. Moreover, the SSLS of a 3 ppm solution of the NOM-2000 sample shows one band in the high-energy region. This band was

quenched and a broad band appeared in the low-energy region as the concentration of the solution increased, indicating that the NOM samples might be forming oligomers at higher concentrations. The polymerized products were also found to affect the photodecomposition rate of carbaryl.

Silver-doped Y-type zeolites with different silver loadings were prepared and analyzed spectroscopically. Several emission bands were observed for each AgY sample. Each emission band becomes dominant over the others by selecting the suitable excitation wavelength. Similarly, different SSLS bands were observed and tuned by choosing the reasonable $\Delta\lambda$ indicating the presence of several luminophores. Both emission and SSLS indicate the presence of different silver clusters in zeolite Y.

The prepared AgY samples were found to catalyze the photodegradation of carbaryl. The study shows that the AgY catalysts were found to increase the photodegradation rate of carbaryl by 3-79 times depending on the amount of silver that was loaded on the Y-type zeolites. The effectiveness of the catalysts was monitored in the presence of Suwannee River NOM. The results indicated that in the presence of 3 ppm NOM and the AgY catalysts, the rate of photodegradation was enhanced, whereas, increasing the concentration of NOM to 15 and 30 ppm decreased the photodecomposition reaction rate.

The carbaryl photodegradation products in the absence and presence of the AgY zeolites were quantified using the technique of GC-MS. In the absence of the catalysts, only α-naphthol was produced after a solution of carbaryl was irradiated for up to 12 hours. However, in the presence of the AgY catalysts, α-naphthol and phthalic acid are major photodegradation products that were produced.

This thesis is dedicated to my husband, Sofian. May Allah reward you the best in this life and in the hereafter.

In the name of Allah, Most Gracious, Most Merciful.

"Say: He is Allah,
The One;

Allah, the Eternal, Absolute;

He begetteth not,
Nor is he begotten;

And there is none
Like unto Him."

From: *The Holy Quran,*
***Sura Al-Ikhlas,* or the Purity (of Faith)**

ACKOWLEDGEMENTS

In the name of Allah, Most Gracious, Most Merciful. First and foremost I thank Allah, our creator, for all the blessings He has given me.

I would like to sincerely thank my husband, Dr. Sofian Kanan, for his help and companionship. Without his constant support and encouragement, this work would not have been possible. I appreciate his love, friendship, patience, and care and will never forget how wonderful he has made my life.

My heartfelt gratitude goes out to my family and Sofian's family for their love and support throughout my years of study at the University of Maine. Special thanks are due to my parents, grandmother, brothers, and sister for always standing by me.

I also need to thank my advisor Dr. Howard Patterson for his help with my research. My sincere appreciation goes out to Dr. Alice Bruce and Dr. Carl Tripp for serving on my graduate committee and reading my thesis. I especially need to thank Dr. Tripp for teaching me how to perform error analysis on experimental data! I would also like to thank Dr. Rachel Austin for performing ICP-AES measurements, donating samples, chemicals, and equipment, as well as for serving on my committee and showing sincere interest in my work. Last but not least, special thanks go out to Dr. Chris Cronan for donating equipment and samples that made this research possible, as well as showing interest in this research.

I would like to thank all the graduate students in the chemistry department for their friendship. In particular, I will always cherish my friendship with Ruvinie Hettiarachchi. My sincere gratitude goes out to the brothers and sisters in the Muslim

Community in Orono for their friendship and kindness. I hope that Nichole and Jessica continue to grow in Islam, for years to come.

A special acknowledgement should be made to the National Science Foundation's K-12 Teaching Program for funding my graduate studies. I especially want to thank Rhonda Shirland, Rachel Byther, Alyce Masters, and Matthew Cyr for helping me teach their students this year. I enjoyed working with the third graders at Old Town elementary, the fourth and fifth graders at Dr. Lewis Libby School in Milford, and the sixth graders at Leonard Middle School in Old Town because of their enthusiasm and interest in learning science.

TABLE OF CONTENTS

LIST OF TABLES

LIST OF FIGURES

Chapter 1

INTRODUCTION

This thesis summarizes an investigation into the photodegradation of the widely used pesticide carbaryl. In particular, the influence of natural organic matter on the reaction will be discussed in depth. Finally, results regarding the use of silver(I)-exchanged zeolite Y as a catalyst for the photodecomposition of carbaryl will be analyzed and explained.

The following sections present background information and a literature review of topics that are relevant to this study. Section 1.1 outlines the environmental importance of this research work. The toxicity, environmental fate, and a brief review of the literature involving the pesticide carbaryl is presented in section 1.2. Information about the make up of natural organic matter is discussed in section 1.3 with a focus on its interaction with organic contaminants. Finally, section 1.4 provides a general introduction about zeolites with a discussion about the particular zeolite used in this study, and a look at the silver(I)-exchanged Y zeolite.

1.1. Importance of this Study

This research involves an in-depth investigation into the breakdown of the toxic pesticide, carbaryl. The extensive use of pesticides to produce food is of great concern for our generation and future generations because they enter our lakes, rivers, oceans, and contaminate our groundwater supplies. Therefore, studies that look at the breakdown of pesticides in the environment have become very important. Our goal

should be to try to clean up our water sources so that future generations will still have water available for their daily needs.

The research work described in this thesis is particularly important because it looks at how the degradation of carbaryl is affected by natural organic matter. By doing so, the study simulates what is occurring in the actual environment. Additionally, the use of silver(I) doped zeolites as catalysts allows the photodecomposition of carbaryl to occur at a much faster rate than it would under normal conditions. Being able to increase the breakdown rate of the pesticide without producing more toxic products is of extreme importance because this will allow us to clean up our water supplies.

1.2. Carbaryl

Carbaryl (1-naphthyl, N-methylcarbamate) belongs to a broad class of carbamate insecticides that are substituted esters of carbamic acid (NH_2COOH) with aliphatic or aromatic substituents on the oxygen or nitrogen atoms.[1] The structure of carbaryl and the carbamate functional group can be seen in Figure 1.1. The chemical properties of carbaryl are determined by the carbamate functional group on the molecule. For example, carbaryl is only slightly soluble in water under normal conditions (0.004% at 30°C).[2] Additionally, a high melting point (142°C) and low vapor pressure (1.17×10^{-6} mm Hg at 25°C), contribute to excellent shelf stability and make carbaryl an ideal compound to work with in the laboratory.[2]

Carbaryl was introduced in 1956 by Union Carbide Corporation as a contact insecticide with slight systemic properties.[3] It is widely used to control insect pests of

Figure 1.1. The structure of carbaryl and the general structure of carbamate pesticides.

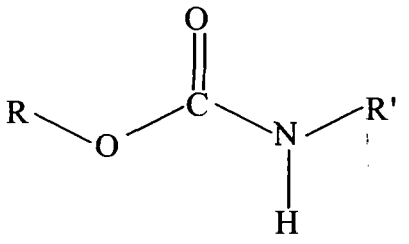

The Carbamate Functional Group

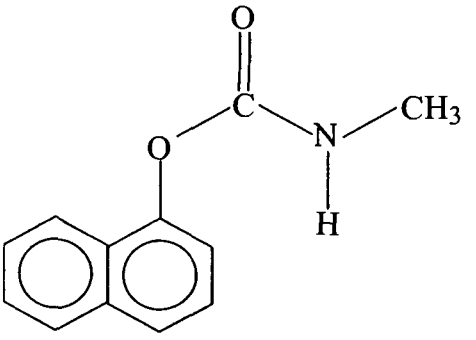

Carbaryl

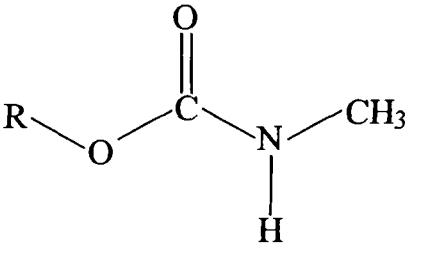

Generic N-methyl carbamate

fruit, vegetables, cotton, and many other crops.[4] Carbaryl is also effective against earthworms and insects in turf.[5] Poultry farmers use carbaryl to control mites in poultry, while the agriculture industry utilizes it to protect apples and other soft fruit from being attacked by moths and mites.[6]

1.2.1. Toxicity and mode of action

Carbaryl is considered to be moderately to very toxic depending on the dosage amount, the form of contact, and the type of animal that is exposed to it. In general, this carbamate pesticide is slightly toxic to mammals and moderately to highly toxic to aquatic organisms and honeybees. For example, the LD_{50} value for carbaryl when ingested by male rats is 850 mg/kg.[7] This value means that a dosage of 850 mg per kilogram of body weight will kill 50 percent of the rat population. Therefore, carbaryl does not pose a significant threat to the rat population. In contrast, carbaryl is considered moderately highly toxic to rainbow trout with an LC_{50} value of 1.3 ppm.[8] Since 1971, the maximum permissible amount of carbaryl in food products of seasonal consumption in the United States has been set at 10 mg/kg.[9]

Almost all insecticides are toxic because of their ability to disrupt the transmission of impulses through the nervous system of animals. Carbaryl and the other carbamates are no different, since their mode of action is acetylcholinesterase inhibition.[10] Acetylcholinesterase (AChE) is an enzyme that conveys impulses through the central nervous system of mammals, insects, and other species for the control of basic bodily functions such as breathing, digestion, and blood flow.[11] Specifically, carbaryl enters the synapse (or gap between nerve fibers and a receptor

that typically binds with an enzyme) and binds to the receptor and thereby inhibits AChE so that the enzyme cannot cleave the acetylcholine.[12] When a high concentration of acetylcholine builds up in the nerve cells, prolonged stimulation occurs and the affected nerve tissue eventually stops functioning.

Symptoms of acute exposure to high doses of carbaryl include sweating, blurring of vision, incoordination, convulsions, and respiratory failure.[7] In addition, inhalation or ingestion of very large amounts can be toxic to the nervous and respiratory systems resulting in nausea, stomach cramps, diarrhea, and excessive salivation.[13] Carbaryl can penetrate the skin mucous membranes, respiratory tract and gastrointestinal tract of mammals. However, it can be rapidly metabolized by various animals, and excreted in the urine as glucuronides or sulfates.[14,15] Overall, carbaryl does not appear to be a significant chronic health risk to humans at or below normal levels set by the EPA.

1.2.2. Environmental fate

Given the toxicity of carbaryl to fish, honeybees, and other animals, it is important to discuss the fate of this pesticide once it enters the environment. Although carbaryl shows a relatively short residual lifetime (a few weeks in soils), its biological half-life is usually larger (e.g., 5-6 months in fish), and some of its toxic metabolites are rather persistent in the environment (until 1-4 months).[16] Table 1.1 provides information regarding the environmental fate of carbaryl in different media.[17-26]

In water, carbaryl is known to degrade into α-naphthol, methylamine, and carbon dioxide.[18,27] The major photolysis product is also α-naphthol, which will

Table 1.1. The half-lives of carbaryl in water and soil under a variety of conditions.

Environmental Media	Degradation Pathway	Specific Conditions	Half-life of Carbaryl
Water	Hydrolysis	27°C, pH = 5	> 1500 days
Water	Hydrolysis	25°C, pH = 7	10~17 days
Water	Hydrolysis	25°C, pH = 9	3.2 hours
Water, Distilled & Sterile	Artificial sunlight	10.1 ppm, pH = 5	21 days
Natural Waters	Hydrolysis	variable	23-25 hours
Surface Water	Photolysis	seasonal variation	2-6.6 days
Seawater, Sterile & Filtered	Hydrolysis	24°C, pH = 8.2, 7.9	23, 24 hours
Seawater, Sterile	Artificial sunlight	10.1 ppm	5 hours
Topsoil	Artificial sunlight	9.8 ppm, 1-mm layer	41 days
Soil	Microbes (bacteria)	none	36 hours
Aerobic Soil	Hydrolysis	sandy loam soil	4-17 days
Anaerobic, Aquatic Soil	Hydrolysis	none	78 days
Topsoil	Field dissipation	0.3-0.45 m layer	0.76-10.9 days

further photooxidize to 2-hydroxy-1,4-naphtho-quinone under basic conditions.[28] Carbaryl is not persistent in soil, it is degraded through hydrolysis, photolysis and by microorganisms. Minor degradates of 1,4-naphthoquinone, 5-hydroxy-1-naphthyl methylcarbamate and 1-naphthyl-(hydroxymethyl)carbamate have been found in soil.[24]

1.2.3. Biological and chemical transformations of carbaryl

Abiotic transformations of carbaryl are equally likely to occur in the environment; therefore, it is important to look at the nature of the chemical reactions that the pesticides undergo because they often lead to the same products as the biological reactions. For example, the degradation pathways of carbaryl may be the same whether sunlight causes its decomposition or a bacterium ingests the molecule. Therefore, examining the chemical transformations first will provide us with insight into the reactions that occur when carbaryl is biodegraded as a result of microbial activity.

The first abiotic transformation that carbaryl undergoes is hydrolysis. Under neutral to basic conditions the hydrolysis of carbaryl is very rapid. For example, at pH = 7, the hydrolysis half-life of carbaryl was found to be 12.1 days, and at a pH = 9, the hydrolysis half-life was 3.2 hours.[19] On the other hand, under acidic conditions, the hydrolysis process takes a lot longer. At pH = 5, the hydrolysis reaction for carbaryl was found to take more than 1500 days.[17] The process of hydrolysis cleaves the C-O of the carbamate functional group leaving α-naphthol and methyl carbamic acid. The

hydrolysis reaction is shown in Figure 1.2. Methyl carbamic acid is very unstable and rapidly degrades to carbon dioxide and methylamine.[11]

Figure 1.2. Hydrolytic pathway for carbaryl.

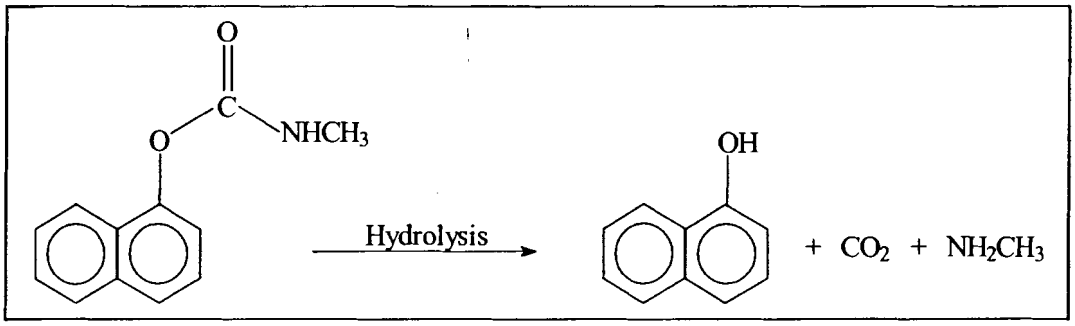

In the presence of UV light, carbaryl can also break down via a multi-step oxidation process. Although the mechanism of this degradation process is not well known, five different products have been identified. These species include α-naphthol, 1,4-naphthoquinone, 5-hydroxy-1,4-naphthoquinone, phthalic acid, and 1-hydroxy-phthalic acid.[29]

Carbaryl can also be degraded naturally via biological pathways. The metabolism of carbaryl is known to occur in vertebrates, insects, plants, and soil. Most animals readily hydrolyze a portion of the administered carbaryl, although hydrolysis does not seem to be a significant pathway in the metabolism of carbaryl in monkeys or pigs.[2] Overall, carbaryl is mostly metabolized via oxidative mechanisms.

In animals, several investigations revealed that carbaryl was metabolized by hepatic enzymes primarily into 1-naphthyl N-hydroxy-methylcarbamate, 4-hydroxy-1-naphthyl N-methylcarbamate, 5-hydroxy-1-naphthyl N-methylcarbamate, and to conjugates of these hydroxylated materials.[30] Investigations of the comparative

metabolism of carbaryl by different insect larval tissues revealed that the most efficient metabolic sites were fat body and gut.[31] The products of this oxidative process as well as those found when plant stems are injected with carbaryl, are similar to those found in vertebrates.

The mineralization, or complete biodegradation, of an organic molecule in water and soil is almost always a consequence of microbial activity.[32] Carbaryl metabolism by microorganisms in soil proceeds via a predominantly hydrolytic mechanism or a predominantly oxidative mechanism; rarely are the two processes combined as they are in animals. The degradation of carbaryl in soil goes further than in animals, plants, and insects because the bacteria are able to break down the naphthalene ring in the molecule.

When carbaryl is added directly to soil, it appears to follow the same metabolic pattern observed in isolates of the fungus *Fusarium solani*.[2] Two studies that were conducted using ^{14}C-carbonyl carbaryl and 1-naphthyl-^{14}C carbaryl produced hydroxylated metabolites.[33] However, the data suggested that the metabolites are not necessarily conjugated as they are in animals and plants because they could not be extracted with acetone or methanol.

A proposed mechanism of the oxidative breakdown of carbaryl in soil is shown in Figure 1.3.[33,34] This mechanism is based on the following products that the authors were able to identify: 1-naphthol, pyruvate, and catechol.[33,34] The process involves the breakdown of the naphthalene ring that is found in the carbaryl molecule. The metabolism of the naphthalene ring is a known degradation pathway that occurs through mineralization by soil microorganisms.[34]

Figure 1.3. Hypothetical pathway of carbaryl in soil, based on the release of ^{14}C-carbon dioxide from 1-naphthol-^{14}C, carbonyl-^{14}C carbaryl, and 1-naphthyl-^{14}C carbaryl, and a known pathway of naphthalene degradation by soil microbes. Products underlined have been identified as soil metabolites of carbaryl.

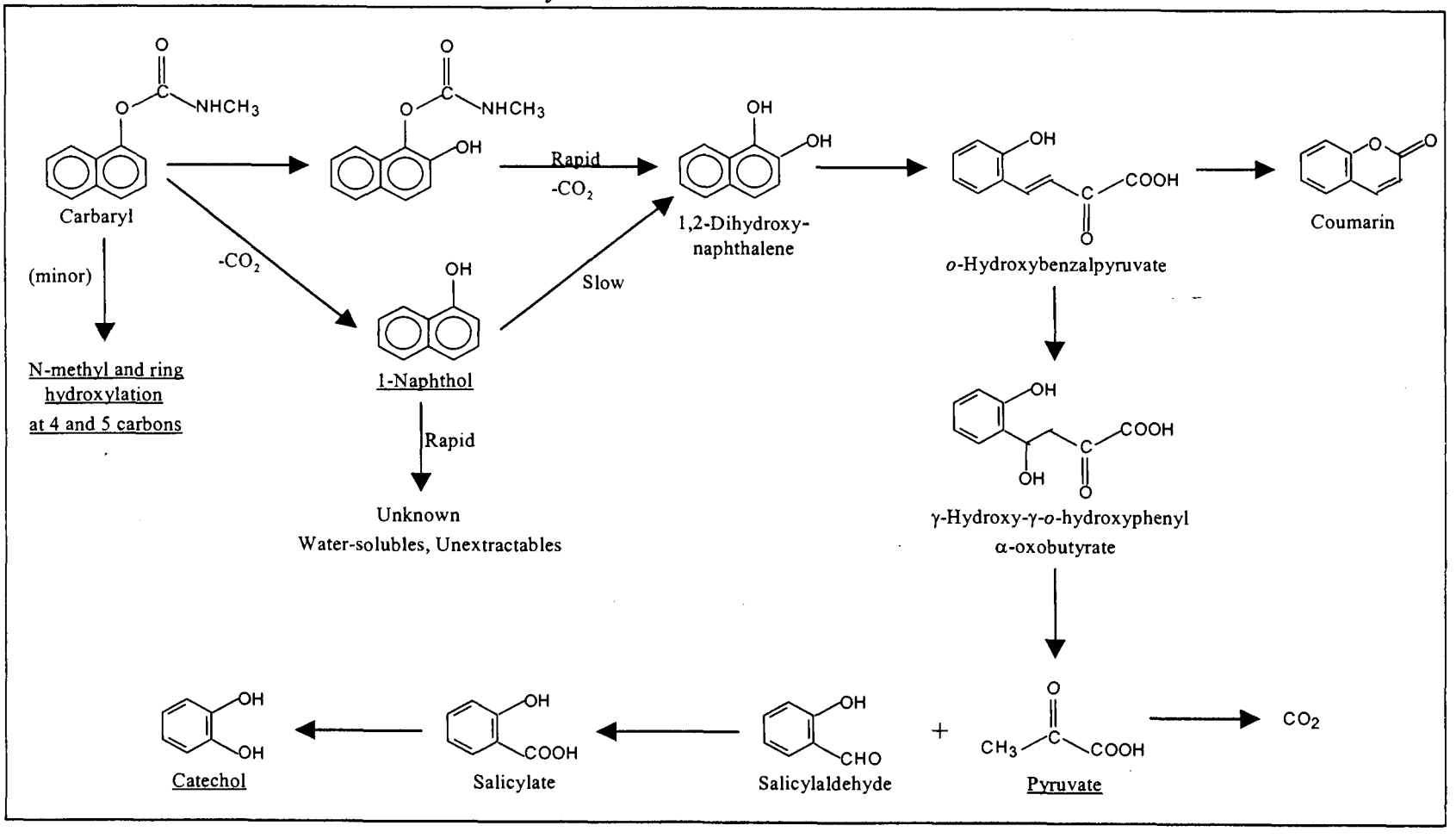

1.2.4. Literature review of relevant investigations

A majority of the research surrounding carbaryl has focused on finding a technique that will efficiently detect the pesticide when it is present in low concentrations. Several instrumental methods have been used for the determination of carbaryl in different media. These methods include HPLC,[35] TLC,[36] fluorimetry,[37] and phosphorimetry.[38] The spectrophotometric methods are usually based on coupling of a diazonium ion with the phenols obtained by hydrolysis of the carbamate in alkaline medium.[39] Additionally, some work has focused on extracting carbaryl from pond and well water. This method involves the use of solid-phase extraction to remove the organic chemical from water.[40]

During the last decade, scientists have focused on trying to decompose carbaryl into less harmful products so that it will not be present in soil and groundwater supplies. One of the first studies in this area looked at the photodegradation of carbaryl, aldicarb, and carbofuran in water.[1] Carbofuran and aldicarb are insecticides that also belong to the carbamate family. De Bertrand and Barceló looked at the effect of the photodegradation rate of these carbamates in different types of water, namely sea water, pond water, and distilled water. These authors also varied the type of lamp (i.e. mercury or xenon arc lamp) used to shine light on their samples.[1] The degradation of carbaryl was also studied in natural waters using fluorimetric methods to study the kinetics of the reaction. González *et al.* found that the hydrolysis rate of carbaryl increased in the presence of a micellar solution under alkaline conditions.[41]

In the most recent years, researchers have focused their attention on using catalysts to speed up the photodegradation of carbaryl. For instance, the photocatalytic degradation of carbaryl in aqueous solutions containing titanium dioxide suspensions has been studied.[16,42] TiO_2 was used in these studies because scientists previously found that in its anatase form, this semiconductor allowed for the complete decomposition and mineralization of several aromatic compounds.[42] Among other interesting results, Peris-Cardells *et al.* found that the degradation of carbaryl decreases as the concentration of the insecticide increases.[42] In the presence of TiO_2 suspensions, Pramauro *et al.* discovered that carbaryl was completely mineralized to CO_2, with nitrate and ammonium ions becoming the nitrogen-containing end products.[16]

The use of catalysts to increase the photodecomposition rate of pesticides has sparked interest in our research group. In particular, zeolites are being used as catalysts for the photodecomposition of carbaryl.[29,43] Zeolites A, X, and mordenite have been used in recent studies. Silver(I) doped in Zeolites A, X, and mordenite led to photodecomposition rates that were 164, 182, and 168 times faster, respectively than when carbaryl was alone in solution.[29] These photodecomposition rates varied slightly depending on the percentage of silver that was loaded onto the zeolite. The photoassisted degradation of carbaryl was also studied using silver and gold dicyanide clusters doped in A-type zeolite.[43] With the $Ag(CN)_2^-$ and the $Au(CN)_2^-$ complexes encapsulated in zeolite A, photodecomposition rates were 40 and 60 times faster, respectively than rates observed with carbaryl alone in solution.

1.3. Natural Organic Matter

Humic substances occur in soil, natural waters, and sediment and arise from the decomposition of plant and animal tissues. The size of the molecules, molecular weight, elemental composition, structure, as well as the number and position of functional groups on the molecules vary, depending on the origin and age of the material.[44] Three fractions, namely humic acids, fulvic acids, and humin are discussed in most of the literature on humic substances. Specifically, the natural organic matter (NOM) samples that were used in this investigation are made of a combination of humic and fulvic acids. Humic and fulvic acids, are naturally occurring, biogenic, heterogeneous organic substances that can generally be characterized as being brown in color.[45]

1.3.1. Humic acids

Humic acids comprise the fraction of natural organic matter that are not soluble in water under acidic conditions (i.e., below a pH of 2), but become increasingly soluble at higher pH.[45] On average, the amount of carbon found in humic acids ranges from 51-62 %, while oxygen levels range from 31% to 36%.[46] In general, scientists have discovered that humic acids contain more hydrogen, carbon, nitrogen, and sulfur and less oxygen than fulvic acids.[44]

Although the exact structure of humic acids is still a mystery, scientists have proposed some hypothetical structures. A "type" molecule for humic acid is made of micelles of a polymeric nature, of which the basic structure is an aromatic ring of the di- or trihydroxy-phenyl type bridged by –O–, –NH–, –N=, –S–, and other functional

groups that contain both free OH groups and the double linkages of quinones.[45] In its natural state, the type molecule contains attached protein and carbohydrate residues. Figure 1.4 shows a structure of humic acid that was proposed by Stevenson.[45,47] The structure shows the presence of aromatic rings of the di- and trihydroxybenzene type, the presence of the quinone group, as well as the occurrence of carbohydrate and protein residues.

Figure 1.4. Hypothetical structure of humic acid showing free and bound phenolic OH groups, quinone structures, oxygens as bridge units, and carboxyls variously placed on the aromatic ring.

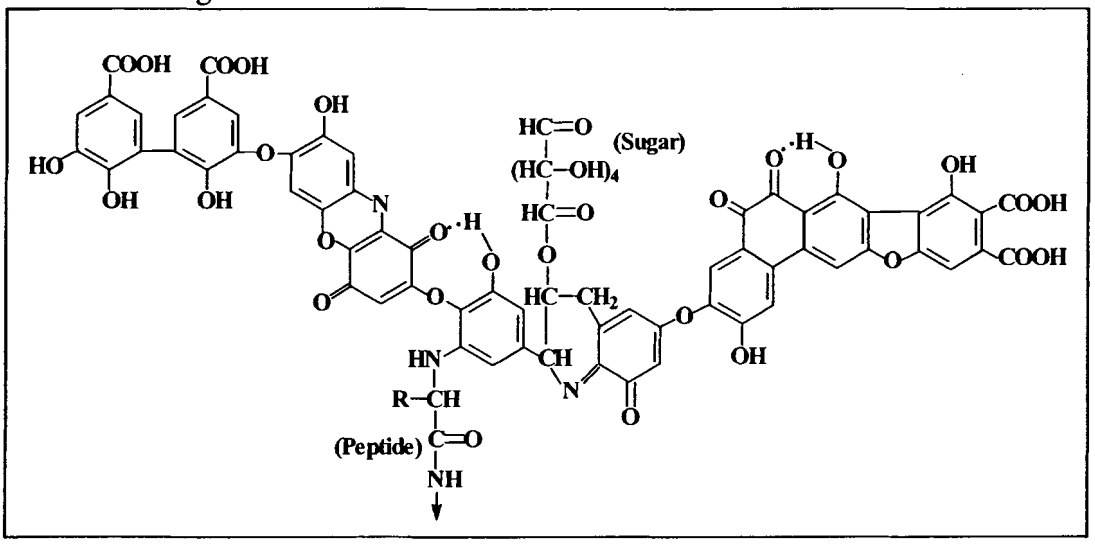

1.3.2. Fulvic acids

While humic acids are soluble under alkaline conditions, fulvic acids are soluble under both acidic and basic conditions. Fulvic acids also comprise the smaller fractions of humic substances, having a molecular weight that ranges from hundreds of daltons to a few thousand daltons.[48] In contrast to humic acids, the low-molecular-

weight fulvic acids contain higher oxygen levels (45 to 49%) but lower carbon contents (43 to 47%).[45,46]

The structures of fulvic acids are slightly more aliphatic and less aromatic than humic acids; and fulvic acids contain more carboxylic acid, phenolic and ketonic functional groups.[44] Like humic acids, the exact structure of fulvic acids is still unknown simply because so many different types of fragments exist together making it difficult to separate and characterize individual molecules. For example, the elemental composition and the hypothetical molecular weight of about 2500 daltons led to an average molecular formula of $C_{100}H_{109}O_{69}N_2$ for a fulvic acid sample that was isolated from aquatic humic material. The important thing to note is that several thousand possible isomers exist for this general formula.[49] Figure 1.5 shows one hypothetical structure of fulvic acids that consists of phenolic and benzenecarboxylic acids held together through hydrogen bonds, forming a polymeric structure having considerable stability.[45,50]

Figure 1.5. Structure of fulvic acid as proposed by Schnitzer and Khan.

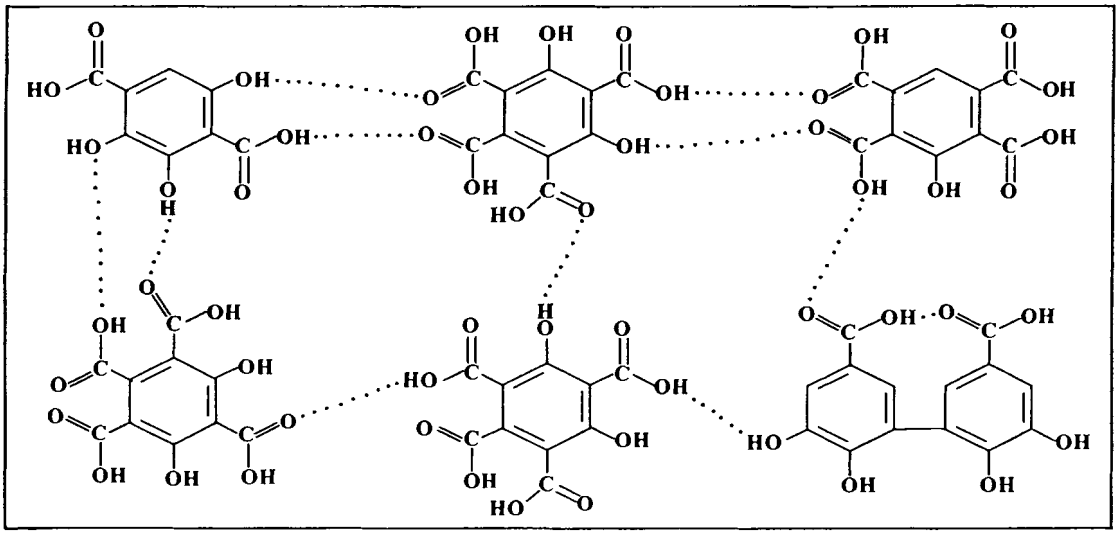

1.3.3. Interaction of pesticides with natural organic matter

Natural organic matter is a very important part of ecological systems and serves many functions, including: (1) retaining micronutrients like Fe, B, and Mo that are essential for plant growth, (2) playing an important role in nitrogen and sulfur cycling, (3) maintaining the water regime of a soil environment, (4) being necessary for the development of a soil structure that is suitable for plant growth, and (5) acting as a pH buffer to prevent rapid fluctuations in soil acidity.[46] Despite all these beneficial roles that natural organic matter has in the environment, it poses some problems when we consider its interaction with organic pollutants such as pesticides and toxic metal ions like mercury(II).[51]

In recent years, it has become very important for scientists to understand the fate of pesticides in the environment so that their application can be regulated. As a result, one problem that needs to be investigated in depth is the interaction of pesticides with natural organic matter. It is well known that the interaction between dissolved organic matter and pesticides not only changes the solubility and mobility of pesticides in the environment, but also affects the photodegradation and hydrolysis rate of the pesticides.[52] The major problems that researchers face in pursuing this type of investigation is that scientists have been unable to characterize the molecular structure of natural organic matter (NOM), so NOM that is taken from a river may interact differently with the pesticide of interest than NOM that is taken from a lake.

The way in which natural organic matter typically affects the fate of pesticides in the environment is through a binding interaction. In particular, binding interactions between pesticides and dissolved organic matter have been shown to decrease the rate

of microbial degradation of the pesticides.[53] Additionally, when sunlight is absorbed by the colored natural organic matter in surface waters, a rich variety of photochemical reactions ensue. The resulting excited states of the NOM and reactive transients that are produced participate in energy transfer, electron transfer, and free radical reactions that affect the fate of aquatic contaminants like pesticides.[54] Reports in this area provide data revealing that dissolved organic matter can either enhance or inhibit the rate of pesticide photolysis.[53]

1.4. Zeolites

The term "zeolite" was first used by Cronstedt in 1756 as a name for an extraordinary aluminosilicate mineral that seemed to boil when heated.[55] Since that discovery, 41 naturally occurring zeolites have been found. Zeolites that exist naturally in the environment can be found in the cavities of basaltic volcanic rock, in metamorphic rocks, and in sedimentary tuff deposits.[55] Despite the numerous naturally occurring zeolites that have been discovered, recently scientists have been focusing their attention on synthesizing zeolites for industrial purposes or to understand more about their chemistry.

Zeolites are microporous crystalline solids with well-defined pore and channel structures. Generally they contain silicon (Si), aluminum (Al), and oxygen (O) in their framework and cations, water, and/or other molecules within their pores. The framework of each zeolite is constructed from tetrahedral building blocks, TO_4, where T is a tetrahedrally coordinated atom (i.e. Si or Al). The tetrahedral building blocks, $(SiO_4)^{4-}$ and $(AlO_4)^{5-}$, by themselves have formal charges of –4 and –5, respectively.

However, in the zeolite framework the O/T ratio is 2, making the SiO_4 units neutral because each oxygen atom forms a bridge between two tetrahedral atoms.[56] The net formal charge on the AlO_4 units is –1, causing the zeolite framework to be negatively charged. This negative charge is typically balanced by metal cations or protons that are not actually a part of the zeolite framework. Figure 1.6 depicts how the tetrahedral building blocks are put together to form the zeolite framework.[56]

Figure 1.6. The building blocks that are common to every zeolite, and the way they are combined to create the zeolite framework.

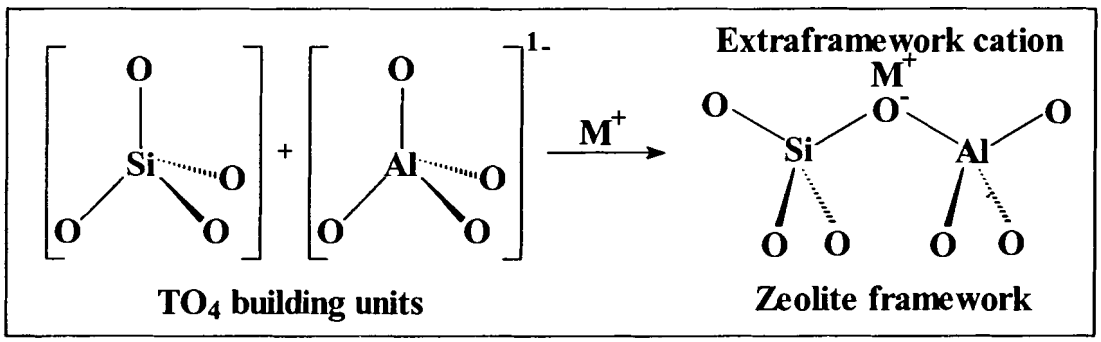

1.4.1. Zeolite Y

Zeolite Y exhibits the faujasite (FAU) structure. Its aluminosilicate framework may be viewed as an assemblage of sodalite cavities that are composed of $(Si_{24-x}Al_xO_{48})^{x-}$ where $0 < x < 12$, which are arranged in space like the carbon atoms in diamond.[57] The sodalite units in Zeolite Y have T_d symmetry, whereas in others such as zeolite A the sodalite units exhibit O_h symmetry.[57]

In general, the different types of zeolites vary in their silicon to aluminum ratio, their pore diameter, and the number of oxygen atoms at the pore-opening ring of

the zeolite. For zeolite Y, the Si/Al ratios generally vary from 1.5-6.0, the number of oxygens at the pore-opening of the zeolite is 12, and the pore diameter ranges from about 8-10 Å.[29] Zeolite Y has a three dimensional pore structure with pores running perpendicular to each other in the x, y, and z planes.[55] Figure 1.7 shows the framework structure of a sodalite unit and the structure of zeolite Y.[57] It is interesting to see how the geometry of the sodalite unit changes when it becomes incorporated into this particular zeolite framework.

1.4.2. Silver clusters doped in zeolite Y

Studies within the past twenty years show that silver ions have an incredible tendency to bond to one another, forming silver clusters.[58-61] Silver is of interest to scientists because it is isostructural with nickel, palladium, and platinum.[62] These three transition metals have been extensively studied because of their pronounced catalytic activity.[57] By studying silver clusters in different media, the hope is to learn more about silver agglomeration, which plays a very important role in heterogeneous catalysis.[63] For example, scientists have already discovered that catalysts containing both Ag^0 and Ag^+ are important in partial oxidation processes such as the formation of ethylene oxide from ethylene and oxygen.[62]

Silver clusters can be synthesized in the cages and channels of zeolites by vacuum dehydration, by reduction using reducing agents, by ion exchange procedures, and by using γ- or X-ray irradiation.[57] Some different types of silver clusters that have been impregnated in zeolite Y include: Ag_2^+, Ag_2, Ag_3^{2+}, and Ag_6^{4+}.[57,64-66] Silver ions and silver atoms have also been found in the channels of zeolite Y. In particular, the

photostimulated luminescence and optical absorption of silver atoms and silver clusters in zeolite Y have been studied extensively.[67,68] Ag exchanged zeolite Y has been used to photoreduce methyl-viologen to its π-cation radicals.[65]

Figure 1.7. (a) The structure of a sodalite cavity and (b) the framework structure of zeolite Y.

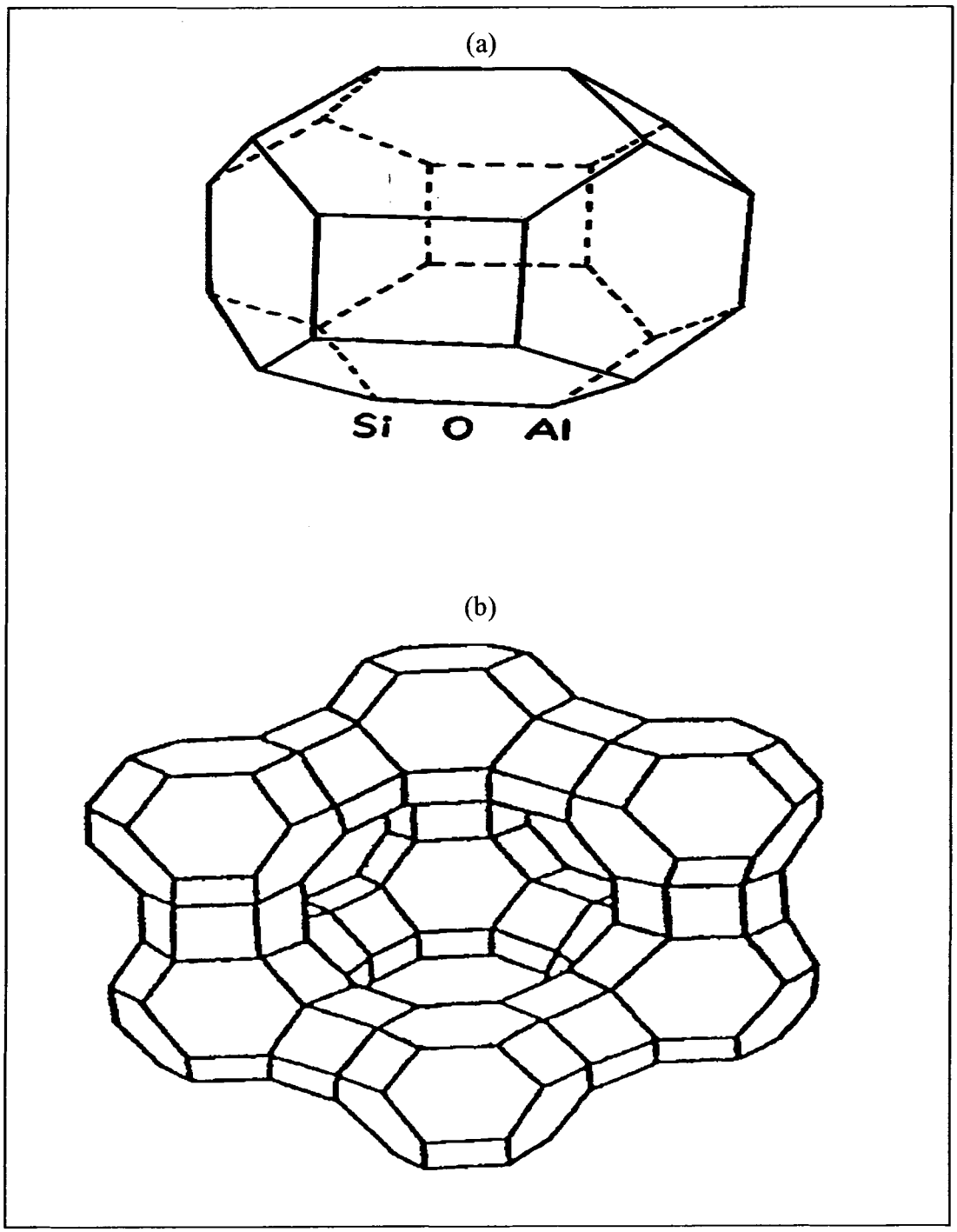

Chapter 2

MATERIALS AND METHODS

2.1. Chemicals and Samples

Carbaryl (1-naphthyl, N-methylcarbamate) crystals having a 99% purity were purchased from Chem Service. HPLC grade methanol and acetone as well as α-naphthol were purchased from Aldrich Chemical Company. Silver nitrate, potassium chromate, and ammonium hydroxide were purchased from Fischer Scientific. Phthalic acid and NaY zeolite were donated by Dr. Rachel N. Austin, Department of Chemistry, Bates College. All chemicals were used as received without further purification.

One sample of Suwannee River natural organic matter (NOM) was purchased from the International Humic Substances Society (IHSS) in 2000 and donated by Dr. Christopher S. Cronan, Department of Biological Sciences, The University of Maine. From this point on, this natural organic matter sample will be referred to as NOM-2000. A second sample of Suwannee River NOM was purchased from the International Humic Substances Society in 2001 and also donated by Dr. Rachel N. Austin. This natural organic matter sample will be referred to as NOM-2001 throughout the remainder of this thesis. The Suwannee River NOM samples had the same reference number (1N101), so according to the IHSS the two samples were collected from the Suwannee River in Georgia at the same time and from the same area. The elemental composition of the dry Suwannee River NOM is: 48.8 %C; 3.9 %H; 39.7 %O; 1.02 %N; 0.60 %S; 0.02 %P; and 7.0 % Ash.

2.2. Preparation of the Silver Doped Zeolite Catalyst

The silver exchanged Y zeolite was prepared via ion-exchange of 1 gram of zeolite Y with a solution of $Ag(NH_3)_2^+$ at 70°C for about 48 hours. The aqueous solution of $Ag(NH_3)_2^+$ was prepared by reacting silver nitrate with aqueous ammonia. To begin with, a known mass of silver nitrate was placed in an erlenmeyer flask, then enough water was added to dissolve the solid silver nitrate crystals. Upon adding a small amount of ammonia to the flask, a brown precipitate appears, and then more ammonia is added very slowly until the precipitate completely dissolves and a clear solution of $Ag(NH_3)_2^+$ results. The amount of water and ammonia that are used in each preparation vary depending on the mass of silver nitrate that is originally placed in the flask. Four samples of AgY zeolite were prepared using different masses of silver nitrate to create samples that contained various silver loadings. Table 2.1 gives the masses of zeolite Y and silver nitrate that were used in each preparation. After the 48-hour period, the AgY zeolite samples were filtered, washed three times with distilled water and then dried in an oven at 100°C for 24 hours. The samples were then transferred to small vials and stored in the dark.

The amount of silver loaded on each zeolite was determined using the technique of inductively coupled plasma-atomic emission spectroscopy (ICP-AES). These experiments were conducted by Dr. Rachel N. Austin and the samples were then sent to Gailbraith for a follow-up analysis of the silver loadings.

Table 2.1. The masses of silver nitrate and zeolite Y that were used to prepare each AgY zeolite catalyst.

Sample	Mass of Zeolite Y (g)	Mass of $AgNO_3$ (g)
AgY #1	1	0.2
AgY #2	1	1
AgY #3	1	5
AgY #4	1	10

2.3. Irradiation of Carbaryl and Related Samples

30 ppm or 3 ppm solutions of carbaryl and 3 ppm solutions of α-naphthol were prepared in a 10:90 v:v% methanol:water mixture. All solutions were prepared immediately before beginning the irradiation experiments. All irradiations were performed with a model M-57 mid-range UV lamp from VWR Scientific, Inc. The lamp emits a narrow band of irradiation at 300 nm. Each sample was irradiated in quartz test tubes that have an inside diameter of 12.5 mm, a length of 10 mm, and were 1 mm thick. Only one test tube was irradiated at a time. The distance from the light source to the sample tube was 2 cm and the test tubes were placed parallel to the light source.

Each irradiation experiment was performed at a pH of 6.5 and at room temperature using a total of 5 ml of solution. The 30 ppm solutions of carbaryl were irradiated in the absence and presence of 10 mg of each AgY zeolite catalyst. The 3 ppm solutions of carbaryl and α-naphthol were irradiated in the absence and presence of the Suwannee River natural organic matter samples and in the presence of both the catalyst and the NOM samples. At various time intervals, the test tubes were removed

from the UV light, 2 ml of solution was pipetted into a cuvette, and measurements of the luminescence intensity of the pesticide were recorded. The solution was then pipetted back into the original test tube and the sample was put back under the UV lamp.

2.4. Description of Binding Experiments

Binding experiments between carbaryl and the NOM samples were conducted in order to investigate the interaction between the luminophore and the quencher. In all cases, the NOM samples were used as the quencher, and the luminophore was carbaryl. In addition, one binding experiment was conducted in which carbaryl was the luminophore and α-naphthol was the quencher, to see the interaction between the pesticide and its major degradation product.

In general, the experiments were conducted in the following manner. The concentration of the quencher was typically varied from 0 ppm to a maximum of 95 ppm. The concentration of the luminophore was held constant at 3 ppm for all experiments. At the beginning of each experimental run, the absorption spectrum of the quencher was scanned and the absorbance was recorded at the maximum excitation and emission wavelengths of the luminophore. Then the luminescence of the quencher was scanned at the excitation wavelength of the luminophore. After that, the luminophore was added and the solution was stirred and allowed to incubate for 5 minutes so that the luminophore and the quencher could interact in solution. After the 5-minute period, the luminescence spectrum of the luminophore/quencher solution was taken. This process was repeated for different concentrations of the quencher. If

the quencher was interacting with the luminophore, the luminescence intensity of the luminophore gradually decreased as the concentration of the quencher increased.

To analyze the data in the luminescence binding experiments, a series of steps were followed to collect the necessary data and process it. To begin with, for each experiment in the laboratory the following data was collected: (1) the concentration of the quencher before and after adding the luminophore, (2) the luminescence intensity of the quencher at its maximum wavelength of emission, (3) the absorbance of the quencher at its maximum wavelength of emission, (4) the absorbance of the quencher at the luminophore's wavelength of excitation, and (5) the luminescence intensity of the luminophore/quencher system at the quencher's maximum wavelength of emission.

The data analysis involved creating linear plots of the absorbance data versus the concentration of the quencher, and a quadratic regression of the luminescence data gathered for the quencher. The best-fit lines for these plots provide equations that are used to produce a Stern-Volmer plot. The slope of a Stern-Volmer plot gives the quantitative value of the binding interaction between the luminophore and the quencher. The technique used for the data analysis of the luminescence binding experiments was performed using the same method that was explained in detail by Feng Fang.[46]

2.5. Ultrafiltration of the Natural Organic Matter Sample

Ultrafiltration is a method of separating macromolecules according to molecular size, by filtering samples under an applied hydrostatic pressure through a

membrane. Solute molecules within the molecular weight cutoff of the membrane pass through the micropores of the membrane along with the solvent.[46] The Suwannee River natural organic matter sample that was donated by Dr. Chris Cronan was separated into different molecular weight fractions using the technique of ultrafiltration. This technique is based on a pressure differential across a semipermeable membrane so the separation occurs quite rapidly. Effective molecular filtration processing requires equipment and operating conditions, which minimize the concentration of solutes at the surface of the membrane and avoid formation of a gel layer which can obstruct the membrane, called concentration polarization.

A stirred cell pressurized system was employed in which the retentate is in continuous contact with the molecular filtration membrane and the solution is continuously stirred. The stirred cells use a magnetic rotary stir bar positioned above the surface of the membrane to keep the solution in motion and control concentration polarization. The solution of NOM was pressurized from 10 to 70 psi by a nitrogen gas flow, while in contact with a supported semipermeable membrane. Species below the membrane molecular weight cut-off emerge as ultrafiltrate, and the retained species are progressively concentrated on the pressurized side of the membrane.

Two molecular filtration membranes were used for the ultrafiltration process. The first membrane was labeled YM1 and allowed particles with a molecular weight that was less than 1,000 g/mole to pass through it. The second membrane was labeled YM10 and filtered particles that had a molecular weight (MW) less than 10,000 g/mole. Using these two filtration membranes, three different MW fractions were produced in the following manner. First, the YM10 membrane was placed in the

stirred cell and 250 ml of a 30 ppm solution of the NOM sample was added to the cell. About 25 ml of the retentate was retained and diluted to a volume of 50 ml. This solution contained MW fractions that were greater than 10,000 g/mole. The 225 ml of filtrate that passed through the membrane was collected. After the cell was rinsed thoroughly, the YM1 membrane was placed in it, and the 225 ml of filtrate was added to the cell. About 200 ml of filtrate from the YM1 membrane was collected. This filtrate contained molecules with a molecular weight that was less than 1,000 g/mole. The third NOM fraction was obtained from the solution that was retained by the YM1 membrane. This retained portion had molecules with molecular weights between 1,000 and 10,000 g/mole.

When the ultrafiltration procedures were complete, experiments to determine the concentration of dissolved organic carbon (DOC) in each fraction were conducted by Dr. Chris Cronan. A model 700 Total Organic Carbon Analyzer (detection limit: 0.5 ppm) from O.I. Corporation, College Station, Texas, was used to conduct the quantify the DOC in each sample.

2.6. Spectroscopic Measurements

Solid state luminescence measurements of the silver(I)-exchanged zeolite Y catalysts were recorded at various temperatures within a range of 77 – 298 K. For the luminescence measurements, the samples were first mixed with a small amount of KBr and made into a pellet. The pellet was then attached to a copper surface using a mixture of vacuum grease and copper powder. The copper plate was then attached to the transfer tube for the low temperature experiments. The shroud that covered the

sample had two perpendicular quartz windows, which allowed the incident beam of light to reach the sample and the emitted light beam to reach the detector. Liquid nitrogen was used for the low temperature experiments. The stainless steel transfer tube allowed the sample to reach the temperature of liquid nitrogen with the help of a vacuum pump and a flow of nitrogen gas.

After the carbaryl or α-naphthol solutions were irradiated for a certain increment of time, about 2 ml of the solution was transferred into a quartz cuvette. If the solution contained 10 mg of the AgY zeolite, the test tube was removed from the lamp, and the sample was centrifuged for 2 minutes prior to placing 2 ml of the sample into the quartz cuvette. Emission spectra were monitored at the excitation wavelengths that produced the maximum emission intensity of carbaryl or α-naphthol, as a function of irradiation time.

2.7. Instrumentation

All photoluminescence spectra were obtained using a model QM-1 luminescence spectrometer from Photon Technologies International, (PTI). The instrument is equipped with excitation and emission monochromators, a 75-watt xenon arc lamp, and a photomultiplier tube serving as the detector. The excitation and emission slits widths varied depending on the experiment that was being conducted. Quartz fluorometry cuvettes having a pathlength of 1 cm were used for all luminescence and absorption measurements. Excitation, emission, and synchronous scan-luminescence spectra were obtained using this instrument. Excitation and

synchronous-scan spectra were corrected for variations in lamp intensity using the quantum counter rhodamine B.

UV-vis absorption measurements were obtained using a DU-640 spectrophotometer from Beckman Instruments, Inc. The luminescence spectra of the AgY zeolites were recorded as a function of temperature, using liquid nitrogen as the coolant in a model LT-3-110 Heli-Tran cryogenic liquid transfer system equipped with a temperature controller. Experiments to determine the amount of silver that was doped in zeolite Y were performed by Dr. Rachel N. Austin using the coupled technique of ICP-AES. The ICP that was used was a Perkin-Elmer Optima with a rf power of 1300 W. The samples were then sent to Gailbraith for a follow-up analysis.

GC-MS measurements were made on a Hewlett Packard 5890 Gas Chromatograph with a Hewlett Packard MSD 5970 serving as the detector. A 30 x 0.25 mm DB-5MS GC column from J & W Scientific was used for the GC measurements. The components of various samples were separated using the following parameters: the injector temperature was set at 200°C, and the detector temperature was 300°C. The initial oven temperature was set at 100°C and held constant for 5 minutes. After the initial 5 minutes, the temperature was ramped to 180°C at a rate of 20°C/min and held constant for 5 minutes. Finally, the temperature was ramped to 250°C at a rate of 20°C/min and held constant for 5 minutes. Helium was used as the carrier gas with flow rate of 1 ml/min. All samples were filtered prior to being injected into the GC-MS to remove any particles that would potentially obstruct the GC column.

Chapter 3

THE PHOTODEGRADATION OF CARBARYL AND THE INFLUENCE OF NATURAL ORGANIC MATTER ON THE REACTION

3.1. Spectroscopic Analysis of Carbaryl

3.1.1. Emission and excitation spectra

In luminescence spectroscopy a molecular sample is illuminated by light from an external source, and light is emitted at a wavelength that is generally longer than the wavelength of excitation. Substances which display significant luminescence usually possess delocalized electrons present in conjugated double bonds, such as aromatic rings.[46] Carbaryl molecules have aromatic rings and display strong luminescence properties. As a result, the photodegradation of this molecule is easy to study using the technique of luminescence spectroscopy.

To determine where to excite the carbaryl molecule to produce the maximum luminescence intensity, a 3 ppm solution of carbaryl was placed in a quartz cuvette and the absorption spectrum of the solution was taken. The absorption spectrum of the solution of carbaryl showed a maximum absorbance at 276 nm with an extinction coefficient of $1.530 \pm 0.006 \times 10^3$ L mol^{-1} cm^{-1} (see Figure 3.1 top). Since the absorption spectrum usually mirrors the excitation spectrum in luminescence spectroscopy (for most cases), an excitation wavelength of 276 nm was used to excite the carbaryl solution and observe the emission spectrum. Upon excitation at 276 nm, carbaryl displays a broad luminescence band that spans from 300–400 nm and has maxima at 323 and 333 nm (Figure 3.1), which are longer in wavelength than 276 nm.

Figure 3.1. Absorption, excitation, and emission spectra of a 3 ppm solution of carbaryl.

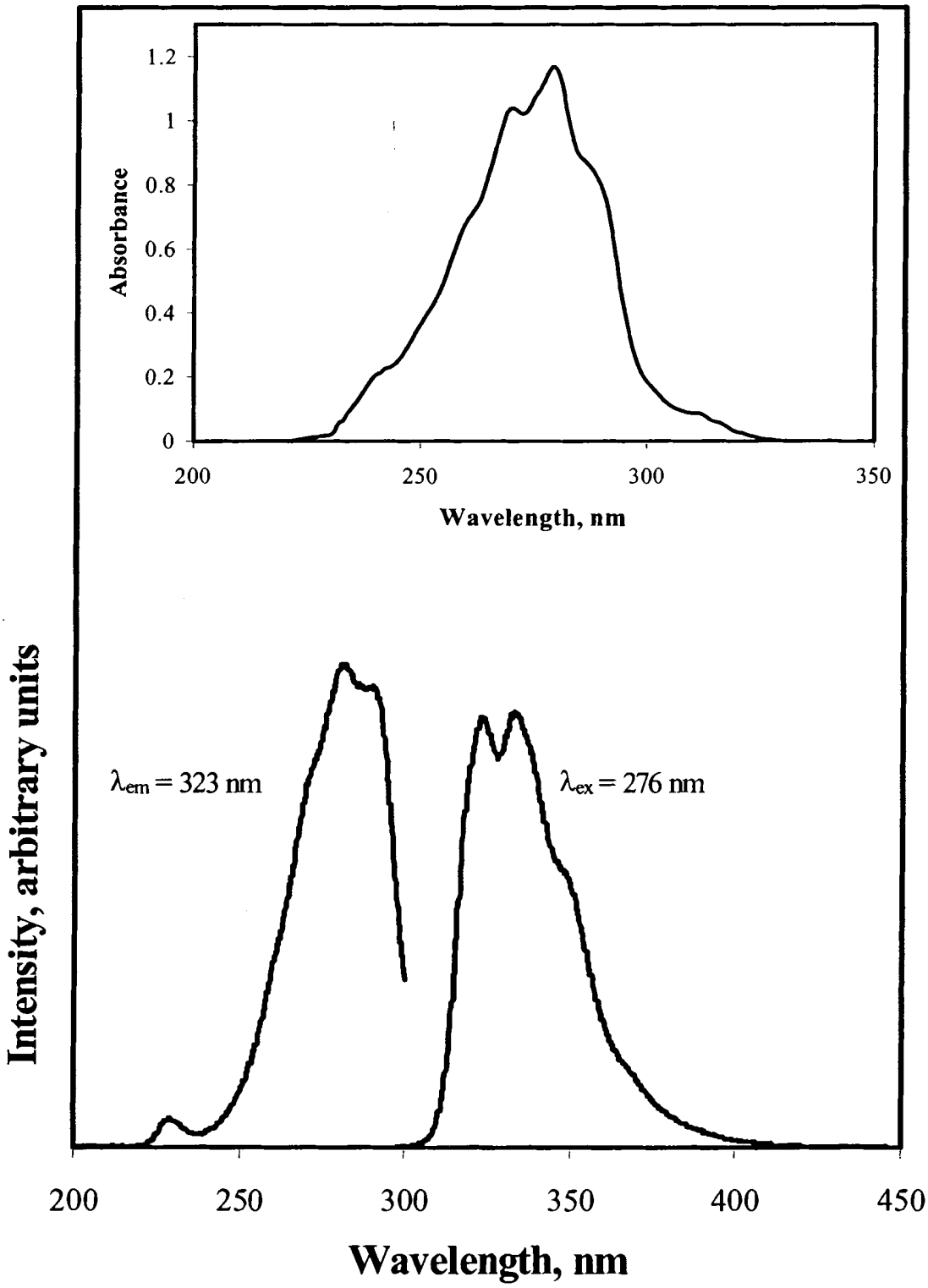

3.1.2. Synchronous-scan luminescence spectra

Synchronous-scan luminescence spectroscopy (SSLS) is a very valuable technique typically used to investigate the presence of several different luminophores in a mixture. The technique involves scanning the excitation and emission wavelength drives of a luminescence spectrometer simultaneously, while maintaining a constant wavelength difference between them.[69] As a result, synchronous-scan luminescence spectra have more well-defined peaks compared to emission and excitation spectra.

Figure 3.2 shows the synchronous-scan luminescence spectra (SSLS) of a 3 ppm solution of carbaryl as a function of $\Delta\lambda$. The most intense SSLS peak is found by subtracting the wavelength of maximum intensity of the excitation band from the wavelength of maximum intensity of the emission band. This calculation allows for the determination of the delta lambda that will be most suited to probe carbaryl. Doing this calculation we have: 333–276 nm, and 323–276 nm; giving us two delta lambda's since there are two maxima in the emission spectrum of carbaryl. Therefore, the two wavelength differences that should give the most intense SSLS band for carbaryl are $\Delta\lambda = 57$ nm and $\Delta\lambda = 47$ nm.

Figure 3.2 displays the spectra of the two primary wavelength differences that need to be probed for carbaryl, along with a few others. In this figure, the peak maxima are slightly shifted in each SSLS, however they become more intense at $\Delta\lambda =$ 57 and 47 nm. As shown in the figure, the SSLS bands appear between 325-350 nm, with peak maxima at 323, 333, 340, and 350 nm. As a result, the technique of synchronous-scan luminescence spectroscopy is another method that can be used to characterize a solution of carbaryl.

Figure 3.2. SSLS of a 3 ppm solution of carbaryl as a function of Δλ.

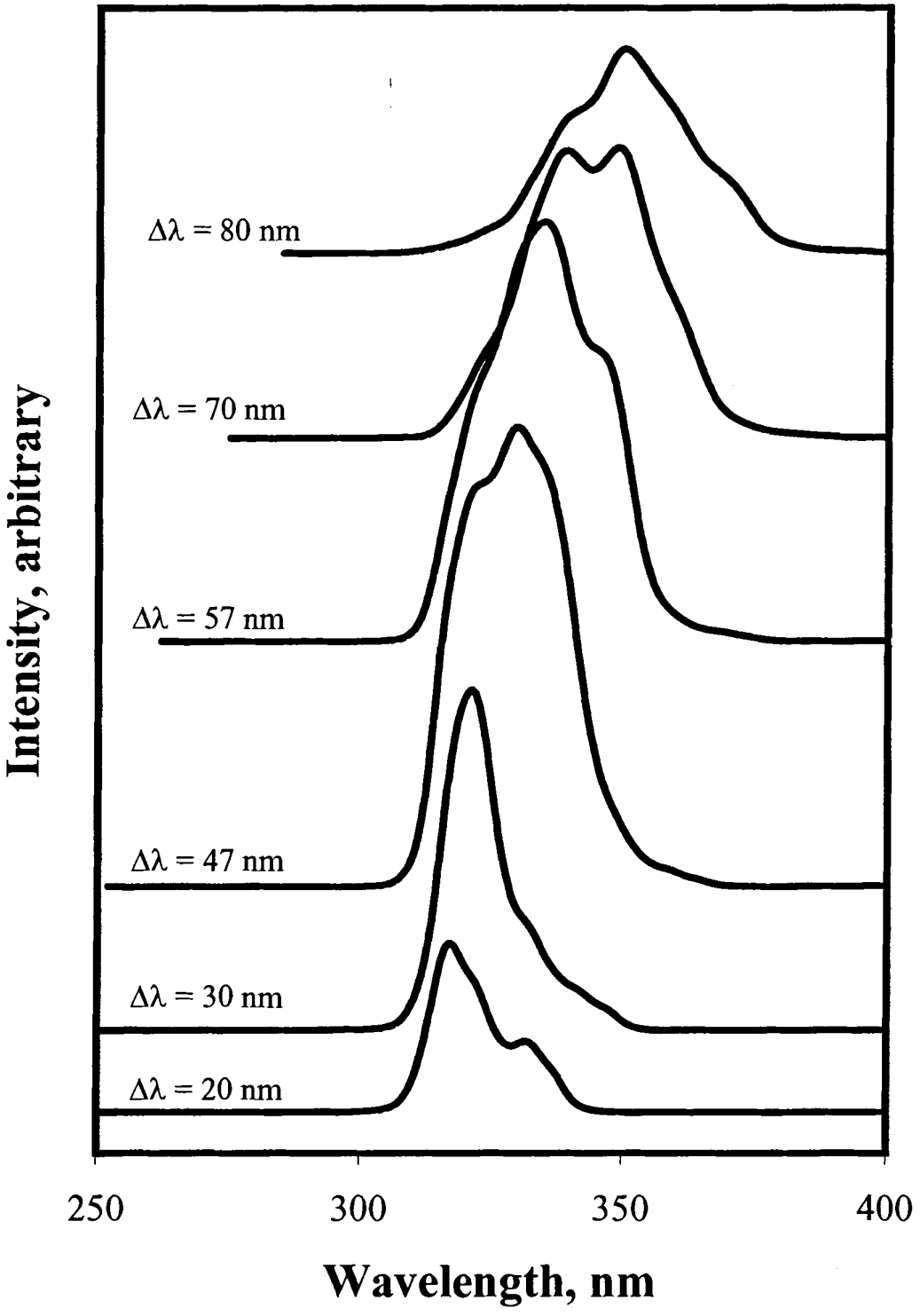

3.2. Spectroscopic Analysis of the Natural Organic Matter Samples

3.2.1. Emission and excitation spectra

The emission and excitation profiles of both Suwannee River natural organic matter samples were taken to investigate the similarities and/or differences between the two samples. Aqueous solutions having a concentration of 30 ppm were made for this set of experiments. For the Suwannee River NOM-2000 and NOM-2001 samples, the absorption spectrum revealed maxima at 333 and 345 nm, respectively. Upon exciting each solution at the maximum absorption intensity, broad luminescence bands between 360-600 nm appear with peak maxima at 437 and 455 nm, respectively. Figure 3.3 shows the excitation and emission spectra of the NOM-2000 and NOM-2001 samples.

From the luminescence data that is shown in Figure 3.3, it appeared that the two Suwannee River NOM samples that were purchased from the same company and collected from the same river in Georgia, were showing similar characteristics. However, separate experiments were still conducted after this similarity was found, because the samples were purchased a year apart from each other and not enough information was obtained at this point to allow them to be considered the same sample.

3.2.2. Synchronous-scan luminescence spectra

Since the molecular structure of humic and fulvic acids is complex, it becomes a challenge to fully understand the chemical structure of natural organic matter. Fortunately, some methods can be utilized to understand some of the chemical

Figure 3.3. Excitation and emission spectra of the Suwannee River NOM-2000 and NOM-2001 samples.

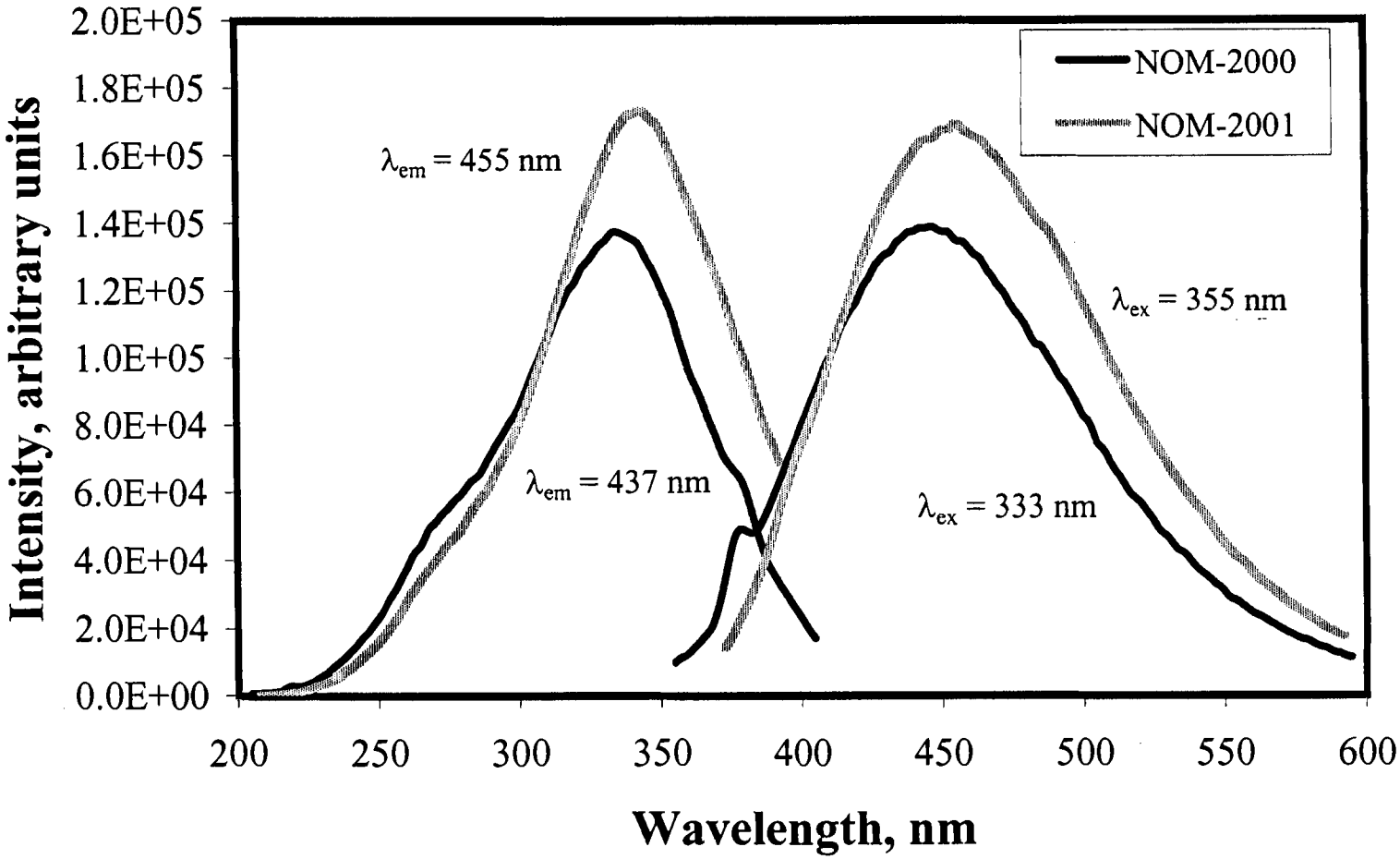

structures and properties of NOM. Synchronous-scan luminescence spectroscopy (SSLS) is one technique available for this purpose, and has revealed some special advantages when dealing with humic substances.[70-72]

The synchronous-scan luminescence spectra of the Suwannee River NOM-2000 and NOM-2001 samples were taken as a function of $\Delta\lambda$. Figures 3.4 and 3.5 show the SSLS of 3 ppm solutions of NOM-2000 and NOM-2001, respectively. The SSLS of NOM-2000 shows several peaks with maxima at 313, 338, 356, 403, 425, and 470 nm; whereas, the NOM-2001 sample displays bands with maxima at 325, 403, 418, 430, and 448 nm as the wavelength difference was varied: $\Delta\lambda$ = 30, 50, 70, and 100 nm.

Unlike the ordinary luminescence spectra (excitation and emission spectra), SSLS show different bands that were distinguished at various $\Delta\lambda$'s which indicate the presence of different luminophores in each NOM sample. The SSLS also shows that the two NOM samples are different. For example, three peaks are observed in the high-energy region between 300-360 nm for NOM-2000; whereas, the NOM-2001 sample shows only one band in this region at 325 nm. Moreover, in comparison to the SSLS of the NOM-2000 sample, NOM-2001 shows more luminescence bands in the low energy region.

It is worth mentioning that not only the number and the energy of the synchronous-scan luminescence bands are different, the relative band intensities were also found to be different. For example, at $\Delta\lambda$ = 30 nm, the SSLS of the NOM-2000 sample shows a unique intense band at 313 nm. This band became weaker for the

SSLS of the NOM-2001 sample with the appearance of another band at lower energy with a maximum at 403 nm (see Figures 3.4 and 3.5).

Since the structure of the NOM is very complicated, it is not easy to analyze the chemical structure of these compounds. However, throughout the past two decades, scientists have tried to assign bands that appear in the luminescence spectrum of humic substances to model molecules. Based on these studies, an effort will be made to assign the peaks seen in Figures 3.4 and 3.5. The SSLS bands that appear with maxima around 313-338 nm are attributed to functional groups of the Suwannee River NOM that are similar to the structure of salicylic acid.[73] Cronan *et al.* also postulated that a peak occurring in the 350-nm range in the SSLS may reflect quantitative differences in the amounts of salicylate-type groups or variations in the carboxyl substitutions of single aromatic rings in the NOM.[73]

Scientists have also hypothesized that at longer wavelengths around 395 and 470 nm, the SSLS peaks were associated with luminophore structures characterized by an increasing number of condensed aromatic rings.[73] The SSLS band that occurred with a maximum at 403 nm could be attributed to a functional group that is similar in structure to 3-hydroxycinnamic acid.[74] The peak at 425 nm was also observed and assigned to a functional group containing 3-hydroxybenzoic acid, while the 470 nm band may be attributed to hydroxy and methoxy coumarins or chromone derivatives.[75] Finally, the observed peak at 448 nm is due to the presence of methyl salicylate or caffeic acid functional moieties.[75]

Figure 3.4. Synchronous-scan luminescence spectra of the Suwannee River NOM-2000 sample, as a function of $\Delta\lambda$.

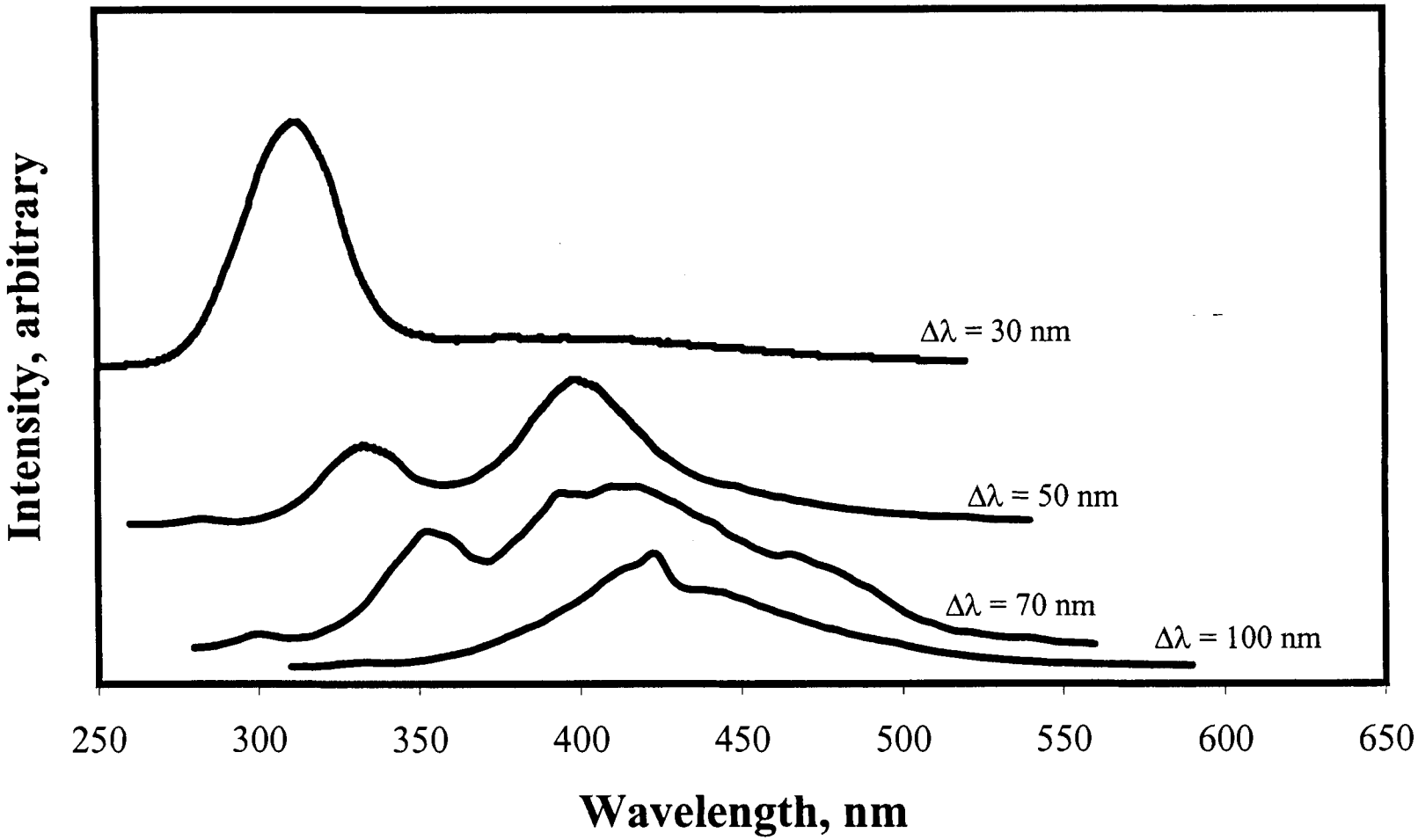

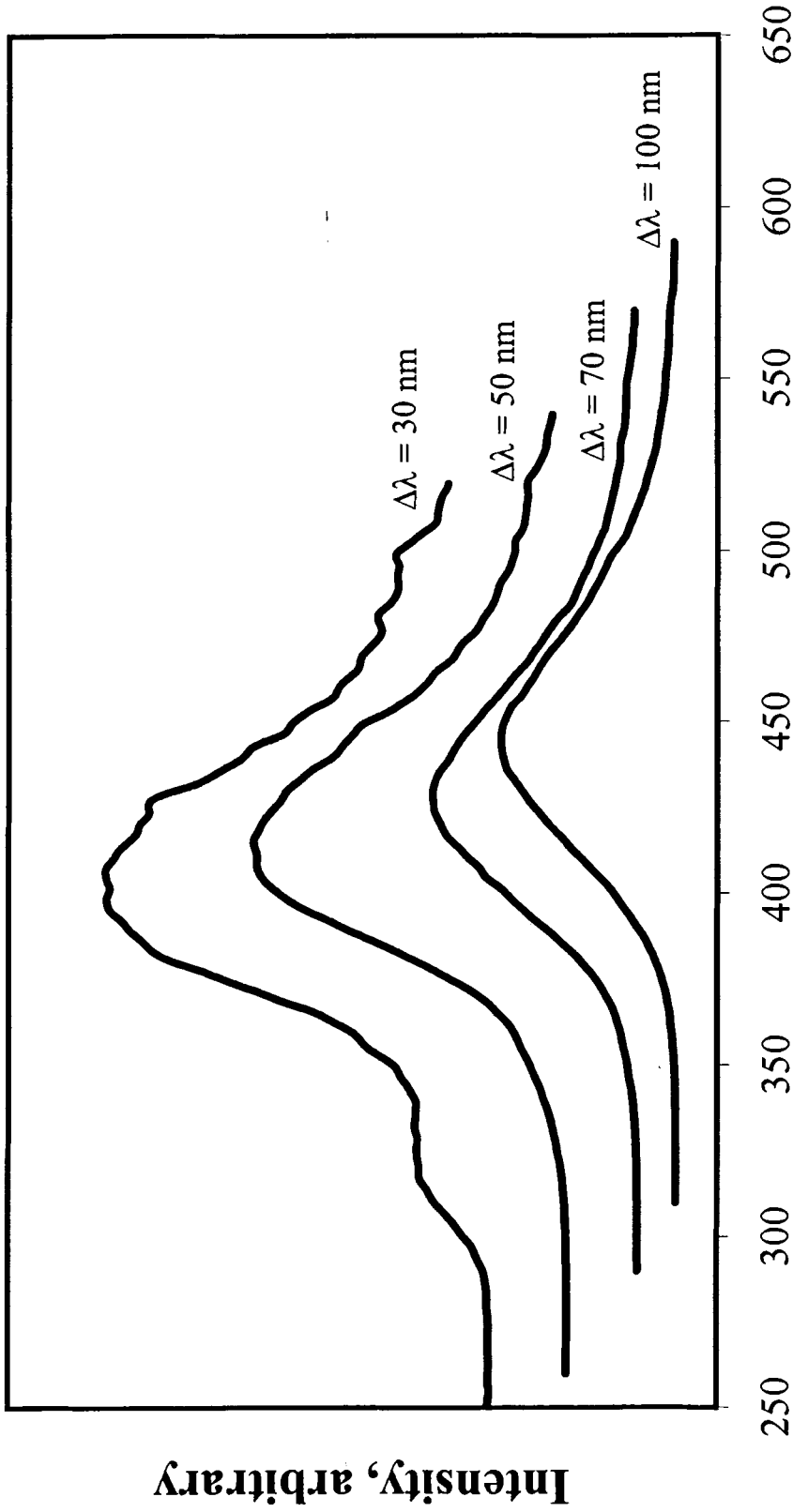

Figure 3.5. Synchronous-scan luminescence spectra of the Suwannee River NOM-2001 sample, as a function of $\Delta\lambda$.

It is important to note that the peak assignments that have been made for both NOM samples only provide an idea of the makeup of the natural organic matter. Although several structures for humic and fulvic acids have been proposed, scientists are still struggling to uncover the mystery behind the actual structure of humic substances.

In addition to the difference found between the synchronous-scan luminescence spectra of the two Suwannee River NOM samples, it was also found that the SSLS depended on concentration. Figure 3.6 shows an example of the SSLS of the Suwannee River NOM-2000 sample at $\Delta\lambda$ = 30 nm and as a function of concentration. This experiment showed that as the concentration of the NOM-2000 increased, the band in the SSLS shifted to lower energy. This shift indicates the presence of longer oligomers forming or molecules in the NOM aggregating together as a result of the increase in concentration.

3.3. Ultrafiltration of the Natural Organic Matter Sample

The Suwannee River NOM-2000 sample was separated into three molecular weight fractions as described in the materials and methods chapter. The first fraction had molecules with a molecular weight (MW) that was less than 1,000 g/mole, the middle fraction had molecules with a MW between 1,000 and 10,000 g/mole, and the largest fraction contained molecules that had a molecular weight greater than 10,000 g/mole. Once the three different fractions were obtained, the amount of dissolved organic carbon (DOC) in each sample was analyzed. Table 3.1 shows the

concentration of DOC that was found to be in each Suwannee River NOM fraction after ultrafiltration was complete.

Table 3.1. The amount of DOC found in each Suwannee River MW fraction.

Size of MW Fraction	Concentration of DOC, mg C L^{-1}
less than 1,000 g $mole^{-1}$	2.05
between 1,000 and 10,000 g $mole^{-1}$	15.7
greater than 10,000 g $mole^{-1}$	50.6

3.4. Binding Interaction of Carbaryl and Natural Organic Matter

In previous studies, natural organic matter has been found to play an important part in pesticide decomposition. Specifically, the presence of NOM has either enhanced or inhibited the rate of photolysis.[53] Before studying the effect the presence of the Suwannee River natural organic matter samples had on the rate of photodecomposition of carbaryl, it is important to look at the binding interaction between the pesticide and the NOM samples.

One hypothesis is that when carbaryl and NOM are in solution together, a certain fraction of the pesticide is bound to the natural organic matter. Scientists believe that this binding may occur through a hydrophobic partitioning mechanism, with polar interactions playing a much smaller role.[53,76] If the bound carbaryl is represented by Ca-NOM, the following equilibrium interaction can be written:

$$Ca + NOM \leftrightarrow Ca\text{-}NOM \qquad (1)$$

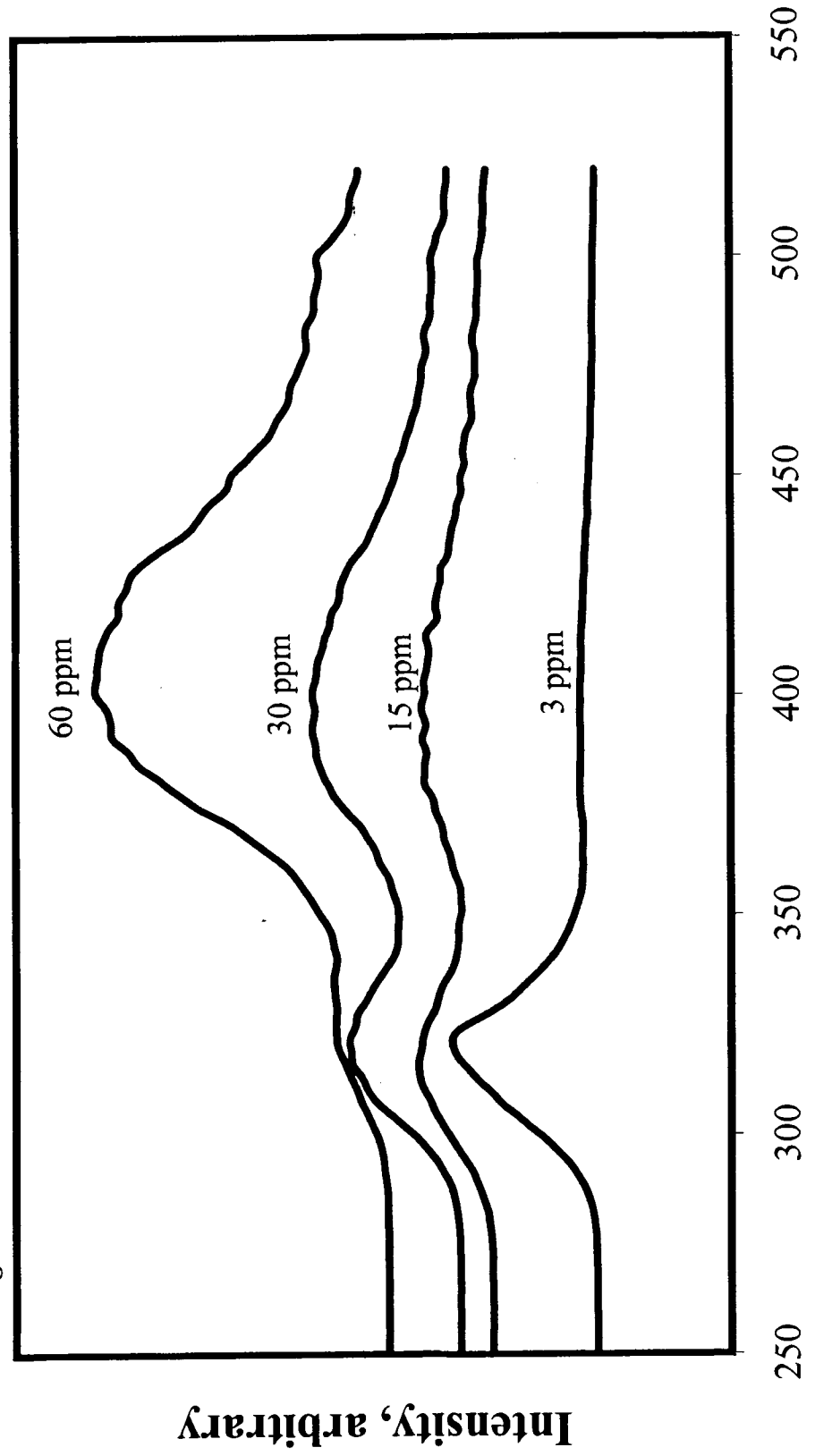

Figure 3.6. SSLS of the Suwannee River NOM-2000 at $\Delta\lambda$ = 30 nm and various concentrations.

The binding constant, K_b, of this reaction can then be found by determining the concentration of each species in Equation 1 and can be calculated using Equation 2:[53]

$$K_b = \frac{[\text{Ca-NOM}]}{[\text{Ca}][\text{NOM}]} \quad (2)$$

Since we are unsure of the concentration of carbaryl bound to NOM in solution, it is more convenient to perform luminescence quenching experiments (or binding experiments) to determine the binding constant. Once K_b has been determined, the percent of carbaryl bound to NOM will be found by performing a simple calculation.

Carbaryl is an excellent compound to use for the binding experiments because of its very strong luminescence peak upon excitation at 276 nm. Typically, as the amount of free carbaryl in solution decreases due to a binding interaction with the natural organic matter, the intensity of its luminescence band also decreases. The magnitude of the reduction in luminescence intensity of the emission band is determined by the NOM concentration and the binding constant as shown below in the Stern-Volmer equation:

$$\frac{L}{L_0} = 1 + K_b[\text{NOM}] \quad (3)$$

In Equation 3, L is the luminescence intensity of the carbaryl/NOM solution, L_0 is the luminescence intensity of carbaryl only, K_b is the binding constant, and [NOM] is the concentration of NOM.[11,53]

Data for the binding experiments were collected as described in Chapter 2 of this thesis and calculations were performed in the same manner as they were done by a former member of Dr. Patterson's research group.[46] Figure 3.7 shows a Stern-Volmer

plot of carbaryl quenched by Suwannee River NOM-2000. To perform this set of binding experiments, the natural organic matter concentration was varied from 0–76 ppm, while the concentration of carbaryl was held constant at 3 ppm. As can be seen in Figure 3.7, a plot of L_0/L vs. concentration of NOM is linear and the slope of the best-fit line yields a binding constant of $7.3 \pm 0.3 \times 10^4$ L kg^{-1}.

Separating the Suwannee River NOM sample into different fractions by ultrafiltration allowed for the determination of the interaction of each molecular weight fraction with carbaryl. As a result, binding experiments were performed on each molecular weight fraction and carbaryl. However, the smallest MW fraction only had a concentration of 2.05 mg C L^{-1}. This concentration was not high enough to perform the binding experiments and obtain adequate results.

Since 134 ml of the smallest MW sample existed, it became clear that some of the solvent (water) needed to be removed from the sample to increase the concentration of DOC in the solution. The solution was put into a round bottom flask, connected to a vacuum line under a pressure of one torr, and a liquid nitrogen trap collected the excess water.

When the procedure was complete, only 34 ml of the solution remained, and the concentration of DOC was immediately measured. The concentration of DOC that was now present in the smallest MW fraction of NOM was 20.2 mg C L^{-1}, so binding experiments on all three NOM fractions were completed successfully. Table 3.2 shows the results of the binding experiments that were performed on the three MW fractions; including the concentration of carbaryl used in the experiments, the range of

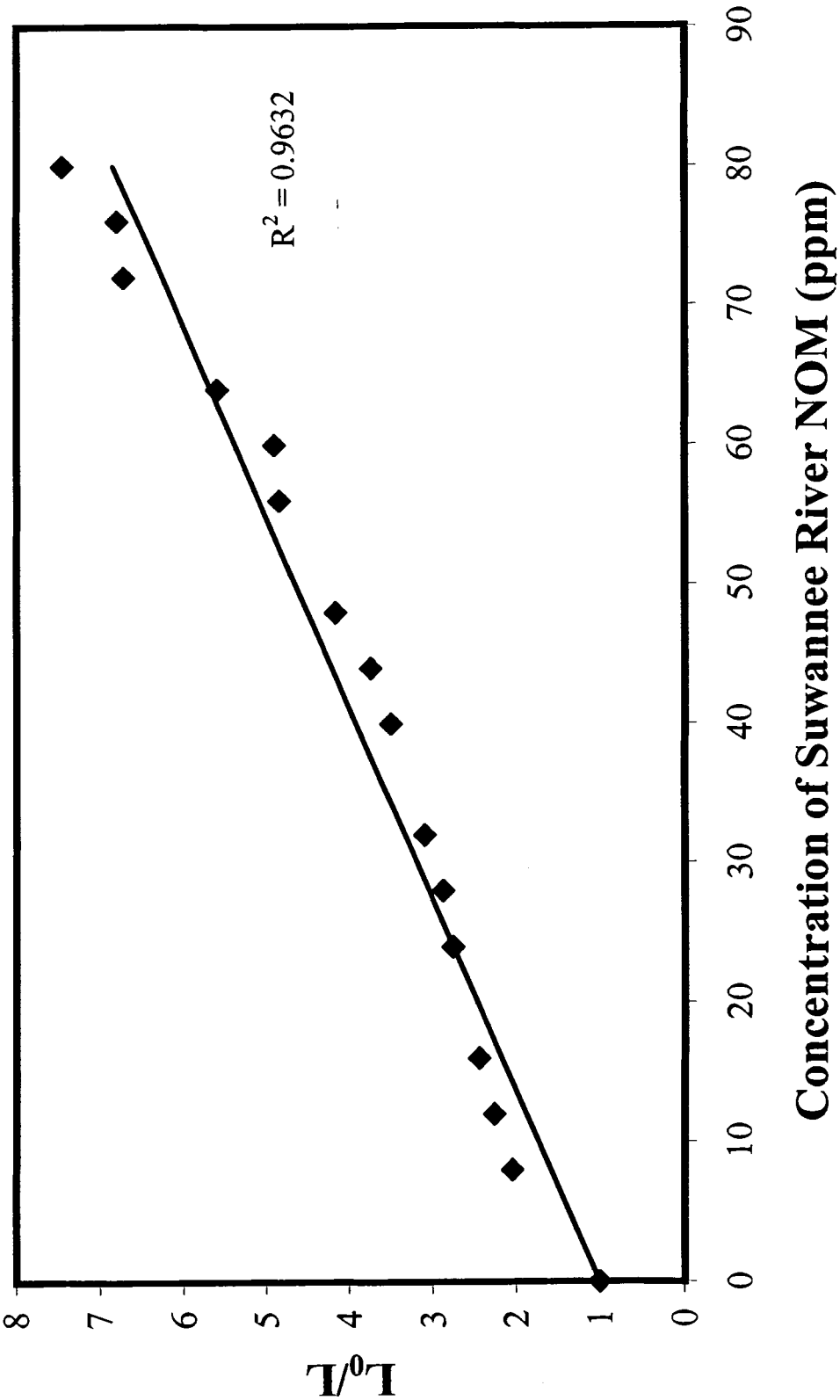

Figure 3.7. Stern-Volmer plot of carbaryl quenched by Suwannee River NOM-2000.

concentrations used for the natural organic matter samples, and the binding constant that was determined from each set of experiments.

Table 3.2. Results of the binding experiments performed with the three Suwannee River MW fractions.

Suwannee River NOM MW fraction	NOM Concentration Range (mg C L^{-1})	[Carbaryl] (ppm)	Binding Constant (L kg^{-1})
< 1,000 g $mole^{-1}$	0 - 16.2	3	$1.29 \pm 0.04 \times 10^4$
1,000 – 10,000 g $mole^{-1}$	0 - 12.6	3	$2.83 \pm 0.06 \times 10^4$
> 10,000 g $mole^{-1}$	0 - 40.5	3	$5.34 \pm 0.09 \times 10^4$

The interaction between the Suwannee River NOM-2001 sample and carbaryl was also studied. The results indicate that the binding constants for the two Suwannee River NOM samples were significantly different. For the Suwannee River NOM-2001, the binding constant was found to be $3.04 \pm 0.02 \times 10^4$ L kg^{-1}, which is lower than the observed binding constant for NOM-2000 ($7.3 \pm 0.3 \times 10^4$ L kg^{-1}). The observed difference in the binding strength between carbaryl and the two NOM samples is mainly due to the presence of different bands in the high-energy region. In specific, three bands were observed in the region between 300–350 nm for NOM-2000 while only one band at 325 nm was observed in the SSLS of NOM-2001. The presence of different luminophores in the NOM-2000 provides more active sites that bind to the pesticide carbaryl.

3.5. Photodegradation of Carbaryl in the Presence of NOM

3.5.1. Luminescence study and kinetics of the reaction

The photodegradation of carbaryl alone in solution, as well as in the presence of the Suwannee River NOM samples was studied extensively. To begin with, a 3 ppm solution of carbaryl was irradiated with 300 nm light and at various time intervals; luminescence data were recorded. Figure 3.8 shows an example of the decrease in luminescence intensity of carbaryl as the solution is irradiated with 300 nm light. The change in the luminescence intensity of carbaryl in the presence of 3, 15, and 30 ppm Suwannee River NOM was also used to study the photodegradation reaction.

The decrease in luminescence intensity that was seen during each photodecomposition reaction needed to be used for an analysis of the kinetics of each reaction. Typically, photodecomposition reactions involving pesticides follow first-order kinetics. So a plot of Ln[pesticide] vs. time will yield a straight line with the slope of the line being the rate constant for the reaction.

For the kinetic analysis, the emission intensity of known concentrations of carbaryl were recorded and a calibration curve for the peak area from 300–400 nm of each carbaryl luminescence band as a function of carbaryl concentration was used to identify the carbaryl concentration as a function of the UV irradiation time. These calculations made it possible for a plot of Ln[carbaryl] vs. time to be constructed.

Figure 3.8. The emission spectrum of a 3 ppm solution of carbaryl, as a function of irradiation time: (a) 0, (b) 20, (c) 60, (d) 100, and (e) 140 minutes.

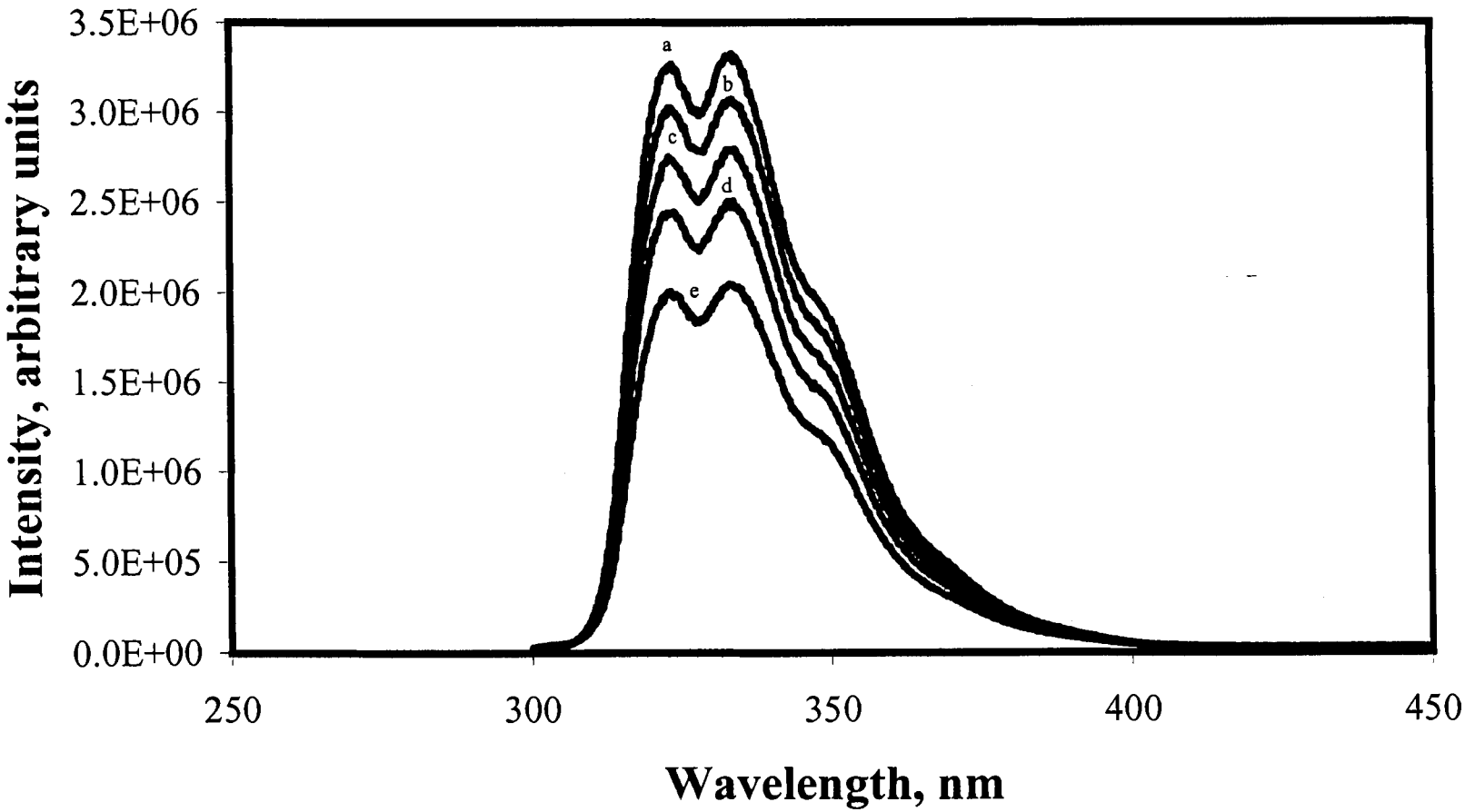

Photodecomposition experiments involving 3 ppm carbaryl in the absence and presence of the Suwannee River NOM-2000 sample were performed. Figure 3.9 shows the kinetic data that resulted from these experiments. In the presence of 3, 15, and 30 ppm concentrations of Suwannee River NOM-2000, the photodecomposition plots are not linear and therefore do not show first-order kinetics. Furthermore, a closer look at the curves reveals that each set of data could actually be fit to two linear best-fit lines as illustrated in Figure 3.10. A summary for the rate constants for each data set is given in Table 3.3. This analysis led to the conclusion that NOM-2000 strongly binds to the products that form from the decomposition of carbaryl.

Table 3.3. First-order rate constants for the photodecomposition of a 3 ppm solution of carbaryl in the presence of various concentrations of the Suwannee River NOM-2000 sample, after each curve was fit to two straight lines.

Concentration of NOM (ppm)	Rate Constants (s^{-1})	
	Slope 1 (Time: 0-70 min)	Slope 2 (Time: ≥ 80 min)
3	$6.04 \pm 0.08 \times 10^{-5}$	$1.764 \pm 0.002 \times 10^{-3}$
15	$5.4 \pm 0.1 \times 10^{-5}$	$4.89 \pm 0.01 \times 10^{-4}$
30	$3.97 \pm 0.09 \times 10^{-5}$	$5.25 \pm 0.07 \times 10^{-4}$

Figure 3.9. Photodecomposition of 3 ppm carbaryl in the presence and absence of the Suwannee River NOM-2000 sample: (a) carbaryl only, (b) carbaryl + 3 ppm NOM, (c) carbaryl + 15 ppm NOM, (d) carbaryl + 30 ppm NOM.

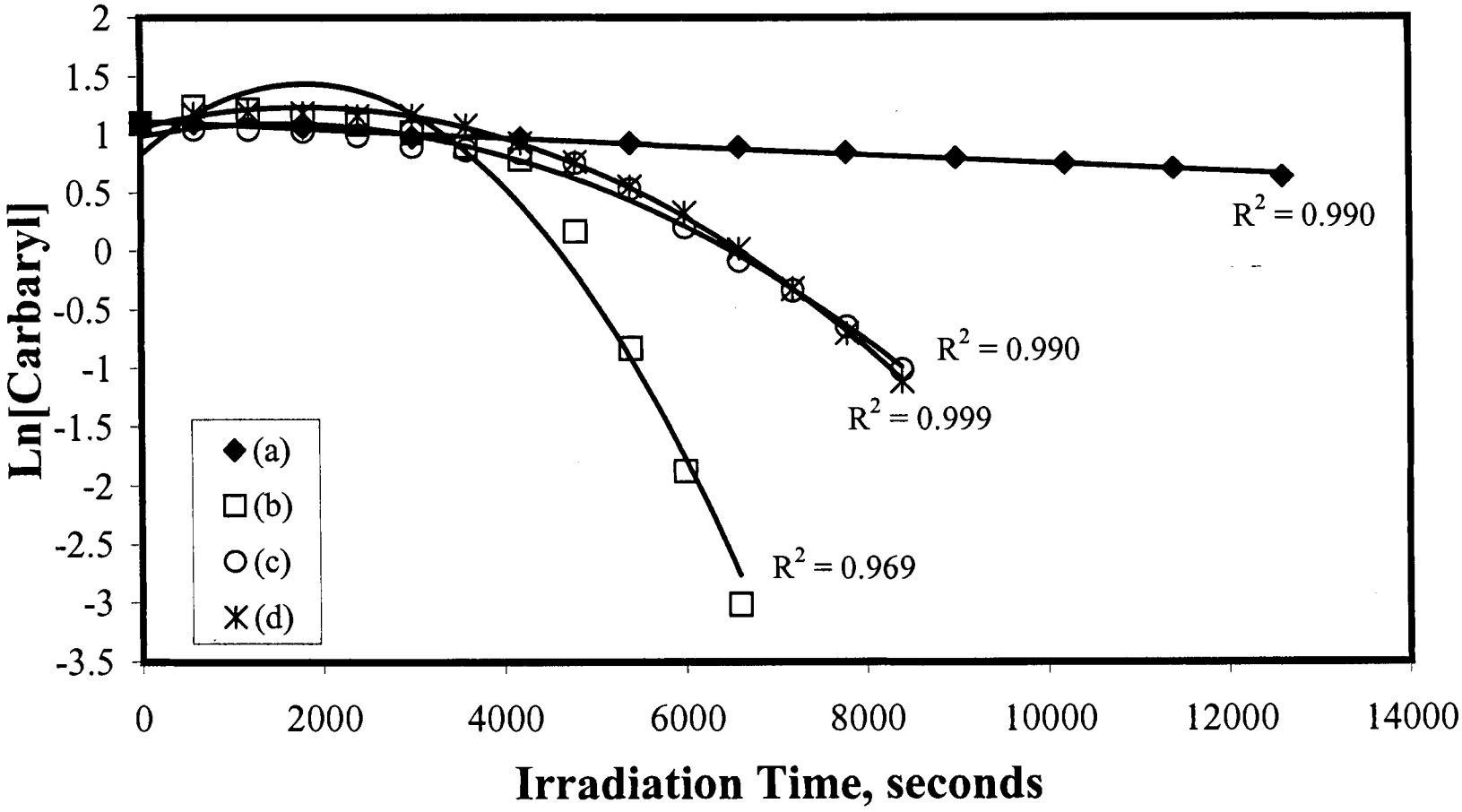

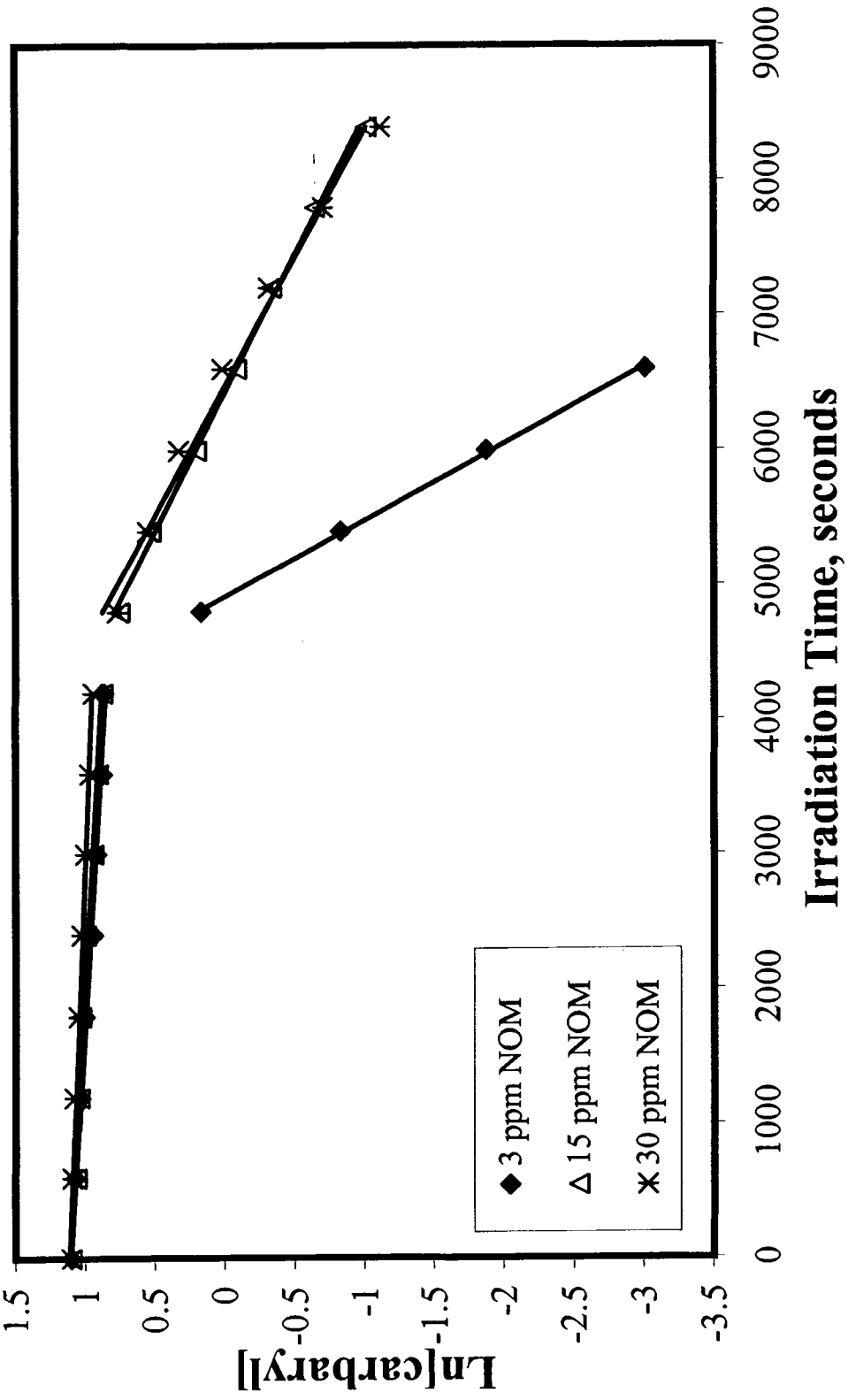

Figure 3.10. Photodecomposition of a 3 ppm carbaryl in the presence of the Suwannee River NOM-2000 sample with each data set fit to two linear best-fit lines.

A final look at Figures 3.9 and 3.10 revealed that the kinetic data shows an increase in the photodecomposition rate of carbaryl in the presence of Suwannee River NOM. The 3 ppm NOM concentration had the largest rate enhancement, and as the concentration increases, the rate enhancement appears to decrease. Based on these results, in the presence of NOM-2000 concentrations below 3 ppm, the rate enhancement would reach a maximum. Photodecomposition experiments in the presence of the three Suwannee River molecular weight fractions also revealed data that fit to a polynomial regression rather than a linear regression analysis.

At this point, a comparison needed to be made between the way the two natural organic matter samples affected the photodecomposition of the widely used pesticide, carbaryl. Figure 3.11 shows the result of experiments conducted in the presence of Suwannee River NOM-2001. The figure indicates that the photodecomposition of a 3 ppm solution of carbaryl follows first-order kinetics because a plot of Ln[carbaryl] versus time is linear.

To begin with, one major difference between the NOM samples is that the Suwannee River NOM-2001 did not alter the kinetics of the photodegradation reaction while NOM-2000 did. Instead, even when 30 ppm of the Suwannee River NOM was present in the solution, carbaryl still degraded via first-order kinetics. In addition, 3 and 15 ppm concentrations of the NOM-2001 sample decreased the rate of photodegradation of carbaryl, while a 30 ppm concentration of the NOM enhanced the photodegradation rate of carbaryl. Table 3.4 shows the rate constants for the photodegradation of carbaryl in the presence and absence of NOM-2001.

Figure 3.11. Photodecomposition of 3 ppm carbaryl in the presence and absence of the Suwannee River NOM-2001 sample: (a) carbaryl only, (b) carbaryl + 3 ppm NOM, (c) carbaryl + 15 ppm NOM, (d) carbaryl + 30 ppm NOM.

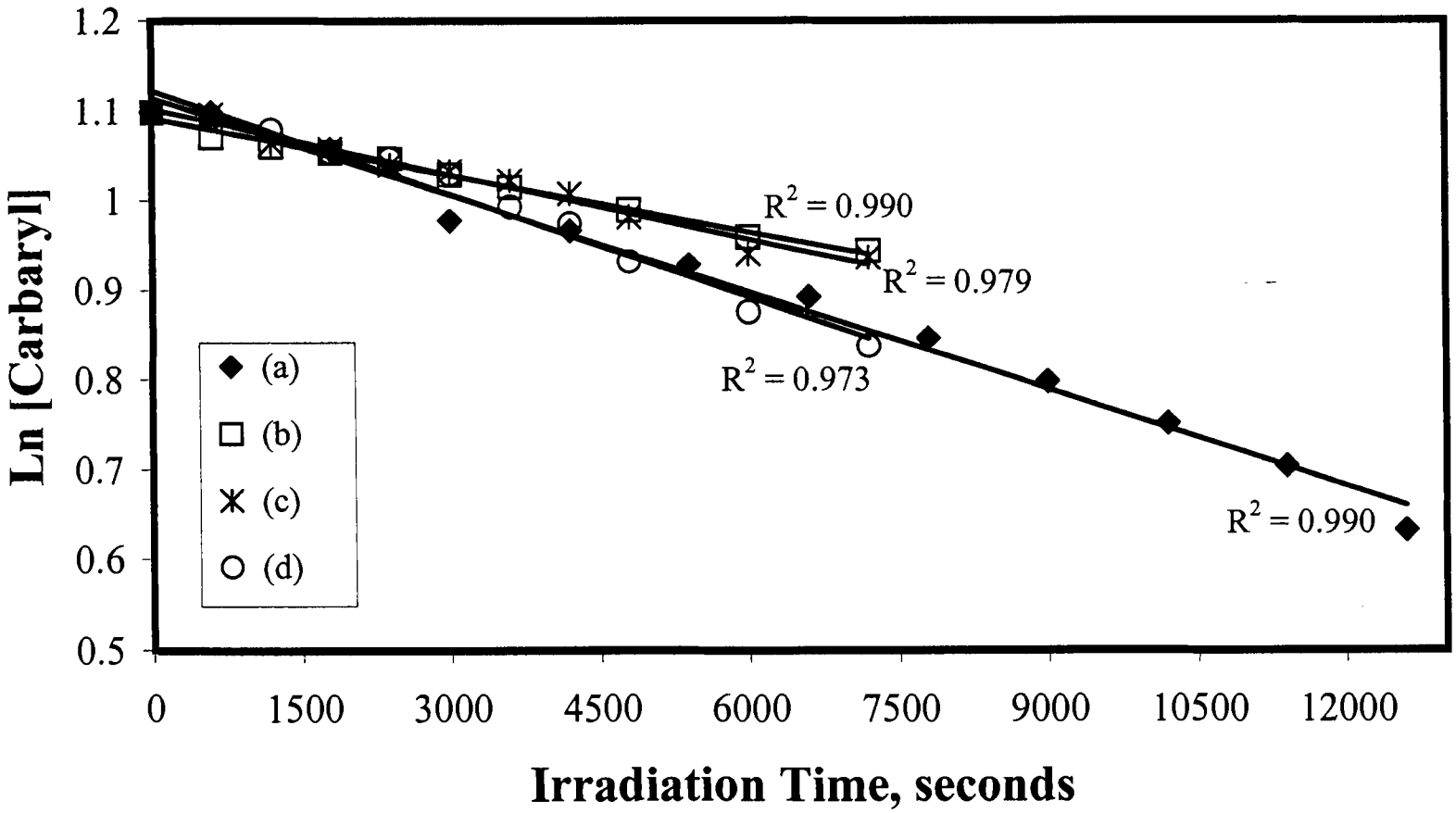

Table 3.4. Rate constants for the photodecomposition of a 3 ppm solution of carbaryl in the presence and absence of the Suwannee River NOM-2001 sample.

	Concentration of NOM			
	0 ppm	3 ppm	15 ppm	30 ppm
Rate Constant (s^{-1})	$3.61 \pm 0.04 \times 10^{-5}$	$2.11 \pm 0.02 \times 10^{-5}$	$2.42 \pm 0.05 \times 10^{-5}$	$3.84 \pm 0.09 \times 10^{-5}$

3.5.2. Analysis of the influence of natural organic matter on the reaction

The influence of Suwannee River natural organic matter on the photodegradation of carbaryl appears to be rather significant, since results show that the two samples have different effects on the reaction rate, and the presence of one sample seems to change the mechanism of the reaction. As a result of these findings and the binding constants for each sample that were found previously, it becomes important to look at the approximate amount of NOM that is bound to carbaryl.

To show the effect of the binding interaction on the photolysis rate constant, one can examine the rate constant data as it relates to the percent of the bound carbaryl in solution. The percentage of bound pesticide is calculated using the binding constant and the NOM concentration:[53]

$$\% \text{ bound} = \frac{(K_b[\text{NOM}])}{(1 + K_b[\text{NOM}])} \times 100 \qquad (4)$$

For example, at a concentration of 3 ppm, the Suwannee River NOM-2000 bound 18.0 ± 0.8% of the total carbaryl concentration, while the NOM-2001 sample bound only 8.36 ± 0.06% of the total carbaryl in solution. Table 3.5 displays the amount of

pesticide that is bound to each Suwannee River NOM sample at the three different concentrations of NOM that were used in the kinetic experiments.

Table 3.5. Percentages of a 3 ppm solution of carbaryl that was bound to different concentrations of the two Suwannee River NOM samples.

Year NOM Purchased	Concentration of NOM		
	3 ppm	15 ppm	30 ppm
2000	18.0 ± 0.8%	52 ± 2%	69 ± 3%
2001	8.36 ± 0.06%	31.3 ± 0.2%	47.7 ± 0.3%

Despite the analysis of the binding interaction between carbaryl and the NOM samples, it is still not clear how the NOM-carbaryl binding controls the photolysis rate effects. This problem occurs mostly because the NOM samples taken from the same river in Georgia have different effects on the photodegradation of carbaryl. As was seen previously, in one case a small amount of the Suwannee River NOM sample enhanced the photodecomposition rate of carbaryl, while a small amount of the other NOM sample seemed to slow down the photodegradation rate. These differences increase the complexity of discovering a theoretical mechanism that can explain the photodegradation reaction in the presence of different Suwannee River NOM samples.

3.5.3. Influence of α-naphthol on the photodecomposition reaction

In previous studies, α-naphthol was found to be the first intermediate and major product in both hydrolysis and photodegradation reactions involving

carbaryl.[18,27,29,33-34] By studying the photodegradation of α-naphthol in the presence and absence of the Suwannee River NOM samples and the influence of the presence of this intermediate on the photodegradation of carbaryl, the hope is to shed some light on the influence of NOM on the breakdown of carbaryl.

To begin with, it was important to discover whether α-naphthol actually shows luminescence upon excitation at a specific wavelength, before performing more complex experiments involving this intermediate. A 3 ppm solution of α-naphthol was made and the absorption spectrum of the compound was taken. The absorption spectrum revealed a maximum at 323 nm with an extinction coefficient of 3.672 ± 0.008 x 10^3 L mol^{-1} cm^{-1}. Upon excitation at 323 nm, a broad luminescence band was seen with a maximum intensity at 462 nm. The excitation spectrum of α-naphthol was then probed by fixing the emission monochromator at 462 nm and scanning the excitation monochromator from 200–400 nm. Figure 3.12 shows the absorption, excitation, and emission spectra of α-naphthol.

It became clear that by following the decrease in the peak area of the luminescence band as a function of the irradiation time, the photodegradation of α-naphthol in solution could be studied. It is important to note that the emission spectrum of α-naphthol appears at lower energy than that for carbaryl; therefore, the luminescence of α-naphthol does not interfere with that of carbaryl. As a result, experiments that looked at the photodecomposition of a 3 ppm solution of α-naphthol in the absence and presence of the Suwannee River NOM samples were completed.

Figure 3.12. Absorption, excitation, and emission spectra of a 3 ppm solution of α-naphthol.

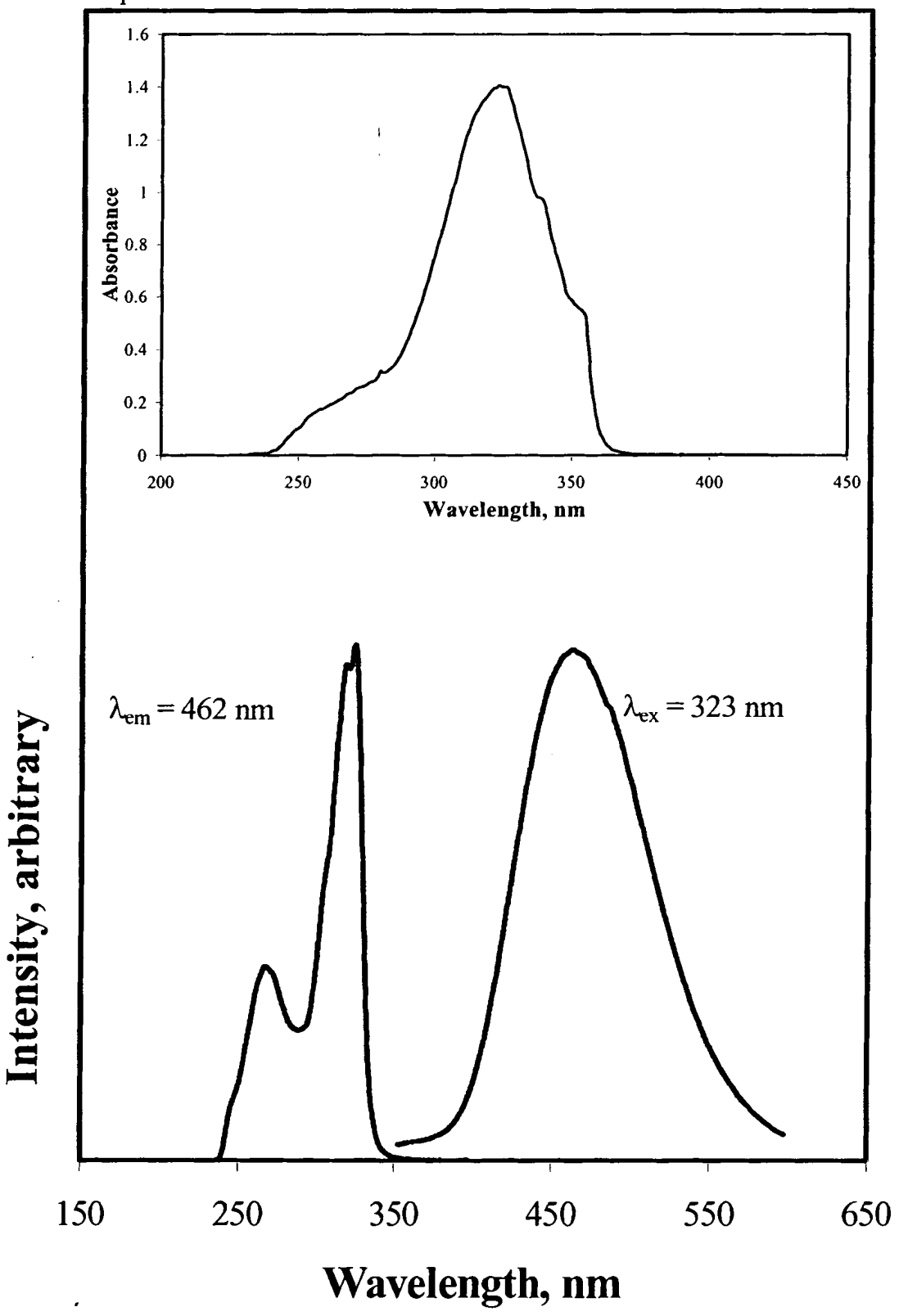

For comparison, the photodegradation of α-naphthol was performed in the presence of the Suwannee River NOM-2000 and NOM-2001 sample. Table 3.6 summarizes the rate constants that were found for the photodegradation of α-naphthol in the absence and presence of the Suwannee River NOM samples. Figure 3.13 shows the photodegradation of α-naphthol in the presence of NOM-2001. It is important to point out that the photodecomposition of α-naphthol in the presence of the NOM-2001 sample follows first order kinetics, but the influence of the natural organic matter on the reaction is different from the influence it had on the photodegradation of carbaryl. As is shown in Table 3.6, a small amount of NOM-2001 present in the reaction appears to slightly enhance the photodecomposition rate of α-naphthol, whereas a large amount inhibits the photodegradation of the intermediate. This trend is opposite from the one seen for carbaryl in the presence of NOM-2001.

Table 3.6. Rate constants in s^{-1} for the photodecomposition of 3 ppm α-naphthol in the presence of various concentrations of Suwannee River NOM.

Year NOM Purchased	Concentration of Suwannee River NOM			
	0 ppm	3 ppm	15 ppm	30 ppm
2000	$1.74 \pm 0.02 \times 10^{-3}$	$1.87 \pm 0.04 \times 10^{-3}$	$4.65 \pm 0.03 \times 10^{-4}$	$5.41 \pm 0.02 \times 10^{-4}$
2001	$1.74 \pm 0.02 \times 10^{-3}$	$1.936 \pm 0.008 \times 10^{-3}$	$1.05 \pm 0.02 \times 10^{-3}$	$7.1 \pm 0.2 \times 10^{-4}$

Figure 3.13. Photodegradation of 3 ppm α-naphthol in the absence and presence of the Suwannee River NOM-2001 sample: (a) 0 ppm NOM, (b) 3 ppm NOM, (c) 15 ppm NOM, (d) 30 ppm NOM.

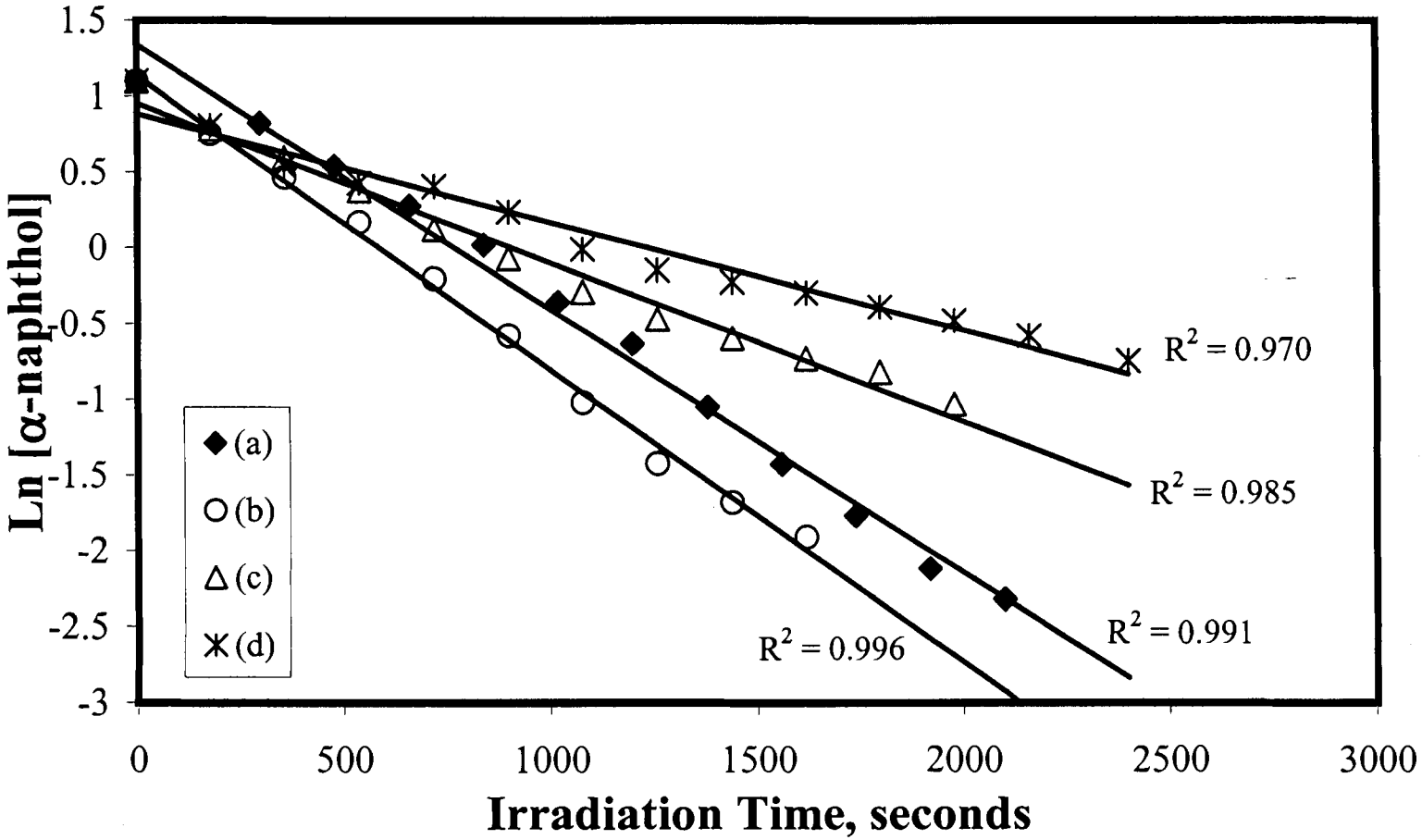

Comparing the photodecomposition rate constants of carbaryl in the presence of NOM-2000 (Figure 3.10 and Table 3.3) with the rate constants of the α-naphthol-NOM-2000 reaction indicate that the observed rate constants for the second curves in the carbaryl-NOM system are similar to the rate constants that were obtained for α-naphthol in the presence of NOM-2000. For example, the second rate constant of carbaryl in the presence of 3 ppm NOM-2000 was found to be $1.764 \pm 0.002 \times 10^{-3}$ s^{-1} which is very similar to the photodecomposition rate of alpha-naphthol in the presence of NOM-2000 ($1.87 \pm 0.04 \times 10^{-3}$ s^{-1}). Similar results were found for the other NOM concentrations. Therefore, we concluded that the photodecomposition of carbaryl in the presence of NOM-2000 shows two rates that are due to carbaryl in the presence of NOM-2000 (having low rate constants) and α-naphthol in the presence of NOM-2000 photodecompositions, respectively.

The next step was to focus on the influence of α-naphthol on the photodegradation of carbaryl. Since the intermediate and major degradation product of the photodecomposition of carbaryl is α-naphthol, carbaryl must be forming α-naphthol as it degrades and perhaps it is the presence of this intermediate that alters the kinetics of the reaction involving the Suwannee River NOM-2000 sample. To investigate the affect α-naphthol has on the photodegradation of carbaryl, an experiment was performed in which a 3 ppm solution of carbaryl was irradiated in the presence of a 3 ppm solution of α-naphthol, and the decrease in the peak areas of both luminescence bands were monitored.

Figure 3.14 shows the kinetics of the photodegradation of carbaryl in the presence of α-naphthol, while Figure 3.15 displays the effect carbaryl had on the photodegradation of α-naphthol. It is important to note that in one figure the Ln[carbaryl] is followed, and in the other figure the Ln[α-naphthol] is shown on the y axis. The two figures were constructed as a result of the same experiment.

A polynomial regression analysis of the data in Figure 3.14 yields a curve with a correlation coefficient (R^2) of 0.983. This is a relatively good fit, and the curve resembles those found for the photodegradation of carbaryl in the presence of the NOM-2000. However, a closer look at the data revealed the idea that two linear regression analyses could be done on separate parts of the data, to see where the increase in the photodegradation of carbaryl occurs in this reaction. The results of this analysis are shown in Figure 3.14.

The analysis in Figure 3.14 reveals that the data fit rather well to two linear best-fit lines, having correlation coefficients of 0.979 and 0.971, respectively for the reaction from time 0–40 minutes, and for the reaction occurring from time 50–90 minutes. The rate constants for these two sets of data were found to be $1.17 \pm 0.02 \times 10^{-4}$ s^{-1} and $1.97 \pm 0.06 \times 10^{-3}$ s^{-1}, respectively.

Figure 3.15 shows that the presence of carbaryl also changed the photodegradation kinetics of α-naphthol. From time 0–20 minutes, α-naphthol appears to be degrading very rapidly and then around 40 minutes, the concentration of α-naphthol begins to increase very slowly probably due to the photodegradation of carbaryl. However, since it is at the end of the reaction that the photodegradation rate

of carbaryl appears to become very rapid, the α-naphthol that is produced as a result of the photodegradation of carbaryl plays a role in influencing the kinetics of the photodegradation reaction. Relating this back to the photodegradation reaction of carbaryl in the presence of NOM-2000 which did not follow first-order kinetics, once a small amount of α-naphthol is produced as a result of the breakdown of carbaryl, the interaction between α-naphthol and carbaryl that is not bound to NOM is strong enough to increase the photodecomposition rate of carbaryl towards the end of the reaction.

The final experiment that was conducted to look at the influence of α-naphthol on the photodecomposition of carbaryl was a binding experiment. In this experiment, α-naphthol was used as the quencher and carbaryl was used as the luminophore. The concentration of α-naphthol was varied from 0–56 ppm and the concentration of carbaryl was held constant at 3 ppm for the purpose of this experiment. The extent of the interaction between carbaryl and α-naphthol was analyzed by determining the binding constant of the reaction. The results of this experiment yielded a binding constant (K_b) of $2.86 \pm 0.08 \times 10^4$ L kg^{-1} indicating that the binding between carbaryl and α-naphthol is lower than the binding between the carbaryl-NOM systems. For example, for the photodegradation of carbaryl in the presence of a 3 ppm solution of α-naphthol, 7.9 ± 0.2 % of the α-naphthol solution would be bound to carbaryl.

Figure 3.14. Photodegradation of a 3 ppm solution of carbaryl in the presence of a 3 ppm solution of α-naphthol.

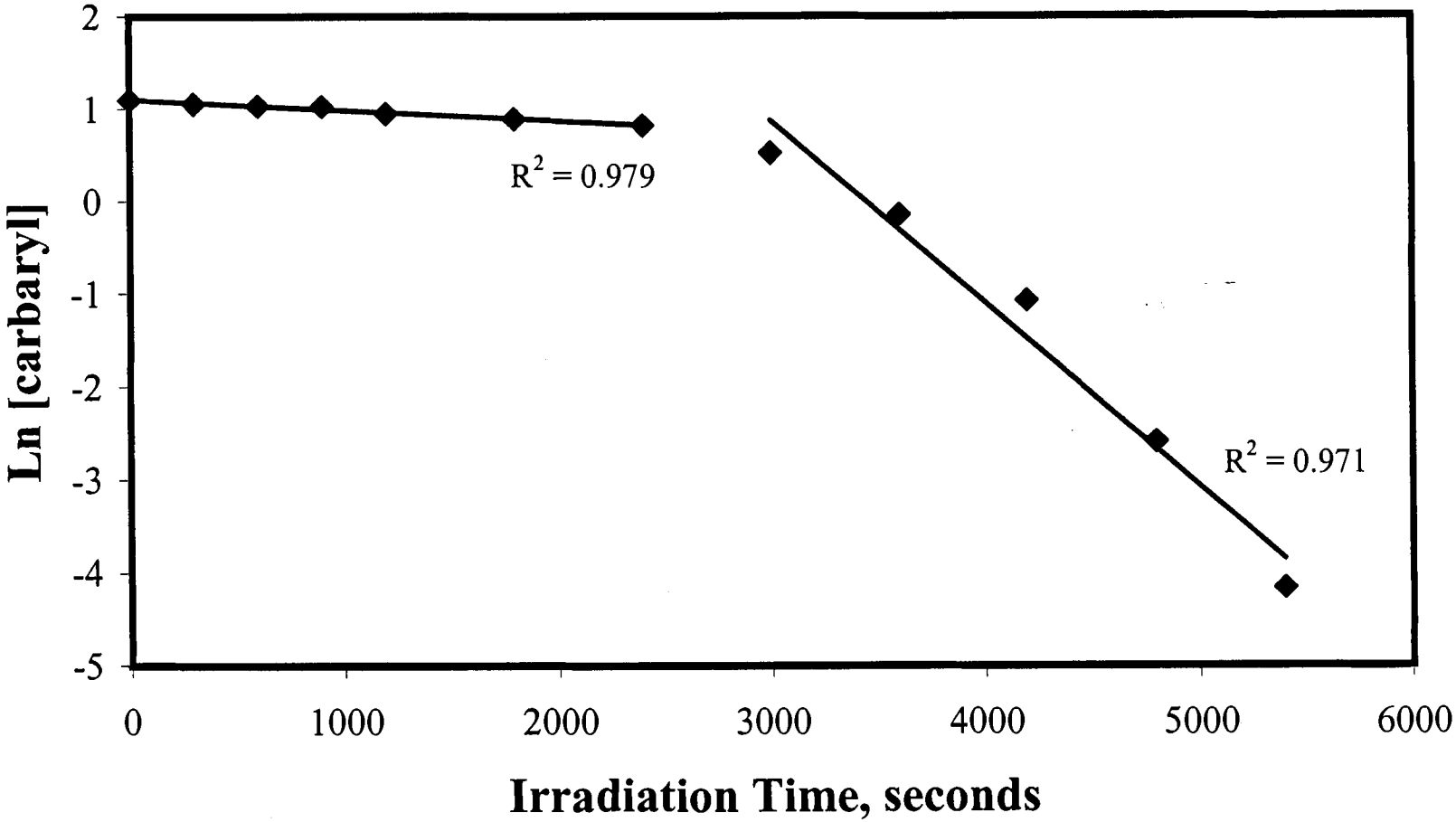

Figure 3.15. Photodegradation of a 3 ppm solution of α-naphthol in the presence of a 3 ppm solution of carbaryl.

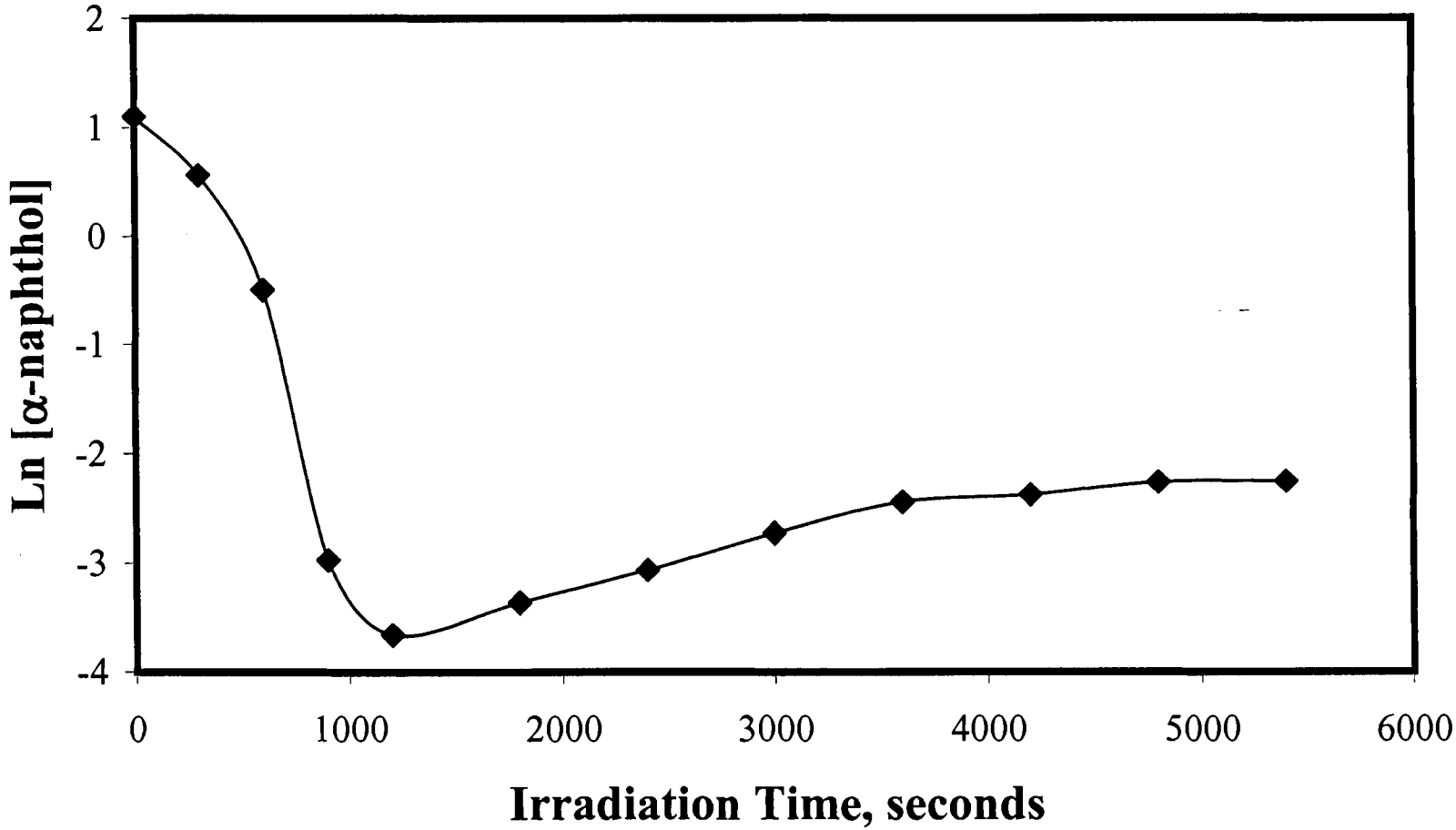

3.6. Conclusions

This chapter focused on the photodegradation of the widely used pesticide carbaryl in the presence of Suwannee River natural organic matter. The results indicate that the two samples of NOM that were collected from the same river in Georgia but purchased one year apart from each other have different affects on the kinetics of the photodegradation of carbaryl. The Suwannee River NOM-2000 actually changed the kinetics of the reaction, and a small concentration of this NOM sample increased the degradation of carbaryl. On the other hand, the Suwannee River sample that was purchased a year later did not alter the kinetics of the reaction, but a small amount of the NOM sample present in solution decreased the photodegradation rate of carbaryl. The results also showed that the binding interaction between carbaryl and the two Suwannee River samples were very different. The NOM-2000 sample bound almost twice as much carbaryl as the NOM-2001 sample did.

The results obtained for the photodegradation of carbaryl in the presence of NOM led to the idea that perhaps the major degradation product, α-naphthol had an influence on the overall reaction. Therefore, the interaction between carbaryl and α-naphthol was studied. To begin with, the photodegradation of α-naphthol in the absence and presence of the Suwannee River NOM samples was studied. The results indicated that α-naphthol degrades via first-order kinetics and the intermediate degrades more rapidly than carbaryl itself. In addition, a 3 ppm solution of carbaryl was irradiated in the presence of 3 ppm α-naphthol. It was found that the presence of α-naphthol actually alters the photodegradation kinetics of carbaryl.

Chapter 4

LUMINESCENCE PROPERTIES OF SILVER(I)-EXCHANGED ZEOLITE Y AND THE PHOTOASSISTED DEGRADATION OF CARBARYL

4.1. Preparation of the Silver Clusters Doped in the Y-type Zeolites

The silver clusters anchored in the Y-type zeolite catalysts were prepared by ion-exchange with $Ag(NH_3)_2^+$ as described in Chapter 2. The ICP-AES analysis of the silver loading in each zeolite was performed, and the results are shown in Table 4.1.

Table 4.1. The initial amount of silver nitrate that was loaded on the zeolites and the ICP-AES analysis of the percentage of silver loading on the zeolites.

Sample	Mass of $AgNO_3$ (g)	ICP-AES Analysis of Ag Loading
AgY #1	0.2	1.46 wt%
AgY #2	1	2.42 wt%
AgY #3	5	2.02 wt%
AgY #4	10	0.3 wt%

The results shown in Table 4.1 reveal that as the amount of silver nitrate used to prepare the AgY zeolites increases, the amount of silver that actually exchanges with the sodium cations in zeolite Y does not show the same trend. For example, AgY #4 was made to have the highest silver loading of the four prepared zeolites because the most silver nitrate was added to this sample, but it turned out to have the lowest amount of silver when analyzed by ICP-AES. As a result, the ICP-AES analysis of

the actual amount of silver that gets loaded on the zeolites is a very important part of this research. Without it the trend for the amount of Ag loaded on the zeolites (based on the initial mass of silver nitrate used) would have been thought to be AgY #1 < AgY #2 < AgY #3 < AgY #4, which is incorrect and would have affected the analysis of other experiments in this study.

4.2. Photoluminescence of Silver(I)-exchanged Zeolite Y

The four Ag(I)-exchanged zeolite Y samples have photoluminescence spectra that depend on the excitation wavelength. This indicates the presence of different luminophores in the Ag-Y zeolites in which their emission is observed upon selecting the correct excitation wavelength (i.e., site selective excitation). The luminescence spectra of the four zeolites have been investigated in detail in this study. The following discussion shows the emission and SSLS of the prepared Ag-Y zeolites as a function of temperature, excitation wavelength, SSLS, and the amount of silver.

For example, Figure 4.1 shows the emission spectra of the AgY zeolite sample that has the lowest silver loading at 77 K and at the indicated excitation wavelengths. Four major luminescence bands with maxima at 300, 360, 410, and 470 nm were observed upon excitation at the wavelengths indicated in the figure. These luminescence bands are labeled A, B, C, and D, respectively. The figure shows that emission bands C and D become dominant over the others at a particular excitation wavelength (above 300 nm). Excitation peaks between 220-245, 250-265, 270-280, and 290-305 nm were observed upon monitoring the emission at the maxima labeled A, B, C, and D, respectively.

Figure 4.1. Emission spectra of AgY zeolite having a 0.3 wt% Ag loading at 77 K and various excitation wavelengths.

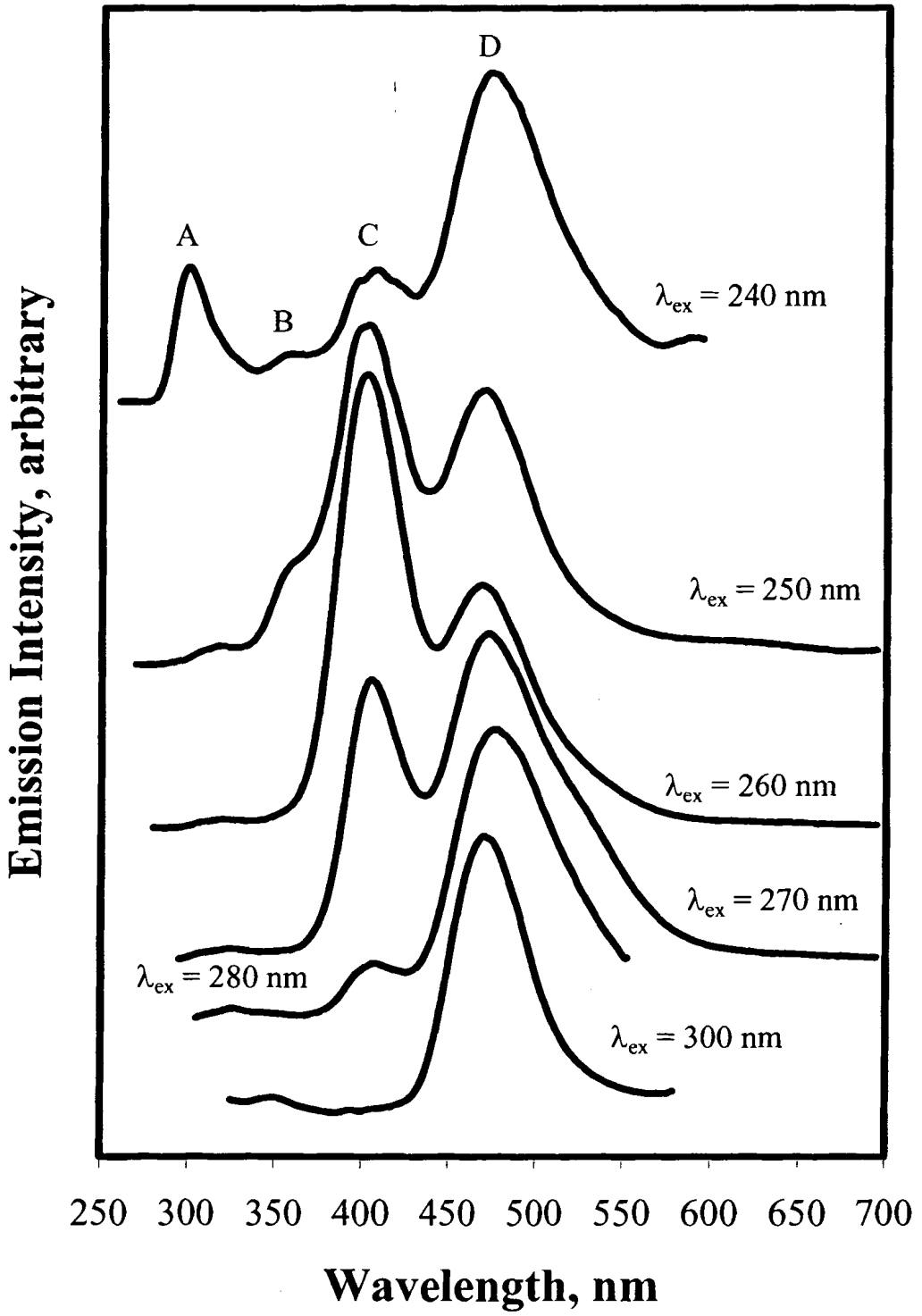

Synchronous-scan luminescence spectroscopy (SSLS) is a technique that can be used to characterize the AgY zeolites because the luminescence spectra provide evidence of the existence of different luminophores in the sample. Figure 4.2 shows the SSLS of the AgY zeolite that was analyzed to have 0.3 wt% silver, as a function of $\Delta\lambda$. The spectra show resolved peaks labeled A-E. Each peak in the SSLS becomes dominant over the others at a particular wavelength difference.

The observed emission and SSLS bands indicate the presence of different silver clusters in the Y-type zeolite. The luminescence data of silver clusters doped in zeolite Y is not common, but a few studies have focused on the types of clusters that form in the zeolite.[64-68] Despite the limited amount of knowledge that exists about the clustering of silver ions in zeolite Y, this is an important aspect to study in this research. Therefore, literature regarding the spectroscopy of silver clusters themselves as well as the assignment of the luminescence bands of silver clusters doped in other zeolites will be used to assign the bands in AgY.

In addition, the formation of Ag(I) clusters doped in the ZSM-5 zeolite were observed and characterized using luminescence, EXAFS, and EXANES spectroscopy as well as extended Hückel and ab-initio calculations. Theoretical calculations have indicated that the formation of $*[Ag^{+}]_n$ excimers and exciplexes that were found to be responsible for the NO photodecomposition.[77] Moreover, the formation of several emission bands for Ag-doped in A zeolite have also been reported. The observed emission bands were assigned based on ground and excited state theoretical calculations.[78]

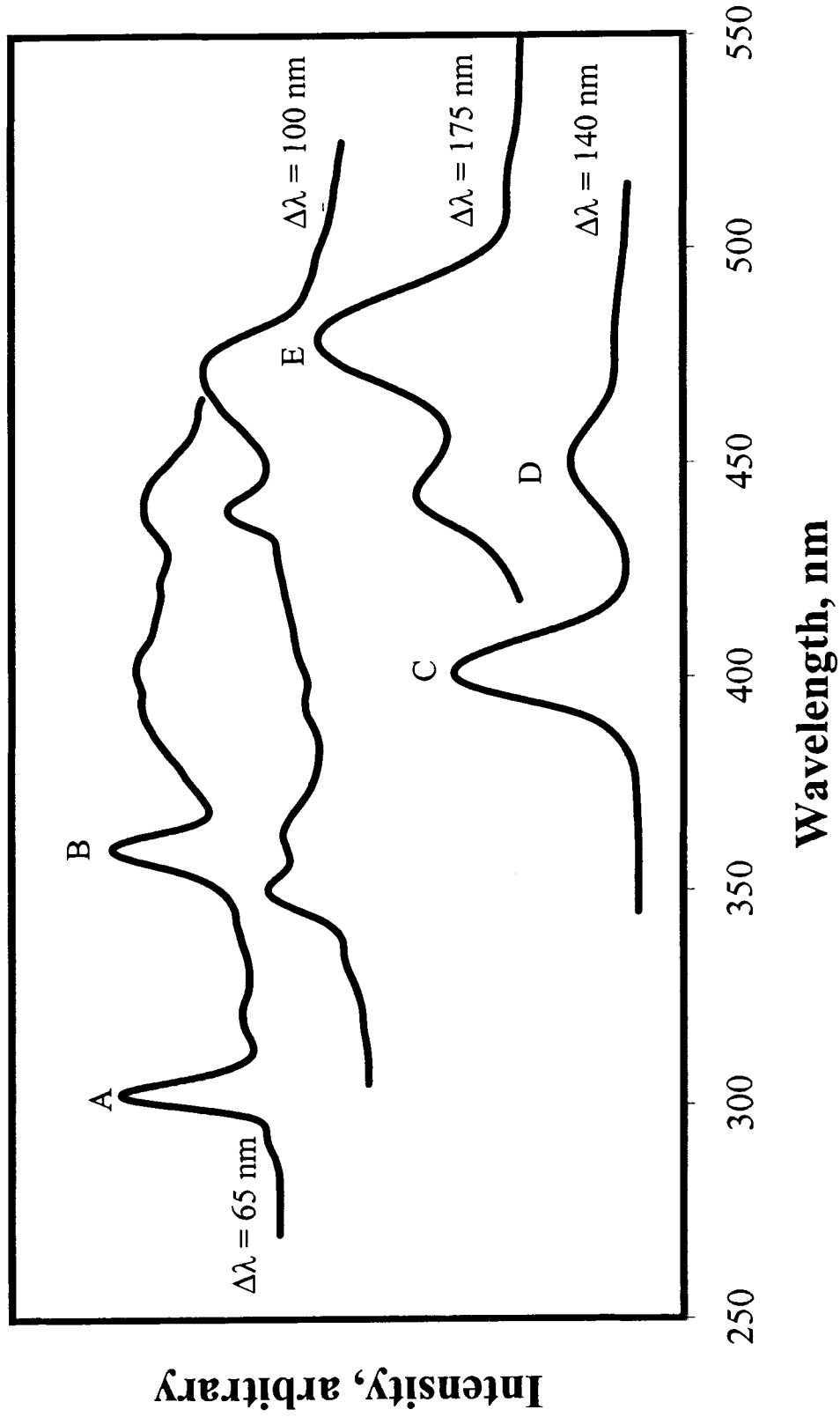

Figure 4.2. SSLS of the AgY zeolite having a Ag loading of 0.3 wt% at 77 K and several Δλ's.

In this study, the observed emission bands for the AgY zeolites as seen in Figure 4.1 are similar to those observed for the AgA zeolites and thus similar assignments are given for the luminescence bands of AgY. Table 4.2. shows the tentative assignments of the silver clusters doped in zeolite Y.

Table 4.2. Tentative assignment of the luminescence bands of AgY zeolite.

Luminescence Band	**λ_{em}, nm**	**λ_{ex}, nm**	**Cluster**
A	280-300	220-245	$*[Ag_2]^+$
B	345-360	250-265	$*[Ag_2]^{2+}$
C	395-435	270-280	Bent $*[Ag_3]^{n+}$ (n = 1, 2)
D	450-470	290-305	Bent $*[Ag_3]^0$
E	480-510	SSLS-only	Linear $*[Ag_3]^{2+}$

It was found that the luminescence properties also depend on the dopant concentration. As shown in Figure 4.3, the spectra of Ag doped in Y zeolite with low silver loading (curve D) shows a very strong emission band at 404 nm. The intensity of this band decreases as the silver loading increases and another band at lower energy appears at 430 nm (see curves B and C). Moreover, at higher silver loadings, bands also appear at 520 nm, which are lower in energy than the other bands (see curve a). This result indicates that an increase in the dopant concentration leads to the formation of larger clusters.

Figure 4.3. Luminescence spectra of the Ag doped Y zeolite at λ_{ex} = 265 nm and various Ag loadings: (a) 2.42, (b) 2.02, (c) 1.46, and (d) 0.3 wt% Ag.

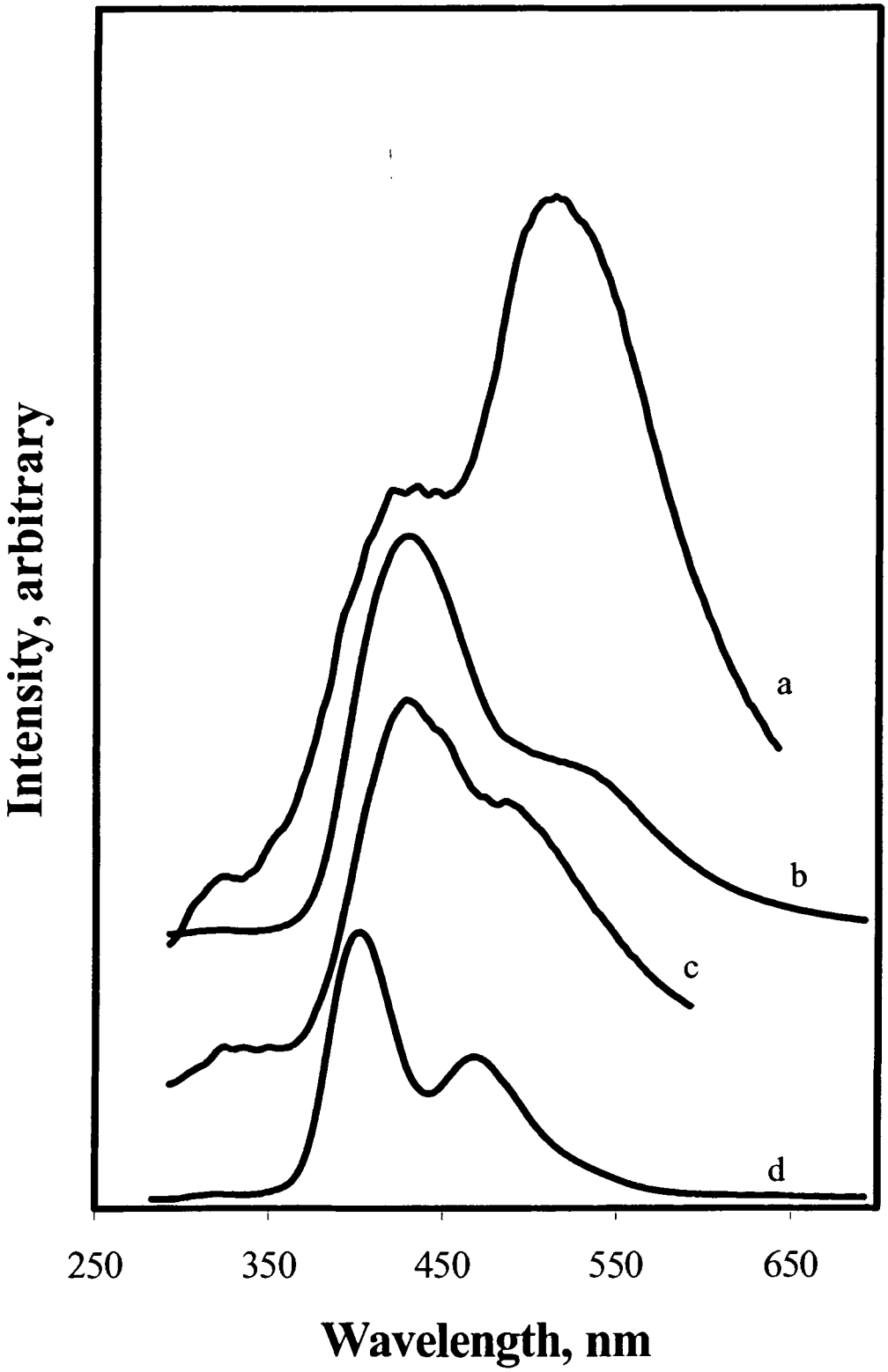

The luminescence spectra are strongly dependent on temperature. Figure 4.4 shows the emission spectra of silver doped in Y zeolite having 2.02 wt% silver at various temperatures and λ_{ex} = 270 nm. As shown in Figure 4.4, a strong emission band at 430 nm was observed at low temperature (77 K). Increasing the temperature accompanies a decrease in the emission band intensity at 430 nm and other bands at lower energy were observed. For example, bands at 455 and 490 nm were observed at 150 and 200 K, respectively. This finding indicated that energy transfer processes from the smaller silver clusters to larger silver clusters within the zeolite channels are thermally activated.

4.3. Luminescence Photodecomposition Rates of Carbaryl in the Presence of the Ag(I) Doped Zeolite Catalyst

Carbaryl shows two strong emission bands at 323 and 333 nm upon excitation at 276 nm (Figure 3.1). A 30 ppm solution of the pesticide itself, and a 30 ppm pesticide solution mixed with 10 mg of the silver Y-type zeolites were irradiated over a period of time. Emission spectra were monitored at the excitation wavelengths that led to maximum emission intensities as a function of irradiation time.

The photodecomposition of carbaryl produces products that do not show luminescence at the monitored wavelengths. This allows the disappearance of the observed luminescence band as a function of the irradiation time to be monitored. For the kinetic analysis, the emission intensity of known concentrations of carbaryl were recorded and a calibration curve for the peak area from 300–400 nm of each carbaryl emission band as a function of carbaryl concentration was used to identify the

Figure 4.4. Emission spectra of the AgY zeolite having 2.02 wt% Ag loading at λ_{ex} = 270 nm as a function of temperature.

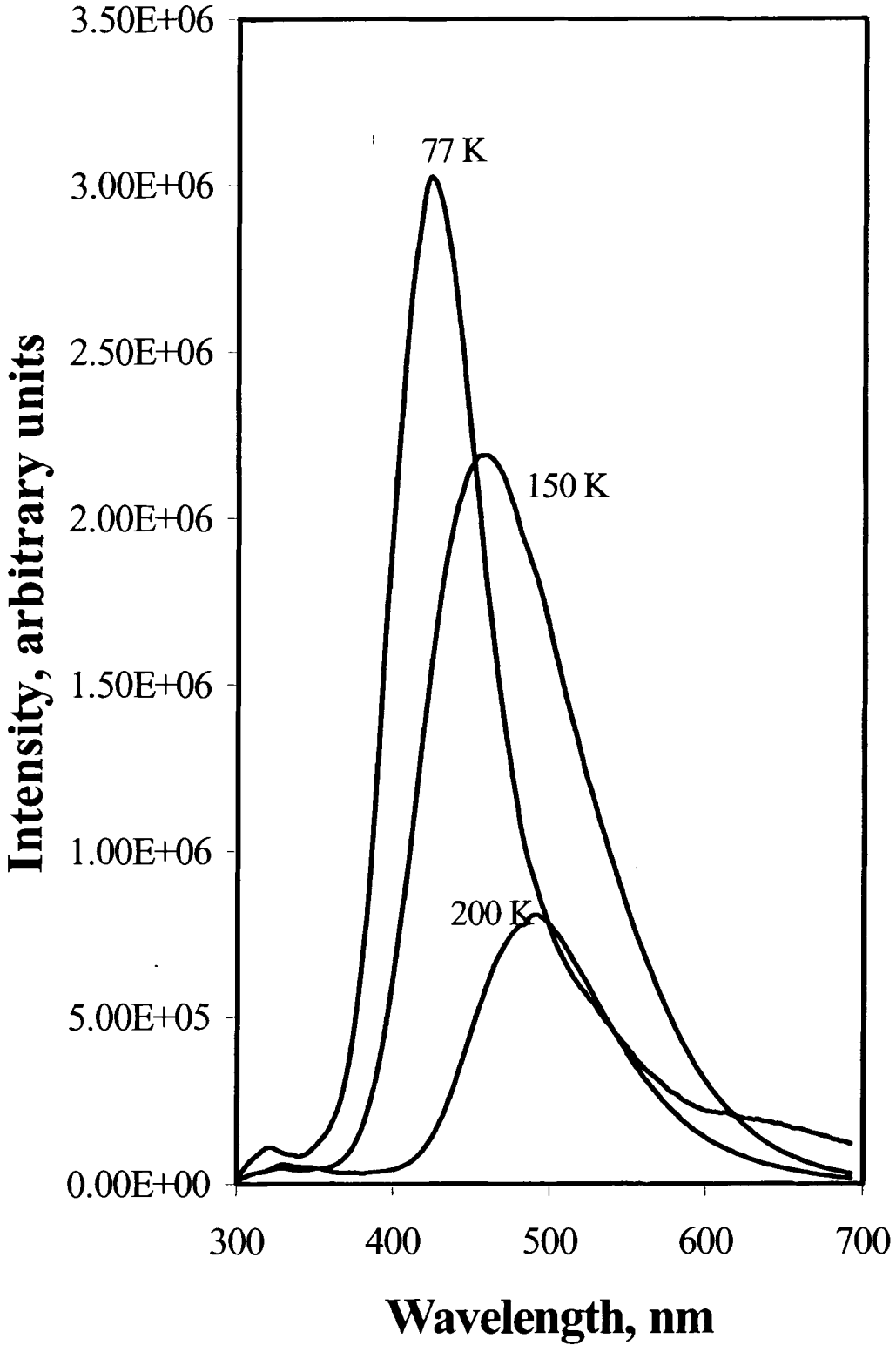

carbaryl concentration as a function of the UV irradiation time. Figure 4.5 shows the emission spectra of carbaryl before UV-irradiation and after UV-irradiation in the presence of the AgY zeolite sample that had 2.42 wt% Ag.

The solutions of carbaryl were irradiated with 300 nm light at 298 K. The photodecomposition rate constants of 30 ppm carbaryl alone in solution at 298 K is 5.6 $\pm$ 0.3 x 10^{-5} s^{-1}. The photodegradation of carbaryl in the presence of the AgY zeolites was found to proceed via first-order kinetics and was also faster than the zeolite-free solution. Table 4.3 summarizes the photdecomposition rate constants of carbaryl in the presence of the four AgY zeolites.

Table 4.3. Rate constants for the photodegradation of a 30 ppm solution of carbaryl in the presence of the AgY zeolites.

Zeolite Sample	Ag Loading (wt %)	Rate constant, s^{-1}
AgY #1	1.46	$6.8 \pm 0.1 \times 10^{-4}$
AgY #2	2.42	$4.44 \pm 0.06 \times 10^{-3}$
AgY #3	2.02	$1.32 \pm 0.04 \times 10^{-3}$
AgY #4	0.30	$1.62 \pm 0.04 \times 10^{-4}$

As shown in Table 4.3, AgY #4 produces the slowest photodecomposition rate, while AgY #2 displays the fastest photodegradation rate for carbaryl. Figure 4.6 is a plot of the rate enhancement versus the amount of silver loaded on the Y-type zeolite. The rate enhancement was determined in the following way: each rate constant in Table 4.3 was divided by the rate constant for the photodegradation of 30 ppm carbaryl alone in solution and the result was rounded to the nearest whole number.

Figure 4.5. An example of carbaryl luminescence photodecomposition as a function of irradiation time, in the presence of the AgY zeolite having 2.42 wt% Ag: (a) 0, (b) 5, (c) 10, (d) 20, and (e) 30 minutes.

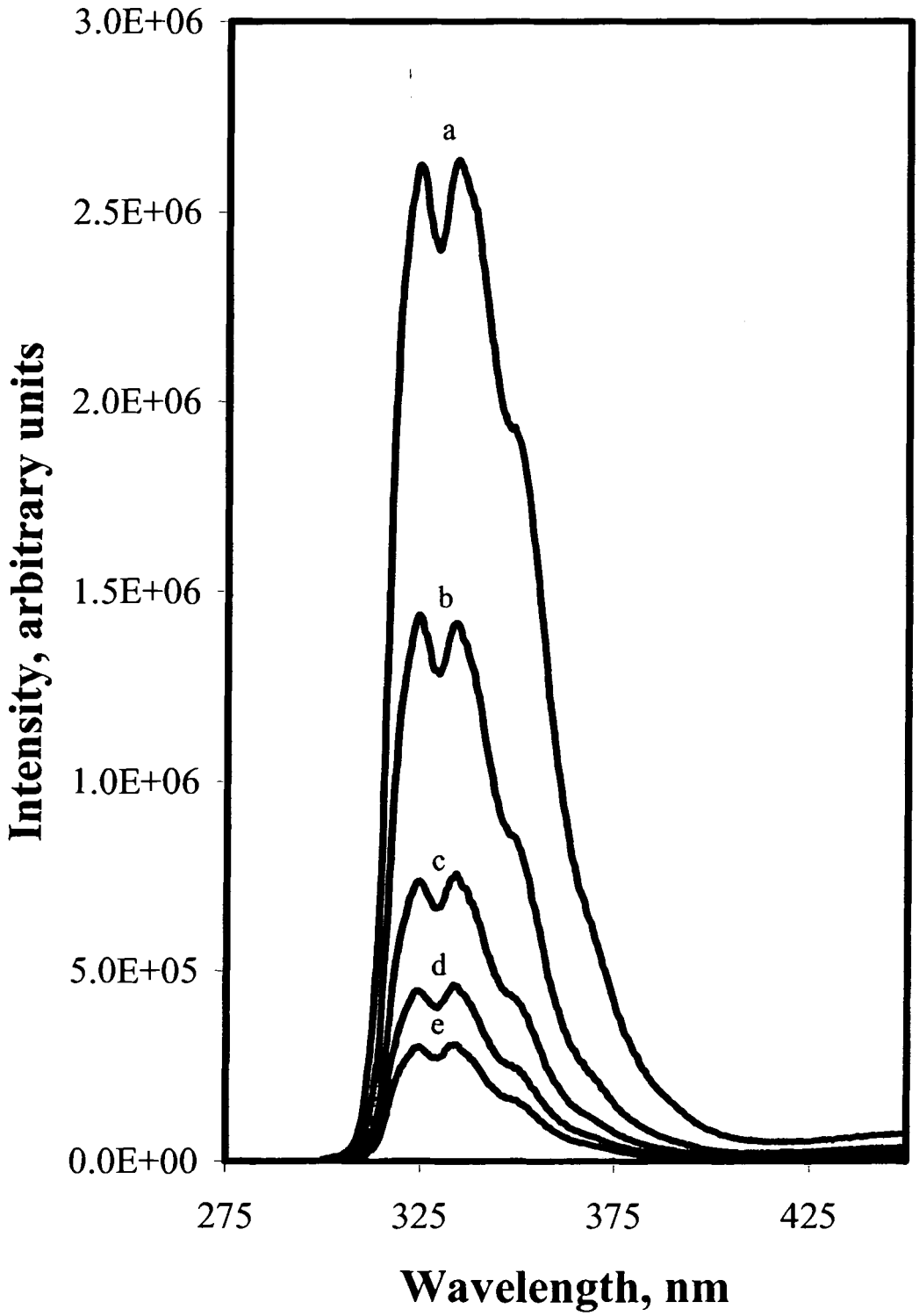

Figure 4.6 shows that as the amount of silver loaded on zeolite Y increases, its catalytic activity toward the photodegradation of the pesticide carbaryl increases. This is mainly due to the formation of more active sites as the amount of silver increases.

A series of control experiments were conducted to test whether the Ag-Y zeolite was needed to catalyze the photodegradation of carbaryl. The same photolysis experiments were performed for a 30 ppm solution of carbaryl in the presence of the Y-type zeolite in the absence of silver ions, and the rate constant was similar to that of the sample of pesticide alone in solution. Subsequently, to see the effect of the silver ion on the decomposition rate, the same experiments were performed in the presence of three different aqueous $AgNO_3$ concentrations. The photodecomposition rates of the pesticide in the presence of the $AgNO_3$ solutions were slightly slower than the silver-free pesticide solution, and no dependence on the $AgNO_3$ solution was found to exist.

Finally, the photodecomposition of carbaryl in the presence of the AgY zeolites was performed in the absence of the UV light. The results of these experiments yielded no significant degradation of the pesticide. As a result of these experiments, the presence of silver clusters in the zeolite channels appear to play a significant role in achieving the strong catalytic activity that was observed. The $[Ag^+]_n$ exciplexes and excimers in the zeolites interact with carbaryl in the presence of light and weaken bonds in the pesticide which causes it to decompose.

Figure 4.6. A plot of the photodegradation reaction rate enhancement versus the amount of silver that was loaded on the AgY zeolites.

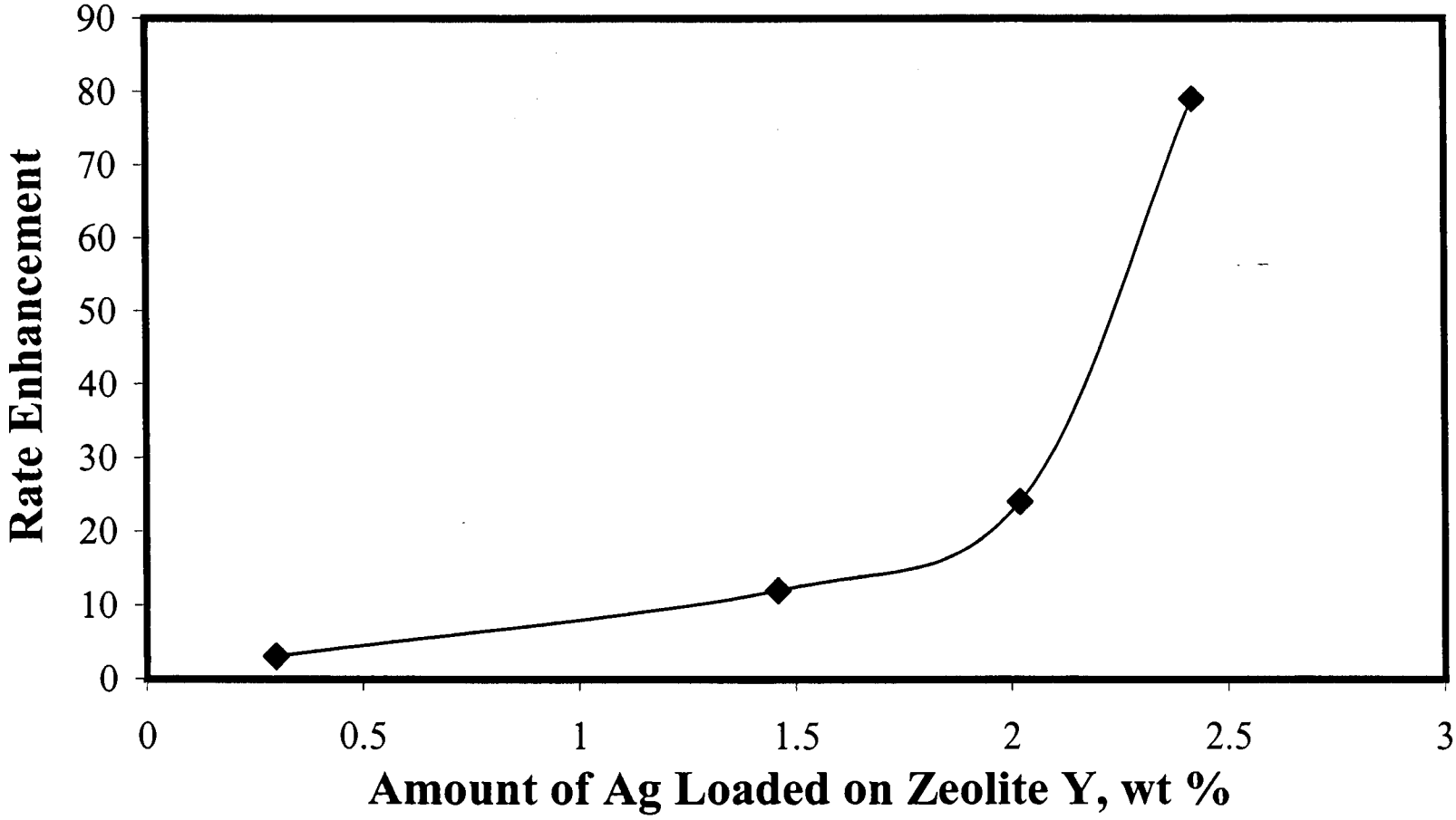

4.4. Rationalization of the Observed Photodecomposition Rate Constants

The enhancement of the photodecomposition rate of carbaryl in the presence of the AgY zeolites is attributed to excimer and exciplex formation between carbaryl and the silver active sites on the zeolite and/or the pesticide-to-zeolite channel sizes that allow the entrapment of the subject compound in the zeolite channels.

Excimers and exciplexes have been reported to form in metal-nitrogen complexes.[79-83] As a result, it is believed that excimer formation between the silver cations and the carbamate nitrogen atom is responsible for the fast photodecomposition rate of carbaryl, where the Ag-N bonding becomes stronger upon excitation. This interaction appears to weaken the bond between the carbamate nitrogen and the carbonyl carbon meanwhile increasing the rate of photodegradation. Since the hydrolysis product (α-naphthol) of carbaryl was obtained in the absence and presence of the AgY zeolites, the photodecomposition of the carbamate pesticide must proceed via a similar reaction mechanism. Figure 4.7 shows a theoretical mechanism of the photodegradation of a carbaryl in the presence of the Ag zeolite.[29] The first step includes the hydrolysis of the carbamate group. Subsequently, the presence of the Ag(I) zeolite leads to the formation of an excimer between the Ag-N atoms which weaken the adjacent C-N group and thus enhances the photodecomposition rate of the carbamate in the presence of the AgY zeolite.

The channel size of the Y-type zeolite is known to be ~ 10 Å and the sizes of carbaryl and α-naphthol were found to be between 5.6–8.0 Å.[29] Therefore, the entrapment of the derivatives of carbaryl inside the zeolite channels is possible. This makes the studied molecule exposed not only to the silver clusters on the surface but

Figure 4.7. Proposed mechanism for the photodegradation of carbaryl in the presence of a silver(I)-doped zeolite catalyst.

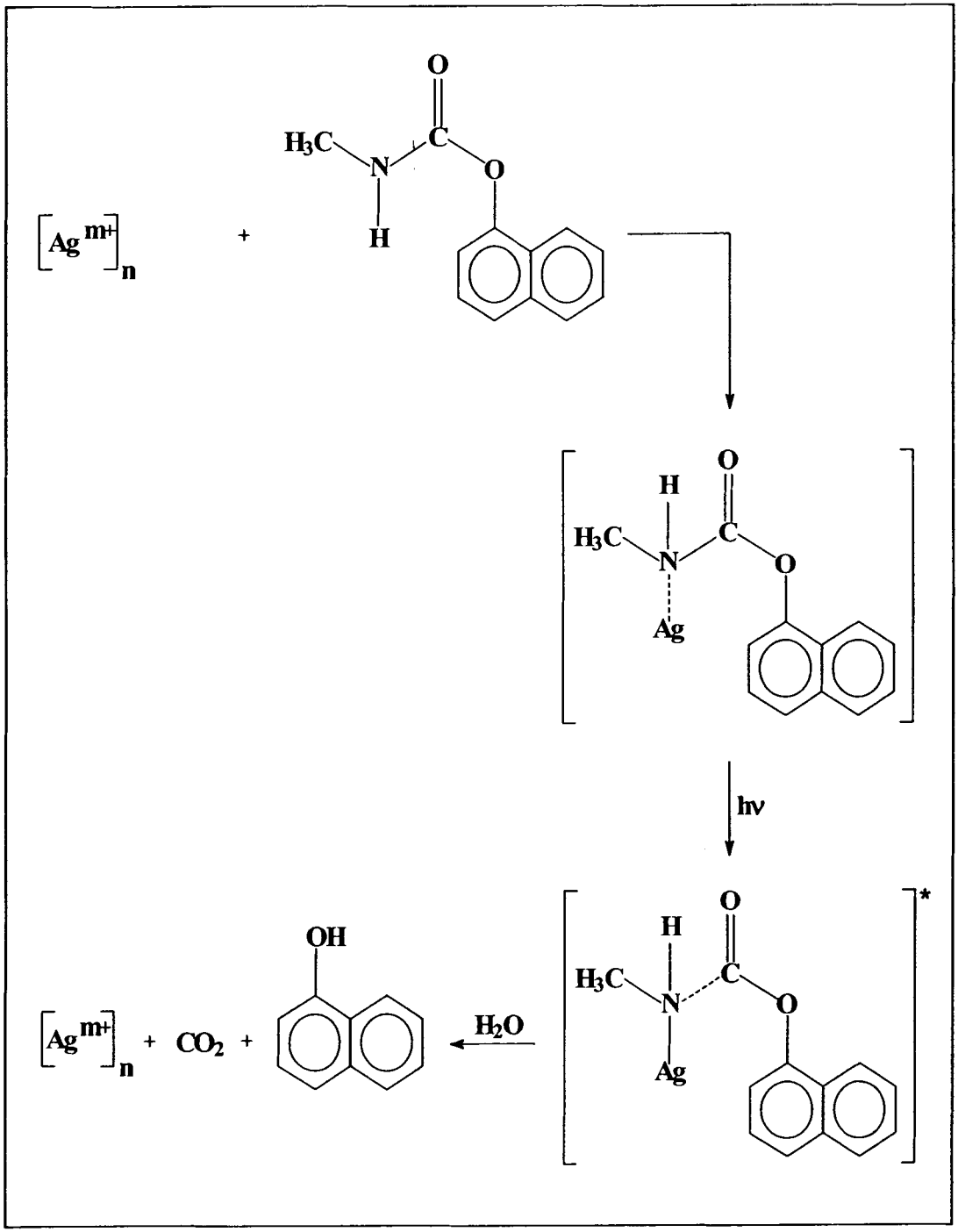

also to the catalysts that form in the zeolite channels and thus a significant increase in the photodecomposition rate is expected.

4.5. GC-MS Analysis of Carbaryl

Samples of a 30 ppm solution of carbaryl in the presence and absence of 10 mg of the AgY zeolites were irradiated with 300 nm light for 30 minutes. The first sample contains a 30 ppm solution of carbaryl only, and the other four samples contain a 30 ppm sample of carbaryl in the presence of the AgY zeolites. After irradiation was complete, the samples were filtered thoroughly and injected into the GC-MS.

Carbaryl generally shows a GC peak at 16.9 minutes. GC-MS analysis of the 30 ppm carbaryl solution that was irradiated for 30 minutes showed GC bands at 10.9 and 16.9 minutes. However, in the presence of the AgY catalysts an additional GC band appeared at 8.6 minutes. Therefore, the presence of the AgY zeolite catalysts causes a more complete degradation of carbaryl to occur, even after being irradiated with 300 nm light for just 30 minutes.

Figure 4.8 shows the gas chromatogram of the 30 ppm solution of carbaryl irradiated in the presence of AgY catalyst for 30 minutes. As was previously explained, peaks at retention times of 16.9, 10.9, and 8.6 minutes were observed. The mass analysis for each peak indicate the presence of carbaryl as well as two other organic products namely, α-naphthol and phthalic acid.

The GC peak at 16.9 minutes had a mass spectrum with major mass ion fragments that appeared at m/z = 144, 115, 89, 57, and a molecular ion peak at m/z = 201 representing the carbaryl molecule. The GC band that appeared at a retention time of 10.9 minutes

had major mass ion fragments at *m/z* = 144, 115, 89, and 63, which was similar to the mass spectrum of a standard solution of alpha-naphthol (MW = 144 g/mole). Finally, major mass ion fragments at *m/z* = 166, 148, 104, 76, and 50 appeared for the GC peak that occurred at a retention time of 8.6 minutes. The GC-MS analysis of the band at 8.6 minutes matched a standard solution of phthalic acid (MW = 166 g/mole).

30 ppm solutions of carbaryl in the presence and absence of the AgY zeolite catalysts were irradiated with 300 nm light for 12 hours. After the 12-hour period, the samples were removed from the lamp light, filtered, and immediately injected into the GC-MS. The GC-MS analysis of 30 ppm carbaryl alone in solution once again revealed the presence of carbaryl and α-naphthol. The samples that contained 30 ppm carbaryl in the presence of the AgY zeolites were also analyzed by GC-MS. The results of this analysis produced the GC bands at retention times of 16.9, 10.9, and 8.6 minutes representing carbaryl, α-naphthol, and phthalic acid, respectively. These results were also seen after the samples were irradiated for only 30 minutes; however, the intensity of the carbaryl GC band had severely decreased while the α-naphthol and phthalic acid GC bands became more intense after 12 hours.

Figure 4.8. The gas chromatogram of a 30 ppm solution of carbaryl in the presence of 10 mg of the AgY zeolite that was irradiated for 30 minutes.

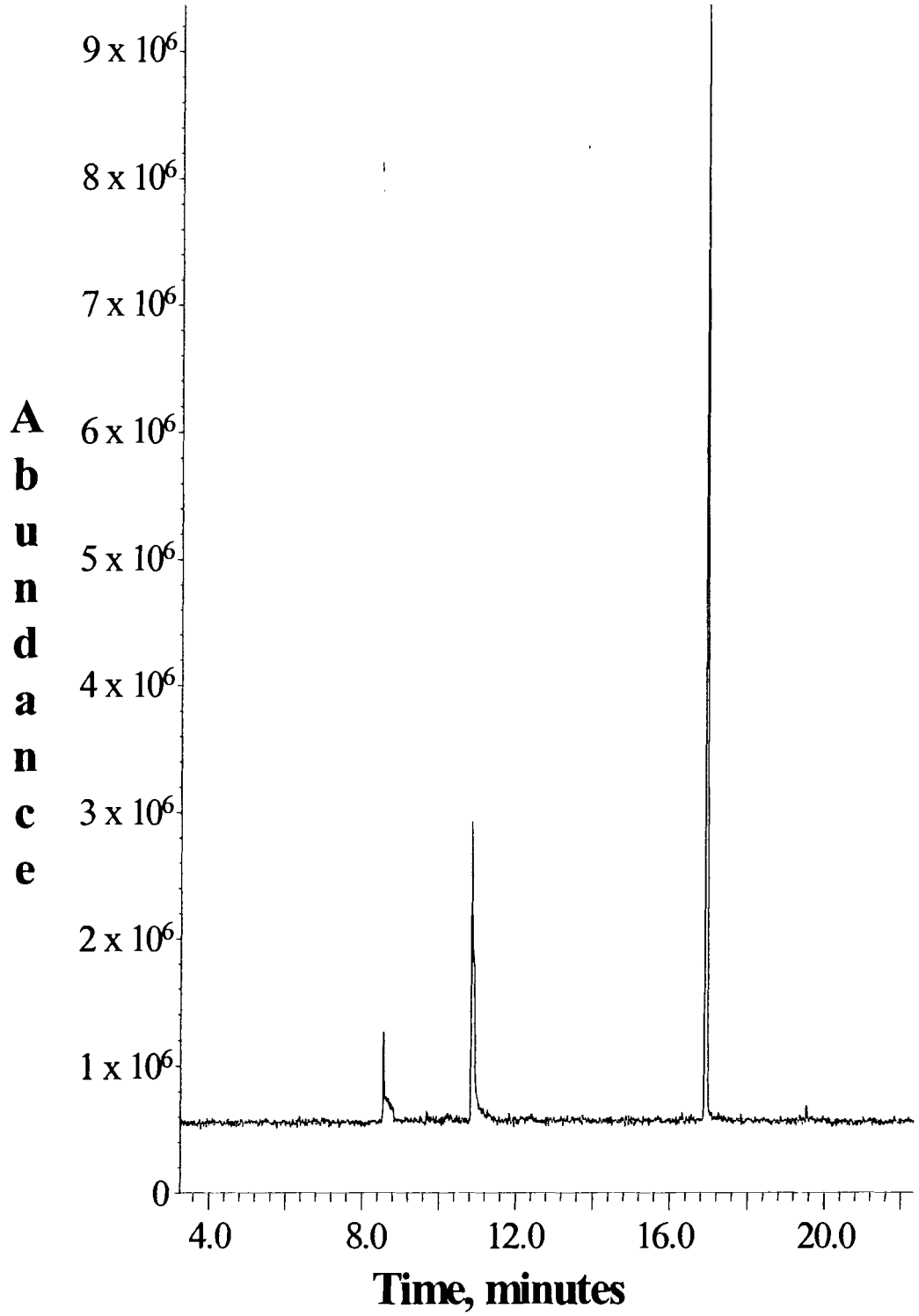

4.6. The Photodegradation of Carbaryl in the Presence of Both the AgY Zeolites and Natural Organic Matter

The photodegradation of 30 ppm carbaryl in the presence of the AgY catalysts as well as NOM-2001 were also studied. In all cases, the photodecomposition of carbaryl proceeds via first-order kinetics. The photodecomposition of carbaryl in the presence of AgY catalysts is 3–79 times faster than the decomposition of 30 ppm carbaryl alone (rate constant = $5.6 \pm 0.3 \times 10^{-5}$ s^{-1}). Table 4.4 summarizes the rate constants for the photodecomposition of carbaryl in the presence of the four AgY zeolites and different NOM concentrations.

The data shown in Table 4.4 indicate that the photodecomposition rate constants of carbaryl increase as the silver loading increases. Moreover, in comparison to the carbaryl in the presence of the AgY zeolites, the presence of 3 ppm NOM was found to enhance the rate constant. In contrast, the presence of 15 and 30 ppm concentrations of NOM slightly decrease the photodecomposition rates.

Table 4.4. Rate constants in s^{-1} for the photodecomposition of a 30 ppm solution of carbaryl in the presence of the Ag-doped Y-type zeolites and various concentrations of Suwannee River NOM-2001.

AgY wt% Ag	0 ppm SR NOM	3 ppm SR NOM	15 ppm SR NOM	30 ppm SR NOM
0.30	$1.62 \pm 0.04 \times 10^{-4}$	$4.38 \pm 0.02 \times 10^{-4}$	$1.02 \pm 0.02 \times 10^{-4}$	$6.01 \pm 0.04 \times 10^{-5}$
1.46	$6.80 \pm 0.01 \times 10^{-4}$	$1.43 \pm 0.05 \times 10^{-3}$	$6.53 \pm 0.01 \times 10^{-4}$	$6.34 \pm 0.05 \times 10^{-4}$
2.02	$1.32 \pm 0.04 \times 10^{-3}$	$1.91 \pm 0.09 \times 10^{-3}$	$1.28 \pm 0.04 \times 10^{-3}$	$1.15 \pm 0.07 \times 10^{-3}$
2.42	$4.44 \pm 0.06 \times 10^{-3}$	$4.97 \pm 0.01 \times 10^{-3}$	$1.81 \pm 0.02 \times 10^{-3}$	$1.69 \pm 0.08 \times 10^{-3}$

Figure 4.9 shows a plot of the rate constant as a function of NOM concentration for the four AgY zeolites. As shown in Figure 4.9, the trend is similar for the four curves; where, the rate constant increases in the presence of 3 ppm NOM and then the rate constant decreases in the presence of 15 and 30 ppm NOM. A similar result was reached for carbaryl in the presence of 3, 15, and 30 ppm concentrations of NOM-2000 (see Chapter 3).

Table 4.5 shows the amount the photodecomposition rate of carbaryl in the presence of the AgY zeolites was enhanced or inhibited in the presence of NOM-2001. The rate enhancement was determined by dividing the rate constants for the photodegradation of carbaryl in the presence of the AgY zeolites and 3 ppm NOM (column 2 of Table 4.4) by the rate constants in column 1 of Table 4.4, depending on which AgY zeolite was being considered. The rate inhibition factor was determined by dividing the rate constants in column 1 of Table 4.4 by the rate constants for the photodegradation of carbaryl in the presence of the AgY zeolites and 15 and 30 ppm NOM (columns 3 and 4 of Table 4.4), depending on which AgY zeolite was being used. Each result was rounded to the nearest whole number. Overall, the rate changes for the photodegradation of carbaryl in the presence of the AgY zeolites were very small in the presence of 3, 15, and 30 ppm concentrations of NOM, showing that the AgY zeolites will be efficient catalysts when placed in the environment.

Figure 4.9. A plot of the rate constant versus NOM concentration for the four AgY zeolites.

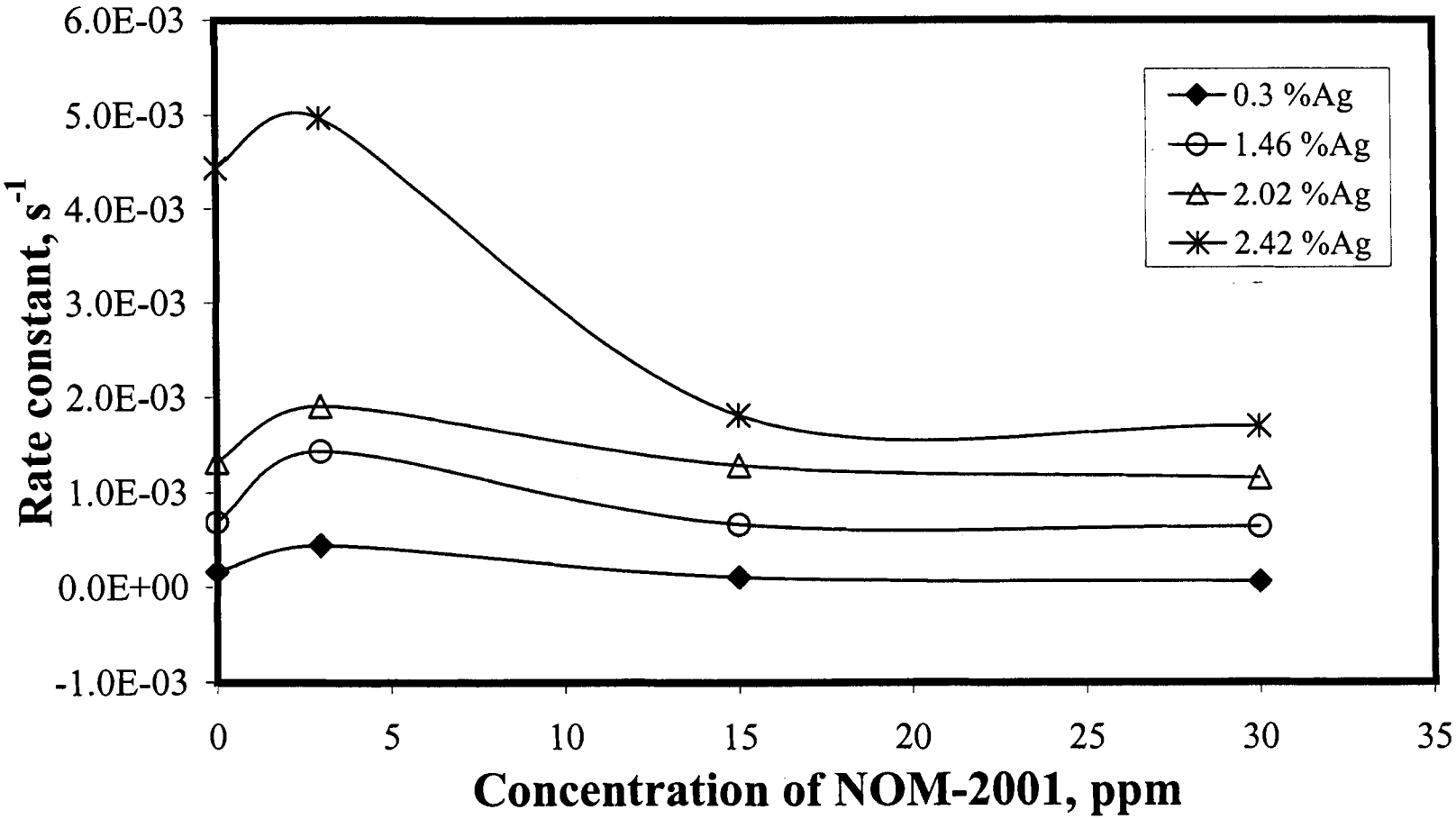

Table 4.5. The factors by which the rate of photodegradation of carbaryl in the presence of the AgY zeolites was enhanced or inhibited by various concentrations of NOM-2001. A negative sign in front of the number designates rate inhibition.

AgY wt% Ag	3 ppm SR NOM	15 ppm SR NOM	30 ppm SR NOM
0.30	3	-2	-3
1.46	2	-1	-1
2.02	1	-1	-1
2.42	1	-2	-3

4.7. Conclusions

This study summarizes the rich luminescent properties of silver doped Y-type zeolites. The results of both conventional and synchronous scan luminescence spectroscopy reveal the presence of multiple environments of $[Ag^{m+}]_n$ clusters in the zeolite channels. This investigation also revealed that the AgY zeolite having the most amount of silver also exhibited the highest catalytic activity toward the photodegradation of the widely used pesticide carbaryl.

The photodecomposition of carbaryl was studied at room temperature in the presence and the absence of each AgY catalyst. GC-MS analysis of each photodecomposition reaction shows that with carbaryl the products remain the same in the presence of the AgY zeolites. The samples of zeolite Y and the presence of silver ion without zeolite Y do not affect the photodecomposition rate constant of carbaryl. As a result, it appears to be the formation of $*[Ag^{+}]_n$ excimers and exciplexes in the zeolite channels as well as excimer formation between the silver cations and the carbamate nitrogen are responsible for the achievement of the observed catalytic

activity. In summary, this study shows that silver doped Y-type zeolites can act as photocatalysts to decompose the carbamate pesticide carbaryl both in the presence and absence of natural organic matter.

Chapter 5

SUMMARY, CONCLUSIONS, AND SUGGESTED FUTURE RESEARCH

This chapter summarizes what has been achieved in this thesis. Two major projects have been studied in this work. The first project is a study of the photodegradation of carbaryl in the presence of Suwannee River natural organic matter. The second project is a study of the photoluminescence properties of Ag(I) clusters doped in Y-type zeolite as a function of silver loadings and temperature, as well as its catalytic properties toward the photodecomposition of the widely used pesticide carbaryl. The following is a summary of the results and conclusions of this thesis.

5.1. Photodecomposition of Carbaryl in the Presence of Suwannee River Natural Organic Matter

5.1.1. Summary

Carbaryl molecules have aromatic rings and were found to display strong luminescence properties in this study. A 3 ppm solution of carbaryl was prepared and the absorption spectrum revealed a peak maximum at 276 nm with an extinction coefficient of $1.530 \pm 0.006 \times 10^3$ L mol^{-1}. Upon excitation at 276 nm, the emission spectrum of carbaryl spanned from 300–400 nm with maxima at 323 and 333 nm. The synchronous-scan luminescence spectra (SSLS) of carbaryl revealed bands between 325–350 nm, with peak maxima at 323, 333, 340, and 350 nm at $\Delta\lambda$'s = 20, 30, 47, 57, 70, and 80 nm.

Two Suwannee River NOM samples were used in this study, (NOM-2000 and NOM-2001). The emission spectra of the NOM-2000 and the NOM-2001 samples revealed broad luminescence bands between 360–600 nm with maxima at 437 and 455 nm upon excitation at 333 and 345 nm, respectively. The synchronous-scan luminescence spectra of NOM-2000 showed several peaks with maxima at 313, 338, 356, 403, 425, and 470 nm. In contrast, the SSLS of the NOM-2001 sample revealed five bands with peak maxima located at 325, 403, 418, 430, and 448 nm. For both NOM samples the wavelength difference was varied in the following way: $\Delta\lambda$ = 30, 50, 70, and 100 nm. The SSLS of the NOM-2000 sample was also found to depend on concentration. For example, at $\Delta\lambda$ = 30 nm a 3 ppm solution of the NOM-2000 sample showed a band at 325 nm. As the concentration of NOM sample increased from 15-60 ppm, the intensity of this high-energy band decreased, while a broad band at 403 nm appeared.

The Suwannee River NOM-2000 sample was separated into three different molecular weight (MW) fractions as described in Chapter 2. One fraction contained molecules with a MW that was less than 1,000 g/mole, the second fraction had molecules with a MW between 1,000 and 10,000 g/mole, and the third fraction contained molecules that had a MW greater than 10,000 g/mole. The concentration of dissolved organic carbon (DOC) in each fraction was determined to be 2.05, 15.7, and 50.6 mg C L^{-1}, respectively. The solvent from the solution of the smallest MW fraction was removed and the new DOC analysis revealed a concentration of 20.2 mg C L^{-1}, which was sufficient to determine the binding interaction between this sample and carbaryl.

To determine the binding interaction of the NOM samples with carbaryl, NOM was used as the quencher and carbaryl was used as the luminophore. A Stern-Volmer plot of carbaryl quenched by the Suwannee River NOM-2000 sample revealed a binding constant of $7.3 \pm 0.3 \times 10^4$ L kg^{-1}. Additionally, experiments to determine the binding constant of the three NOM-2000 molecular weight fractions with carbaryl were performed. The binding constants were determined to be $1.29 \pm 0.04 \times 10^4$, $2.83 \pm 0.06 \times 10^4$, and $5.34 \pm 0.09 \times 10^4$ L kg^{-1} for the MW fraction that was less than 1,000 g/mole, the MW fraction that was between 1,000 and 10,000 g/mole and the MW fraction that was greater than 10,000 g/mole, respectively. For the NOM-2001 sample, the binding constant was determined to be $3.04 \pm 0.02 \times 10^4$ L kg^{-1}, which was lower than the observed binding constant for NOM-2000.

The photodegradation of a 3 ppm solution of carbaryl was studied in the absence and presence of 3, 15, and 30 ppm concentrations of the Suwannee River NOM samples. A plot of Ln[carbaryl] versus irradiation time for the photodegradation of carbaryl in the presence of the Suwannee River NOM-2000 sample did not follow first-order kinetics. Instead, each set of data that resulted from the photodegradation experiment was fit to two linear best-fit lines, one between time 0–70 minutes, and another at a time that was $\geq$ 80 minutes. Overall, the rate of the photodegradation of carbaryl in the presence of NOM-2000 was enhanced and the 3 ppm solution of NOM produced the largest rate enhancement. In contrast, the kinetics of the photodegradation of carbaryl in the presence of the NOM-2001 sample did proceed via first-order kinetics. For this sample, 3 and 15 ppm concentrations of

NOM decreased the photodecomposition rate of carbaryl, while a 30 ppm solution enhanced the photodegradation rate.

To examine the effect of the binding interaction on the photolysis rate constant, the rate constant data was related to the percent of carbaryl bound to NOM in solution using Equation 4 in Chapter 3. For the NOM-2000 sample, the percentages of a 3 ppm solution of carbaryl that was bound to 3, 15, and 30 ppm solutions of NOM were 18 ± 0.8%, 52 ± 2%, and 69 ± 3%, respectively. In contrast, the percentages of a 3 ppm solution of carbaryl that was bound to 3, 15, and 30 ppm solutions of NOM-2001 were 8.36 ± 0.06%, 31.3 ± 0.2%, and 47.7 ± 0.3%, respectively. These results were in agreement with the binding constants that were found for the two NOM samples.

The photodegradation of α-naphthol was studied in the absence and presence of the Suwannee River NOM samples and in the presence of carbaryl. A 3 ppm solution of α-naphthol displays a broad luminescence band with a maximum at 462 nm upon excitation at 323 nm. Since the luminescence spectrum of α-naphthol shows a band at longer wavelength than carbaryl, it was easy to follow the kinetics of the photodegradation reaction using luminescence. Thus, the photodegradation of a 3 ppm solution of α-naphthol was studied in the presence of 3, 15, and 30 ppm concentrations of NOM-2000. The reaction followed first-order kinetics and the rate constants in the presence of NOM-2000 increased as the concentration of NOM increased. The photodegradation of α-naphthol in the presence of 3, 15, and 30 ppm solutions of NOM-2001 was also studied. The results revealed first-order rate constants, and a 3 ppm solution of the NOM-2001 sample enhanced the

photodegradation rate of α-naphthol, while the photodecomposition rate decreased in the presence of 15 and 30 ppm concentrations of the NOM sample.

The photodegradation of a 3 ppm solution of carbaryl in the presence of 3 ppm α-naphthol was studied. The results revealed that a plot of Ln[carbaryl] versus time did not display first-order kinetics. Instead, the data set was fit to two linear best fit lines for the reaction from time 0–40 minutes and 50–90 minutes. The presence of carbaryl also changed the photodegradation kinetics of α-naphthol. From time 0–20 minutes, α-naphthol degrades rapidly and then around 40 minutes, the concentration of α-naphthol begins to increase due to the photodegradation of carbaryl.

5.1.2. Conclusions

The two Suwannee River NOM samples that were collected from the same river in Georgia displayed similar emission and excitation spectra, but the SSLS revealed differences in the two samples. For example, three peaks are observed in the high-energy region between 300-360 nm for NOM-2000; whereas, the NOM-2001 sample shows only one band in this region at 325 nm. Moreover, at $\Delta\lambda = 30$ nm the SSLS of the NOM-2000 sample shows an intense band at 313 nm, but this band was weak for the NOM-2001 sample and another band at 403 nm was seen in the same spectrum.

The SSLS bands that appear with maxima between 313–338 nm were attributed to functional groups in the NOM that are similar to the structure of salicylic acid; whereas, a peak occurring around 350 nm reflects quantitative differences in the

amounts of salicylate-type groups or variations in the carboxyl substitutions of single aromatic rings.[73] The SSLS bands that occurred at 403 and 425 nm were assigned to functional groups similar to the structure of 3-hydroxycinnamic acid and 3-hydroxybenzoic acid, respectively.[74] The band at 470 nm was attributed to hydroxy and methoxy coumarins or chromone derivatives, while the band at 448 nm was due to the presence of methyl salicylate or caffeic acid functional moieties.[75] Therefore, the SSLS allowed for the determination of differences in the two Suwannee River NOM samples. The differences in the SSLS bands do not reveal structural differences in NOM-2000 and NOM-2001, but the variations lead to the conclusion that the isomers composing each sample could be different.

The results of the binding interaction between carbaryl and the two Suwannee River NOM samples revealed that the binding constant for NOM-2001 was lower than that for NOM-2000. The data indicate that the difference in the binding strength between carbaryl and the two NOM samples is due to the presence of different SSLS bands that appeared in the high-energy region. For example, three bands were observed in the region between 300–350 nm for the NOM-2000 sample, while only one band at 325 nm was observed in the SSLS of NOM-2001. Therefore, the presence of different luminophores in NOM-2000 provides more active sites that bind to carbaryl.

The influence of Suwannee River natural organic matter on the photodegradation was found to be significant since the two NOM samples had different effects on the reaction rate. The percentage of carbaryl that was bound to each NOM sample showed that NOM-2000 interacted more with carbaryl than NOM-

2001 at the same concentration. Therefore, the presence of different isomers and the amount of carbaryl bound to NOM caused the photodegradation of carbaryl to be different in the presence of NOM-2000 and NOM-2001. The photodegradation of α-naphthol in the presence of Suwannee River NOM proceeded via first-order kinetics; however, the two NOM samples displayed differences in the way they either enhanced or slowed down the photodegradation rate of carbaryl. When the photodecomposition rate constants of carbaryl in the presence of NOM-2000 (time ≥ 80 minutes) were compared with the rate constants for the photodegradation of α-naphthol in the presence of NOM-2000, they were very similar. In conclusion, the photodecomposition of carbaryl in the presence of NOM-2000 shows two rates that are due to carbaryl in the presence of NOM-2000 and α-naphthol in the presence of NOM-2000.

The photodegradation of carbaryl in the presence of α-naphthol also changed the kinetics of the reaction. In the presence of α-naphthol, carbaryl did not degrade via first-order kinetics, and the data set was fit to two linear best-fit lines that resembled the photodegradation kinetics of carbaryl in the presence of NOM-2000. Therefore, the presence of the intermediate α-naphthol in solution when carbaryl is degrading, alters the kinetics of the reaction. The carbaryl molecules must undergo a binding interaction with α-naphthol causing a rate enhancement and allowing carbaryl to breakdown rapidly.

5.2. Spectroscopic Properties of Ag(I)-exchanged Zeolite Y and the Photoassisted Degradation of Carbaryl

5.2.1. Summary

The AgY zeolites were prepared by ion exchange with $Ag(NH_3)_2^+$. The ICP-AES analysis of the actual amount of silver that was loaded on each zeolite was found to be: 0.3, 1.46, 2.02, and 2.42 wt% Ag. The four silver-exchanged zeolite Y samples have emission spectra that depend on the excitation wavelength. For example, the luminescence spectra of the AgY zeolite with 0.3 wt% Ag loading showed four luminescence bands at 300, 360, 410, and 470 nm (labeled A–D), upon excitation at 220–245, 250–265, 270–280, and 290–305 nm. In the SSLS of the same AgY sample, an additional band occurred that was labeled E. The luminescence properties of the AgY zeolites also depended on the dopant concentration. For example, at λ_{ex} = 265 nm the AgY zeolite with the lowest Ag loading shows a strong band at 404 nm, but at higher silver loadings other bands appear at 430 and 520 nm. Finally, the luminescence spectra were also strongly dependent on temperature. For the AgY zeolite with 2.02 wt % Ag, a strong emission band at 430 nm was observed at 77 K, but as the zeolite was heated, other bands at lower energy were observed.

A 30 ppm solution of carbaryl itself, and 30 ppm solutions of the pesticide in the presence of 10 mg of the Ag doped in Y-type zeolites were irradiated with 300 nm light. The results indicate that the photodegradation of carbaryl in the presence of the AgY zeolites was found to proceed via first-order kinetics and was also faster than the zeolite-free solution. In fact, the presence of the AgY zeolites increases the photodegradation rate of carbaryl by 3–79 times depending on the amount of silver

that was loaded on the zeolites. The photodegradation of carbaryl was also studied in the presence of both NOM-2001 and the AgY zeolites. Overall, the presence of 3 ppm NOM enhanced the photodegradation rate of carbaryl, while 15 and 30 ppm concentrations of NOM decreased the reaction rate. For example, the rate of carbaryl photodegradation in the presence of the AgY zeolite that had 2.42 wt% Ag was enhanced by a factor of 1 in the presence of 3 ppm NOM-2001, and inhibited by factors of 2 and 3 in the presence of 15 and 30 ppm concentrations of NOM-2001, respectively.

The GC-MS analysis of carbaryl in the absence and presence of the AgY zeolites revealed slightly different products. A 30 ppm solution of carbaryl in the absence of the catalysts was irradiated for 30 minutes and the results showed the presence of carbaryl and the major degradation product, α-naphthol. In contrast, a 30 ppm solution of carbaryl in the presence of the AgY zeolites that was irradiated for the same amount of time showed the presence of α-naphthol, phthalic acid, and carbaryl.

5.2.2. Conclusions

This study demonstrated remarkably rich luminescent properties of the silver doped Y-type zeolites. The luminescence spectra of the four AgY zeolites were found to depend on the wavelength of excitation. This indicated that the different luminophores were present in the AgY zeolites and their emission was observed upon site selective excitation. Furthermore, bands A-E that were observed in the emission and SSLS indicated the presence of different silver clusters in the Y-type zeolites. The assignments of the luminescence bands (Table 4.2) indicates the presence of $[Ag^{+}]_n$

oligomers with $n \geq 2$. Additionally, the luminescence properties showed that an increase in the dopant concentration leads to the formation of larger silver clusters. Finally, the luminescence spectra were also dependent on temperature, indicating that energy transfer processes were occurring from smaller silver clusters to larger silver clusters within the zeolite channels.

The photodegradation of carbaryl in the presence of the AgY zeolites proceeded via first-order kinetics and caused a rate enhancement that was 3–79 times faster than carbaryl alone in solution. The AgY sample with the 0.3 wt% Ag showed the smallest rate enhancement, while the AgY zeolite with the highest silver loading showed the largest rate enhancement, indicating that as the amount of silver loading on the zeolite increases, the rate of photodecomposition of carbaryl also increases. The enhancement of the photodecomposition rate of carbaryl in the presence of the AgY zeolites is attributed to excimer formation between silver cations and the carbamate nitrogen in which the Ag-N bond becomes stronger upon excitation. This interaction appears to weaken the bond between the carbamate nitrogen and the carbonyl carbon meanwhile increasing the rate of photodegradation of carbaryl.

The GC-MS analysis of the photodegradation of carbaryl in the presence of the AgY zeolites indicated that the presence of the AgY catalysts causes a more complete degradation of carbaryl to occur, even after being irradiated with 300 nm light for just 30 minutes. The photodegradation of carbaryl in the presence of the AgY catalysts and NOM-2001 showed that the presence of 3 ppm NOM increased the rate of degradation; whereas, larger concentrations of NOM decreased the rate of photodecomposition. However, the rate changes for all the NOM concentrations were

very small indicating that the silver zeolite photocatalysts can still perform in the environment in the presence of natural organic matter.

5.3. Suggested Future Research

Previous studies have shown that carbaryl degrades at different rates depending on the temperature and pH of the solution that it is dissolved in. For example, under alkaline conditions (pH = 9) and at 25°C the compound appears to degrade rapidly, with a half-life of 3 hours.[19] On the other hand, in acidic media carbaryl is rather stable with a half-life of more than 1500 days at 27°C.[17] These results show that the pH of the surrounding solution does make a difference in the degradation of carbaryl. Therefore, research needs to be conducted in which the solution of carbaryl is buffered at a certain pH and monitored throughout the course of the photodegradation reaction. At the same time, the temperature of the reaction should also be monitored to see if this variable also has an affect on the photodecomposition reaction rate. Trying to photodecompose carbaryl as rapidly as possible in the environment, and determining which conditions are best for its degradation is an extremely important aspect of future investigations.

Zeolites encapsulating transition metals have been the subject of many recent studies due to their significant role in different efficient and selective catalytic reactions, such as the partial oxidation of hydrocarbons.[84-87] Many coordination complexes can form within zeolite pores by simply reacting the exchanged metal cations with various organic molecules. For instance, this study shows that silver doped in Y-zeolite displays good catalytic activity toward the photodecomposition of

carbaryl. However, the presence of mixed metal systems might show better catalytic activities toward the photodecomposition of pesticides. Thus, different mixed metals such as Ru-Rh, Pt-Pd, Cu-Ag, and Ag-Au doped in zeolites should be prepared and their catalytic activities toward the photodecomposition of different pesticides will then be tested.

The presence of mixed metal ions should enhance the selectivity toward pesticides rather than other catalysts. For example, silver and gold containing catalysts are expected to bind to sulfur and phosphorus containing pesticides, whereas, Pt, Pd, and Cu containing catalysts are expected to bind to pesticides that have hard ligands such as nitrogen containing molecules. Therefore, we expect to tune the photocatalytic activities toward different types of pesticides by varying the softness or hardness of the catalyst. For example, pesticides that contain soft ligands like sulfur bind strongly to soft metals such as gold; whereas, molecules that contains hard ligands such as nitrogen should bind to hard metals like palladium and copper ions.

REFERENCES

1. de Bertrand, N.; Barcelo, D. *Anal. Chim. Acta*, **1991**, *254*, 235.

2. Kuhr, R. J.; Dorough, H. W. *Carbamate Insecticides: Chemistry, Biochemistry and Toxicology*; CRC Press: Cleveland, **1976**, pp. 17-18.

3. Hayes, W. J., Jr. *Pesticides Studied in Man*; Waverly Press: Baltimore, **1980**, p. 440.

4. Khan, S. U. *Pesticides in the Soil Environment*; Elsevier:Amsterdam, **1980**, pp. 164-170.

5. Cremlyn, R. *Pesticides: Preparation and Mode of Action*; John Wiley & Sons: New York, **1978**, p. 97.

6. Ghauch, A.; Gallet, C.; Charef, A.; Rima, J.; Martin-Bouyer, M. *Chemosphere*, **2001**, *42*, 419.

7. Demirbas, A. *Sci. Tot. Environ.* **1998**, *220*, 235.

8. McKim, J. M.; Schemieder, P. K.; Niemi, G. J.; Carlson, R. W.; Henry, T. R. *Environ. Toxic. Chem.* **1987**, *6*, 313.

9. Melnikov, N. N. *Chemistry of Pesticides*; Springer-Verlag: New York, **1971**, p. 189.

10. Briggs, S. A. *Basic Guide to Pesticides: Their Characteristics and Hazards*; Hemisphere Publishing: Washington, **1994**, p. 201.

11. Bachman, J. G. Kinetic and Mechanistic Examination of the Photodecomposition of the Carbamate Pesticide Carbofuran and the Influence of Dissolved Organic Matter on Reaction Rate. M. S. Thesis, The Graduate School, The University of Maine, **1997**.

12. Kuhr, R. J.; Dorough, H. W. *Carbamate Insecticides: Chemistry, Biochemistry and Toxicology*; CRC Press: Cleveland, **1976**, p. 43.

13. Extension Toxicology Network, Oregon State University, URL: http://ace.orst.edu/cgi-bin/mfs/01/pips/carbaryl.htm?8

14. Dorough, H. W.; Casida, J. E. *J. Assoc. Off. Agric. Chem.* **1964**, *48*, 927.

15. Fukuto, T. R. *Drug Metab. Rev.* **1972**, *1*, 117.

16. Pramauro, E.; Prevot, A. B.; Vincenti, M.; Brizzolesi, G. *Environ. Sci. Technol.* **1997**, *31*, 3126.

17. Wolfe, N. L.; Zepp, R. G.; Paris, D. F. *Water Res.* **1978**, *12*, 565.

18. Aly, O. M.; El-Dib, M. A. *Water Res.* **1971**, *5*, 1191.

19. Carpenter, M. Hydrolysis of ^{14}C-Carbaryl in Aqueous Solutions Buffered at pH 5, 7, and 9. *Vol. 169-218 #92535*, **1990**, Department of Pesticide Regulation, Sacramento, CA.

20. Stanley, J. G.; Trial, J. G. *Bull. Environ. Contam. Toxicol.* **1980**, *25*, 771.

21. (a)Das, Y. T. Photodegradation of [1-naphthyl-^{14}C]Carbaryl in Aqueous Solution Buffered at pH 5 under Artificial Sunlight. *Vol. 169-208 #87094*, **1990**, Department of Pesticide Regulation, Sacramento, CA. (b)Das, Y. T. Photodegradation of [1-naphthyl-^{14}C]Carbaryl on Soil under Artificial Sunlight. *Vol. 169-208 #87095*, **1990**, Department of Pesticide Regulation, Sacramento, CA.

22. Zepp, R. G.; Wolfe, N.; Gordon, L.; Fincher, R. C. *J. Agric. Food. Chem.* **1976**, *24*, 727.

23. Armbrust, K. L.; Crosby, D. G. *Pacific Sci.* **1991**, *45*, 314.

24. (a)Miller, N. E. Metabolism of ^{14}C-Carbaryl under Aerobic Soil Conditions. *Vol. 169-269 #123599*, **1993**, Department of Pesticide Regulation, Sacramento, CA. (b)Miller, N. E. Metabolism of ^{14}C-Carbaryl under Anaerobic Aquatic Soil Conditions. *Vol. 169-268 #123598*, **1993**, Department of Pesticide Regulation, Sacramento, CA.

25. Chapalamadugu, S.; Chaudhry, G. R. *App. Environ. Microbiology*, **1991**, *57(3)*, 744.

26. Norris, F. A. A Terrestrial Field Dissipation Study with Carbaryl. *Vol. 169-223 #89222 & 89223*, Department of Pesticide Regulation, Sacramento, CA.

27. Larkin, M. J.; Day, M. J. *J. App. Bacteriology*, **1986**, *60*, 233.

28. Wauchope, R. D.; Haque, R. *Bull. Environ. Contam. Toxicol.* **1973**, *9*, 257.

29. Kanan, S. M. Study of Argentate, Dicyanoargentate, and Dicyanoaurate Clusters Doped in Zeolites and the Photoassisted Degradation of NO_x, Malathion, Carbofuran, and Carbaryl. Ph. D. Dissertation, The Graduate School, The University of Maine, **2000**.

30. Leeling, N. C.; Casida, J. E. *J. Agric. Food Chem.* **1966**, *14*, 281.

31. Kuhr, R. J.; Davis, A. C. *Pestic. Biochem. Physiol.* **1975**, *5*, 330.

32. Alexander, M. *Science*, **1981**, *211*, 132.

33. Kazano, H.; Kearney, P. C.; Kaufman, D. D. *J. Agric. Food Chem.* **1972**, *20*, 975.

34. Davies, J. F.; Evans, W. C. *Biochem. J.* **1964**, *91*, 251.

35. Jones, A. S.; Jones, L. A.; Hastings, F. L. *J. Agric. Food Chem.* **1982**, *30*, 997.

36. Padalikar, S. V.; Shinde, S. S.; Shinde, B. M. *Analyst*, **1988**, *113*, 1747.

37. Aaron, J. J.; Some, N. *Analusis*, **1982**, *10*, 481.

38. Trawtwein, N. L.; Guxon, J. C. *Mikro Chim. Acta*, **1983**, *3*, 347.

39. Alvarez-Rodríguez, L.; Monferrer-Pons, Ll.; Esteve-Romero, J. S.; García-Alvarez-Coque, M. C.; Ramis-Ramos, G. *Analyst*, **1997**, *122*, 459.

40. Durhan, E. J.; Lukasewycz, M. T.; Amato, J. R. *Environ. Toxicol. Chem.* **1990**, *9*, 463.

41. González, V.; Ayala, J. H.; Afonso, A. M. *Bull. Environ. Contam. Toxicol.* **1992**, *48*, 171.

42. Peris-Cardells, E.; Terol, J.; Maurí, A. R.; de la Guardia, M. *J. Environ. Sci. Health*, **1993**, *B28*, 431.

43. Kanan, S. M.; Tripp, C. P.; Austin, R. N.; Patterson, H. H. *J. Phys. Chem. B*, **2001**, *105*, 9441.

44. Gaffney, J. S.; Marley, N. A.; Clark, S. B. *Humic and Fulvic Acids: Isolation, Structure, and Environmental Fate*; American Chemical Society: Washington, **1996**, pp. 2-3.

45. Aiken, G. R.; McKnight, D. M.; Wershaw, R. L.; McCarthy, P. *Humic Substances in Soil, Sediment, and Water: Geochemistry, Isolation, and Characterization*; John Wiley & Sons: New York, **1985**, pp. 4-23.

46. Fang, F. Prediction of Contaminant Binding in an Upland-Wetland-Stream Drainage Sequence. M. S. Thesis, The Graduate School, The University of Maine, **1997**.

47. Stevenson, F. J. *Humus Chemistry: Genesis, Composition, Reactions*; Wiley-Interscience: New York, **1982**, p. 443.

48. Lakshman, S. Use of SSFS to Probe the Chemistry of Fulvic Acid and its Complexes with Aluminum. Ph. D. Dissertation, The Graduate School, The University of Maine, **1993**.

49. Perdue, E. M.; Gjessing, E. T. *Organic Acids in Aquatic Ecosystems*; John Wiley & Sons: New York, **1990**, pp. 5-23.

50. Schnitzer, M.; Khan, S. U. *Humic Substances in the Environment*; Marcel Dekker: New York, **1972**, p. 327.

51. Lu, X.; Jaffe, R. *Wat. Res.* **2001**, *35*, 1793.

52. Fang, F.; Kanan, S.; Patterson, H. H.; Cronan, C. S. *Anal. Chim. Acta*, **1998**, *373*, 139.

53. Bachman, J.; Patterson, H. H. *Environ. Sci. Technol.* **1999**, *33*, 874.

54. Gao, H.; Zepp, R. G. *Environ. Sci. Technol.* **1998**, *32*, 2940.

55. Newsam, J. M. *Science*, **1986**, *231*, 1093.

56. Zecchina, A.; Areán, C. O. *Chem. Soc. Rev.* **1996**, 187.

57. Sun, T.; Seff, K. *Chem. Rev.* **1994**, *94*, 857.

58. Baetzold, R. C. *J. Phys. Chem. B*, **1997**, *101*, 8180.

59. Mitchell, S. A.; Kenney-Wallace, A.; Ozin, G. A. *J. Am. Chem. Soc.* **1981**, *103*, 6030.

60. Vogler, A.; Kunkley, H. *Chem. Phys. Let.* **1989**, *158*, 74.

61. Eastland, G. W.; Mazid, M. A.; Russell, D. R.; Symons, M. C. R. *J. Chem. Soc. Dalton Trans.* **1980**, 1682.

62. Kim, Y.; Seff, K. *J. Am. Chem. Soc.* **1978**, *100*, 6989.

63. Michalik, J.; Wasowicz, T.; van der Pol, A.; Reijerse, E. J.; de Boer, E. *J. Chem. Soc., Chem. Commun.* **1992**, 29.

64. Ozin, G. A.; Hugues, F. *J. Phys. Chem.* **1983**, *87*, 94.

65. Szulbinski, W. S. *Inorg. Chim. Acta*, **1998**, *269*, 253.

66. Baker, M. D.; Ozin, G. A.; Godber, J. *J. Phys. Chem.* **1985**, *89*, 305.

67. Kellerman, R.; Texter, J. *J. Chem. Phys.* **1979**, *70*, 1562.

68. Chen, W.; Wang, Z.; Lin, L.; Lin, J.; Su, M. *Phys. Lett. A*, **1997**, *232*, 391.

69. Taylor, T.; Patterson, H. H. *Anal. Chem.* **1987**, *59*, 2180.

70. Senesi, N.; Miano, T. M.; Provenzano, M. R.; Brunetti, G. *Sci. Tot. Environ.* **1989**, *81*, 143.

71. Patterson, H. H.; Cronan, C. S.; Lakshman, S.; Plankey, B. J.; Taylor, T. A. *Sci. Tot. Environ.* **1992**, *113*, 179.

72. Lloyd, J. B. F. *Nature*, **1971**, *231*, 64.

73. Cronan, C. S.; Lakshman, S.; Patterson, H. H. *J. Environ. Qual.* **1992**, *21*, 457.

74. Senesi, N. *Anal. Chim. Acta*, **1990**, *232*, 77.

75. Senesi, N.; Miano, T. M.; Provenzano, M. R.; Brunetti, G. *Soil Sci.*, **1991**, *152*, 259.

76. Schwarzenbach, R. P.; Gschwend, P. M.; Imboden, D. M. *Environmental Organic Chemistry*; John Wiley & Sons: New York, **1993**, pp. 255-341.

77. Kanan, S. M.; Omary, M. A.; Patterson, H. H.; Matsuoka, M.; Anpo, M. *J. Phys. Chem. B*, **2000**, *104*, 3507.

78. Kanan, S. M.; Kanan, M. C.; Patterson, H. H. *J. Phys. Chem. B*, **2001**, *105*, 7508.

79. Crutchley, R. J.; Kriess, N.; Lever, A. B. *J. Am. Chem. Soc.* **1983**, *23*, 1170.

80. Hicks, C.; Ye, G.; Gonzalez, M.; Rutenberg, I.; Fan, J.; Helmy, R.; Kassis, A.; Gafney, H. D. *Coord. Chem. Rev.* **1998**, *171*, 71.

81. Lever, A. B.; Seymour, P.; Auburn, P. *Inorg. Chim. Acta*, **1988**, *145*, 43.

82. Stacy, E. M.; McMillin, D. R. *Inorg. Chem.* **1990**, *29*, 393.

83. Kutal, C. *Coord. Chem. Rev.* **1990**, *99*, 213.

84. Notari, B. *Adv. Catal.* **1996**, 253.

85. Corma, A. *Chem. Rev.* **1997**, *97*, 2373.

86. Karge, H. G. *Stud. Surf. Sci. Catal.* **1996**, *134*, 197.

87. Sass, C. E.; Chen, X.; Kevan, L. *J. Chem Soc. Faraday Trans.* **1990**, *86*, 189.

BIOGRAPHY OF THE AUTHOR

Marsha Kanan was born in Lewiston, Maine on December 17, 1978. She graduated as valedictorian from Oxford Hills High School on June 7, 1997. She attended The University of Maine in Orono, Maine starting in September of 1997, and graduated Summa Cum Laude with her Bachelor of Science Degree in Chemistry in May of 2001. She then joined the graduate program in the Department of Chemistry at The University of Maine in June of 2001.

She was married to Sofian M. Kanan on May 14, 1999. Marsha is a candidate for the Master of Science degree in Chemistry from The University of Maine in May, 2002.